# 14. SITE 1020[1]

Shipboard Scientific Party[2]

## HOLE 1020A

**Date occupied:** 1 June 1996

**Date departed:** 1 June 1996

**Time on hole:** 6 hr, 30 min

**Position:** 41°0.051′N, 126°26.065′W

**Drill pipe measurement from rig floor to seafloor (m):** 3052.9

**Distance between rig floor and sea level (m):** 11.3

**Water depth (drill pipe measurement from sea level, m):** 3041.6

**Total depth (from rig floor, m):** 3062.9

**Penetration (m):** 10.0

**Number of cores (including cores having no recovery):** 1

**Total length of cored section (m):** 10.0

**Total core recovered (m):** 10.0

**Core recovery (%):** 100.0

**Oldest sediment cored:**
Depth (mbsf): 10.0
Nature: Clay with diatoms
Age: Quaternary

**Comments:** Missed the mudline.

## HOLE 1020B

**Date occupied:** 1 June 1996

**Date departed:** 4 June 1996

**Time on hole:** 2 days, 6 hr

**Position:** 41°0.051′N, 126°26.064′W

**Drill pipe measurement from rig floor to seafloor (m):** 3049.7

**Distance between rig floor and sea level (m):** 11.3

**Water depth (drill pipe measurement from sea level, m):** 3038.4

**Total depth (from rig floor, m):** 3328.5

**Penetration (m):** 278.8

**Number of cores (including cores having no recovery):** 30

**Total length of cored section (m):** 278.8

**Total core recovered (m):** 265.0

**Core recovery (%):** 95.0

**Oldest sediment cored:**
Depth (mbsf): 278.8
Nature: Claystone with nannofossils, claystone
Age: early Pliocene

**Measured velocity (km/s):** 1.723 at Section 30X-1, 33 cm

**Comments:** Tagged the basement. Approximately 5 cm of basalt was recovered.

## HOLE 1020C

**Date occupied:** 4 June1996

**Date departed:** 5 June 1996

**Time on hole:** 1 day, 2 hr, 45 min

**Position:** 41°0.051′N, 126°26.063′W

**Drill pipe measurement from rig floor to seafloor (m):** 3049.2

**Distance between rig floor and sea level (m):** 11.3

**Water depth (drill pipe measurement from sea level, m):** 3037.9

**Total depth (from rig floor, m):** 3282.4

**Penetration (m):** 233.2

**Number of cores (including cores having no recovery):** 25

**Total length of cored section (m):** 233.2

**Total core recovered (m):** 239.5

**Core recovery (%):** 102.0

**Oldest sediment cored:**
Depth (mbsf): 233.2
Nature: Clay with diatoms, nannofossil clay mixed sediment with diatoms
Age: late Pliocene

## HOLE 1020D

**Date occupied:** 5 June 1996

**Date departed:** 6 June 1996

**Time on hole:** 19 hr, 30 min

**Position:** 41°0.050′N, 126°26.071′W

**Drill pipe measurement from rig floor to seafloor (m):** 3049.1

**Distance between rig floor and sea level (m):** 11.3

**Water depth (drill pipe measurement from sea level, m):** 3037.8

**Total depth (from rig floor, m):** 3205.3

**Penetration (m):** 156.2

**Number of cores (including cores having no recovery):** 17

**Total length of cored section (m):** 156.2

**Total core recovered (m):** 163.7

**Core recovery (%):** 104.0

**Oldest sediment cored:**
Depth (mbsf): 156.2
Nature: Clay with diatoms
Age: late Pliocene

[1]Lyle, M., Koizumi, I., Richter, C., et al., 1997. *Proc. ODP, Init. Repts.*, 167: College Station, TX (Ocean Drilling Program).
[2]Shipboard Scientific Party is given in the list preceding the Table of Contents.

**Principal results:** Site 1020 is located on the east flank of the Gorda Ridge at a water depth of 3038 mbsl. It is about 170 km west of Eureka, California, and forms the deep-water drill site on the Gorda Transect. The site is located on an abyssal hill that trends northeast and rises ~50 m above the surrounding seafloor on 5.1 Ma ocean crust. The primary objective of drilling at this site was to study paleoceanographic conditions near the core of the northern region of the California Current during the critical time interval when the Northern Hemisphere glaciation developed. The development of a correlation between biostratigraphy and the paleomagnetic chronostratigraphy was another key objective at this site. Site 1020 will provide information about organic carbon diagenesis and about minor element geochemistry through interstitial water profiles and through solid phase analyses. Provided that stable paleomagnetic declinations can be obtained, the rotation of the Gorda Plate can be monitored through time. A secondary goal was to obtain a representative sample of the basalt basement for igneous petrology and geochemistry.

Four holes were cored with the APC/XCB at Site 1020 (Fig. 1) to a maximum depth of 278.8 mbsf, recovering an apparently continuous interval of late early Pliocene to Quaternary age (0.0–3.8 Ma). Hole 1020A is a 10-m-long failed mudline core. Hole 1020B was cored with the APC to 169.3 mbsf and extended with the XCB to a depth of 278.8 mbsf. The hole was logged with the density-porosity combination, sonic-Formation MicroScanner, and the GHMT tool strings. Hole 1020C was cored with the APC to 146.8 mbsf and deepened with the XCB to 233.2 mbsf. Seventeen cores were taken at Hole 1020D with the APC down to refusal at 156.2 mbsf. Detailed comparisons between the magnetic susceptibility and the GRAPE density record generated on the MST, and high-resolution color reflectance measured with the Oregon State University system, demonstrated complete recovery of the sedimentary sequence down to 242 mcd, with the exception of coring gaps at 126, 137, and 200 mcd, which could not be covered by overlap.

The uppermost ~229 m of the sedimentary sequence consists of siliciclastic clay with minor calcareous biogenic components (Quaternary to late Pliocene) (Fig. 1). The uppermost part of this interval is calcareous whereas the lower part is diatomaceous. Thin intervals of nannofossil ooze occur throughout, and diatoms rarely exceed 30% of the sediment. Turbidite deposition is relatively unimportant at this site compared to previous sites, except for a few thin, graded beds. The underlying unit (50 m thick) is characterized by interbeds of nannofossil clay and clayey nannofossil chalk. The age range of this unit is early to late Pliocene. The lowest 18 m at the site is composed of sparsely calcareous claystone that immediately overlies approximately 5 cm of brecciated dark gray basalt that was recovered at the base of the hole.

A well-constrained biostratigraphy and chronology are provided by a combination of paleomagnetic reversals and calcareous nannofossil, planktonic foraminifer, radiolarian, and diatom datums. All microfossil groups are clearly dominated by cool, high-latitude elements throughout the late Neogene. Radiolarians are entirely represented by subarctic forms, and the assemblages exhibit noticeably lower diversity than at all other sites cored during Leg 167. Diatoms are dominated by North Pacific subarctic assemblages in addition to rare temperate elements. Planktonic foraminifer assemblages are dominated by subarctic to cool temperate forms, with subtropical elements absent. Radiolarians are represented throughout the entire sequence by forms not characteristic of upwelling regions. Likewise, diatoms are represented by open-ocean forms not characteristic of coastal upwelling regions, except during the early late Pliocene when upwelling forms are present in relatively low abundances.

Alternating field demagnetization at 20 mT revealed a complete magnetostratigraphic record between 0 and 130 mbsf, which allowed the identification of the Brunhes (C1n) and the Jaramillo (C1r.1n) normal polarity intervals.

Calcium carbonate concentrations range between 1 and 20 wt% in the upper 220 mbsf and increase up to 58 wt% below that depth. Organic carbon is of predominantly marine origin and varies around 0.7 wt%. Chemical gradients in the interstitial waters reflect organic matter diagenesis, the dissolution of biogenic opal and calcium carbonate, the influence of authigenic mineral precipitation, and the diffusive influence of reactions in underlying basalt.

Downhole temperature measurements yield a thermal gradient of 189°C/km. Using an average measured thermal conductivity of 0.899 W/(m·K) provides a heat-flow estimate of 170 mW/m$^2$ at Site 1020. The vicinity of the Gorda Ridge explains this relatively high heat-flow value.

Overall log quality was excellent to very good below 170 mbsf, and fair in the washed-out section above 170 mbsf. Core-log comparison suggests that the cored sediment, and therefore the meters composite depth scale, is expanded by about 10% relative to its true depth range.

## BACKGROUND AND OBJECTIVES

### General Description

Site 1020 is located on the east flank of the Gorda Ridge at a water depth of 3038 mbsl (Fig. 2). It is about 170 km west of Eureka, California and is the high-resolution deep-water drill site on the 40°N (Gorda) Transect. The age of the ocean crust is 5.1 Ma based upon magnetic anomalies (base of Anomaly 3N; Atwater and Severinghaus, 1989). The site is located on an abyssal hill that trends northeast and rises ~50 m above the surrounding seafloor. To the east of Site 1020, the floor of the Gorda Basin is covered with thick Pleistocene turbidite deposits, but the site itself has a hemipelagic sediment sequence. The site was surveyed in detail during the *Wecoma* cruise W9406 in 1994 (Lyle et al., 1995a, 1995b; Fig. 3). The sediments at Site 1020 are acoustically transparent with only faint layering. Basement is at a depth of 345 ms TWT, or about 265–275 mbsf.

### Site Objectives

Site 1020 is situated in deep water and has sedimentation rates ~100 m/m.y. in the upper 220 mbsf. Site 1020 was drilled to assess paleoceanographic conditions within the northern region of the California Current during the critical time interval when the Northern Hemisphere glaciation developed. Site 1020 will also be used to develop a correlation between biostratigraphy and the paleomagnetic chronostratigraphy. In the modern oceans, Site 1020 is located beneath a region of high seasonal variability, where the local current regime is strongly affected by the movement of the atmospheric North Pacific high pressure regime (see "Introduction" chapter, this volume). The site is on the fringes of nutrient-enriched waters upwelled along the coast and is not as strongly influenced by upwelling as other sites. Geochemical indices of paleoproductivity and microfossil assemblages from Site 1020 will provide important data on nutrients introduced from the subarctic gyre into the California Current at its northern terminus.

Site 1020 has important geochemical objectives. Organic carbon content varies between 0.3 and 1.3 wt%, and heat flow is relatively high because of the young basement age. Diagenesis driven by moderate thermal conditions may become apparent here. Inorganic geochemical studies through interstitial water profiles and solid phase studies will monitor the reactions of inorganic sediment constituent phases. Site 1020 was drilled to oceanic basement, and 5 cm of basalt was recovered for studies of igneous petrology and geochemistry.

Because this site has high sedimentation rates with stable magnetic mineral phases to at least 100 mbsf, another goal at Site 1020 was to study the structure of paleomagnetic reversals in detail. Paleomagnetic studies will also provide an avenue to study the deformation of the Gorda Plate. The eastern flank of the Gorda Ridge has rotated 40 to 60 degrees in the last 5 million years during its slow incorporation

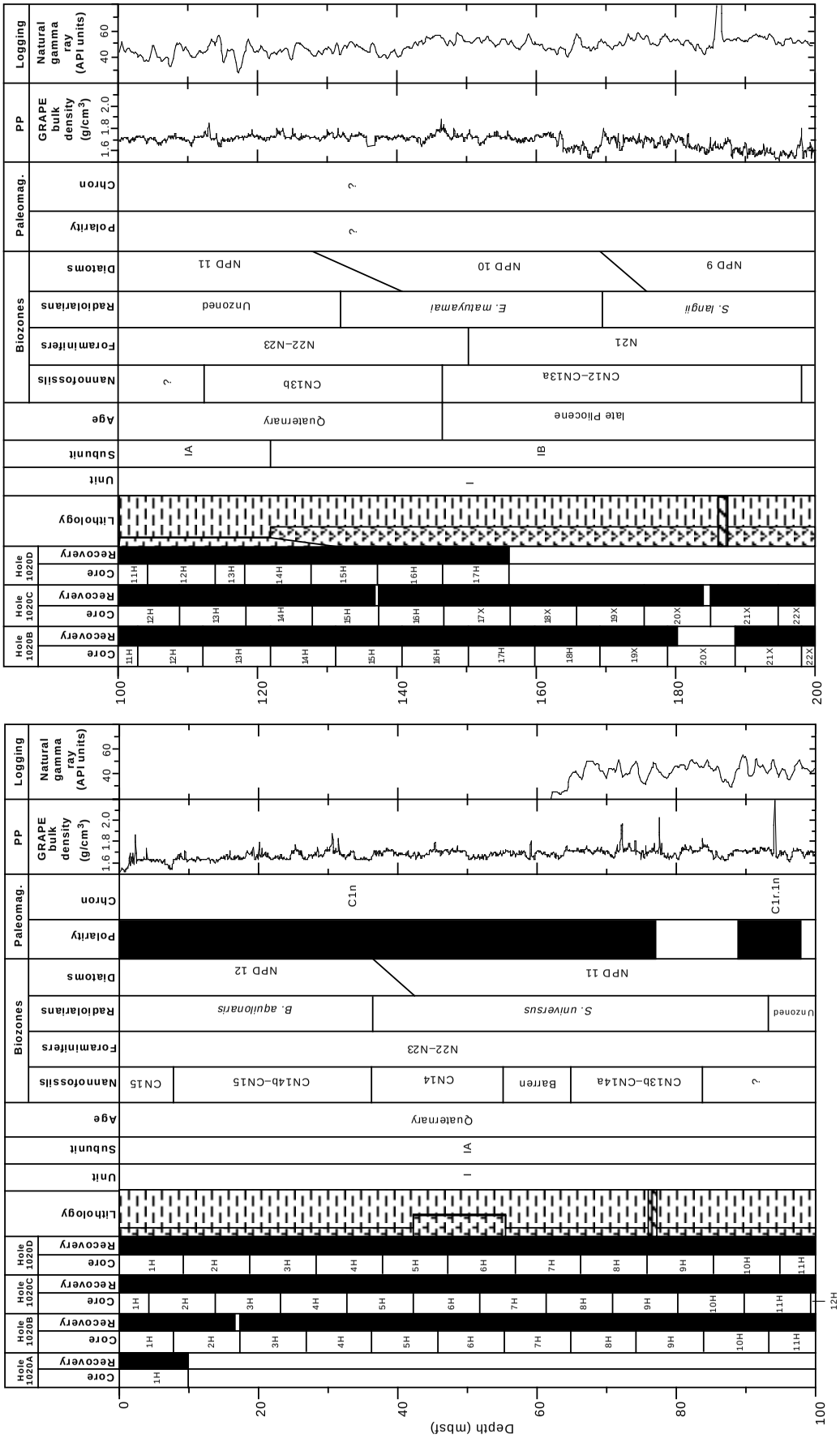


Figure 1. Site 1020 master column.

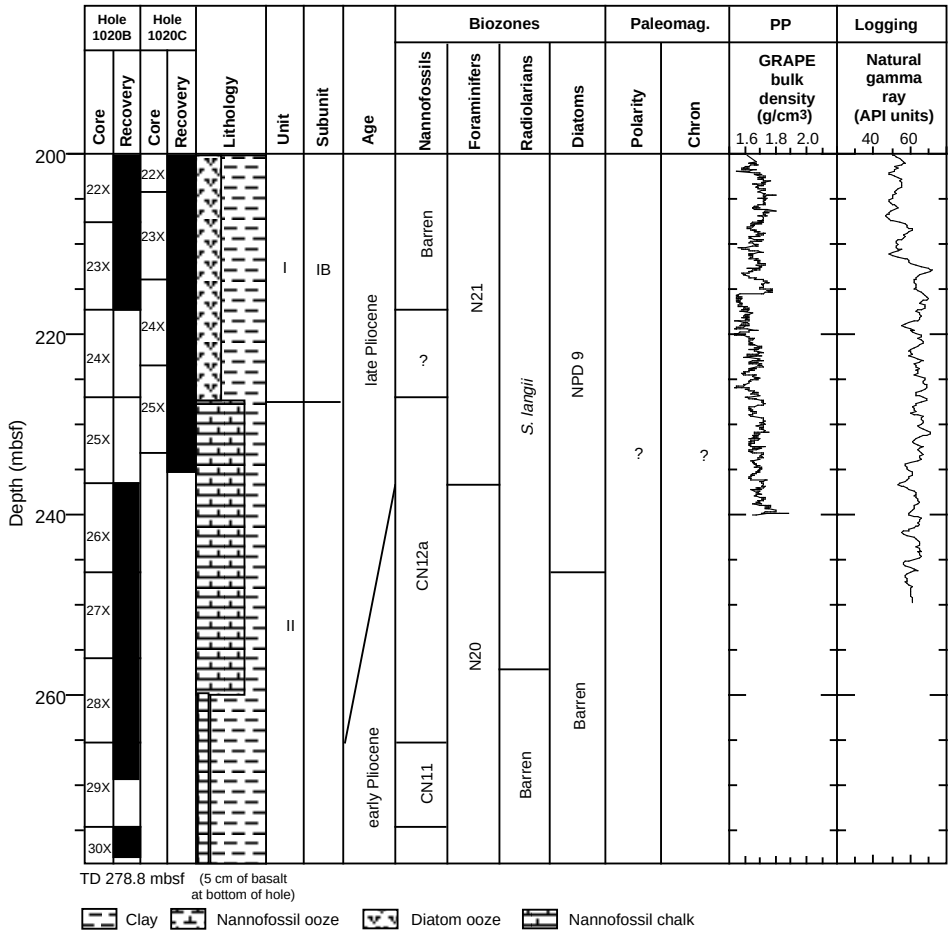


Figure 1 (continued).

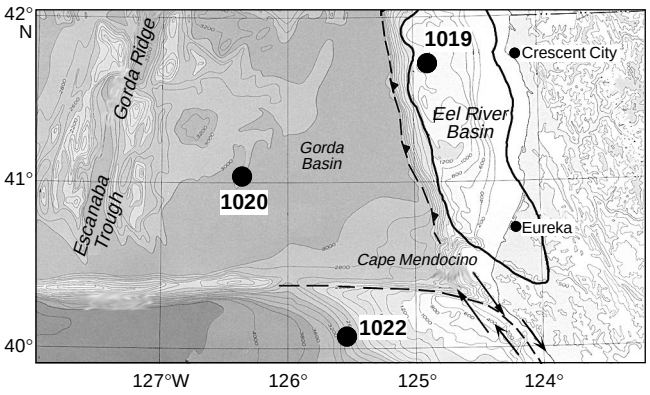


Figure 2. Location map for Site 1020, located on the east flank of the Gorda Ridge, just above the turbidite plain that fills the Gorda Basin.

into the Pacific Plate (Riddihough, 1980; Wilson, 1989). Provided that stable magnetic declinations can be obtained from Site 1020 sediments, the rotation can be monitored through time.

## OPERATIONS

### Transit from Site 1019 to Site 1020

The 79.0-nmi transit from Site 1019 to Site 1020 was accomplished in 7.0 hr at an average speed of 10.9 kt. A 3.5-kHz precision depth recorder survey was performed while approaching Site 1020. The *JOIDES Resolution* arrived at Site 1020 at 1445 hr on 1 June.

### Hole 1020A

Hole 1020A was spudded at 2030 hr on 1 June. A full barrel prevented establishing an accurate mudline, and the hole was abandoned.

### Hole 1020B

The drill string was raised 5 m and Hole 1020B was spudded at 2115 hr on 1 June. APC Cores 167-1020B-1H through 18H were taken down to 169.3 mbsf with 105.1% recovery (Table 1; see Table 2-CD on CD-ROM in the back pocket of this volume for a more detailed coring summary). Adara temperature measurements were taken on Cores 167-1020B-4H, 6H, and 8H (see "Physical Properties" section, this chapter). Oriented cores were obtained starting with Core 167-1020B-3H. XCB Cores 167-1020B-19X through 30X were taken down to 278.8 mbsf with 79.5% recovery. Hole 1020B was logged with the density-porosity combination, sonic-Formation MicroScanner, and GHMT tool strings with excellent results.

### Hole 1020C

The vessel was offset 10 m to the south and Hole 1020C was spudded at 0545 hr on 4 June. APC Cores 167-1020C-1H through 16H were taken down to 146.8 mbsf with 104.0% recovery (Table 1). Sediments became increasingly indurated with Core 167-1020C-15H (Fig. 4). Oriented cores were obtained again starting with Core 167-

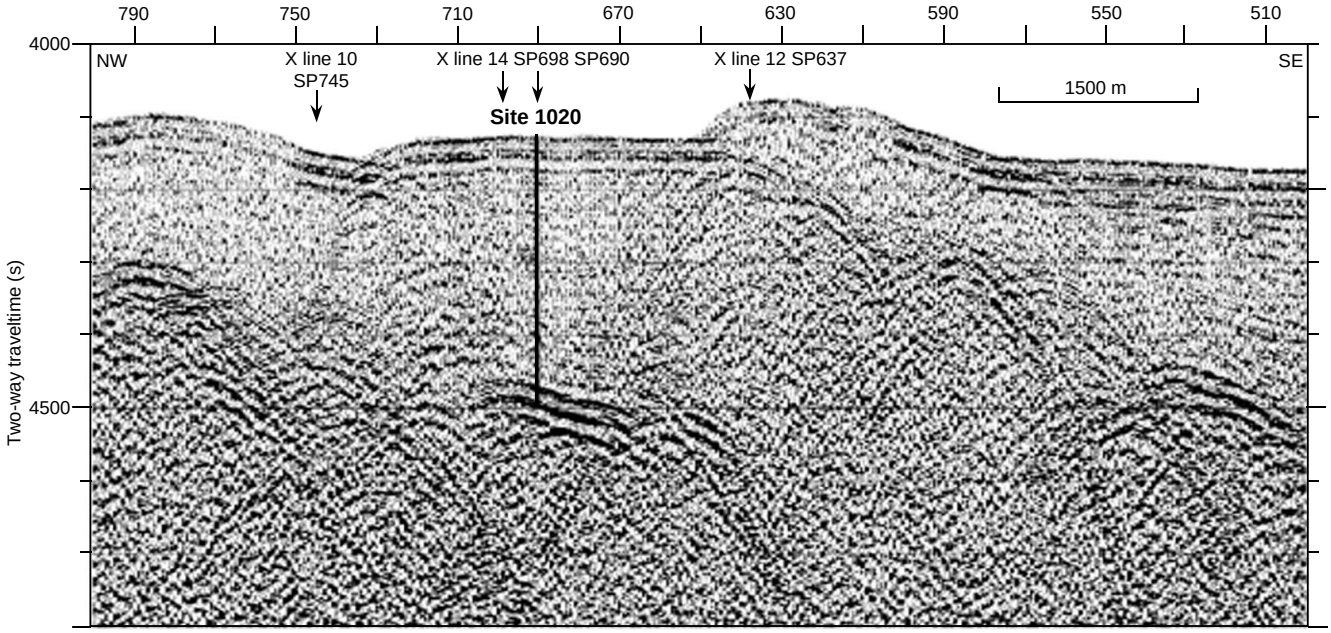


Figure 3. Seismic reflection profile through Site 1020 (Line EW9406 CA4-4; Lyle et al., 1995a, 1995b). The data are single channel, filtered between 30 and 200 Hz. The profile cuts across the abyssal hill on which Site 1020 is located. On y-axis, (s) = milliseconds.

1020C-3H. XCB Cores 167-1020C-17X through 25X were taken down to 233.2 mbsf with 100.5% recovery.

### Hole 1020D

The vessel was offset 10 m to the south and Hole 1020D was spudded at 0715 hr on 5 June. APC Cores 167-1020D-1H through 17H were taken down to 156.2 mbsf with 104.8% recovery (Table 1). The drill string was tripped back to the surface and secured for the 12-hr transit to Site 1021 by 0130 hr on 6 June.

## LITHOSTRATIGRAPHY

### Introduction

A continuous Quaternary to lower Pliocene (0.0–3.8 Ma) sequence was recovered at Site 1020. Siliciclastic clay is present throughout the cored interval and is the dominant component in the upper part. The middle part is dominated by nannofossil clay with frequent interbedding of clayey nannofossil ooze. Diatoms are present in lesser amounts ranging between about 10% and 30% of the total sediment. The lower part is dominated by interbeds of nannofossil clay and clayey nannofossil chalk. Two beds of dolomite are found at about 78 mbsf and 188 mbsf. Compared to previous sites, turbidite deposition is insignificant in these sediments, except for a few thin, graded beds in the uppermost portion and a slightly thicker bed at about 68 mbsf. Pyrite nodules occur through most of the section but are more frequent and larger, occasionally with a diameter of up to 5 cm, in the lower portion. The sediments are divided into two units based on visual core descriptions and smear-slide estimates (Fig. 5). Unit I is predominantly composed of clay-rich sediments mixed with minor quantities of nannofossils and diatoms. Thin intervals (usually <1 m) of nannofossil ooze occur throughout this unit, and diatoms rarely exceed 30% of the sediment. Unit II chiefly consists of clayey nannofossil chalk mixed sediments with abundant pyrite nodules. Clay content increases to nearly 95% at the bottom of the sequence. Approximately 5 cm of basalt was recovered at the base of Hole 1020B.

### Description of Units

#### *Unit I*

Hole 1020A, interval 167-1020A-1; 0–10.0 mbsf (base of hole);
Hole 1020B, interval 167-1020B-1H-1 through 25X-1; 0–228.5 mbsf;
Hole 1020C, interval 167-1020C-1H-1 through 25X-3; 0–226.8 mbsf;
Hole 1020D, interval 167-1020D-1H-1 through 17H-CC; 0–156.2 mbsf (base of hole).
Age: Quaternary to late Pliocene, 0.0–2.9 Ma.

Unit I is characterized by siliciclastic clay with small to moderate amounts of siliceous and calcareous biogenic components. Bioturbation is variable throughout this unit with *Chondrites* and *Zoophycos* trace fossils common. The sediments from Unit I are divided into two subunits based on relative abundance of biogenous components (Fig. 5). Contacts between subunits are not strictly defined because of the gradational nature of changes between the major lithologies, thus "intervals" given below are only approximate.

*Subunit IA*

Hole 1020A, interval 167-1020A-1H; 0–10.0 mbsf (base of hole);
Hole 1020B, interval 167-1020B-1H-1 through 13H-CC; 0–121.8 mbsf;
Hole 1020C, interval 167-1020C-1H-1 through 14H-2, 70 cm; 0–120.5 mbsf;
Hole 1020D, interval 167-1020D-1H-1 through 14H-2, 30 cm; 0–120.0 mbsf.
Age: Quaternary; 0.0–1.3 Ma

Subunit IA consists of gray to pale olive (5Y 5/1 to 10Y 6/1) clay interbedded with nannofossil clay. Interbedding of these lithologies is gradual and indistinct. The average content of calcareous microfossils (nannofossils and foraminifers) ranges from about 0% to 10%, with a few intervals containing up to 75% nannofossils. Several thin beds of very fine sand occur near the top of this subunit, and a thicker (25 cm), graded bed of feldspar quartz silt/sand occurs at about 68 mbsf in Section 167-1020C-8H-5, 51–77 cm. A thin layer of moderately cemented dolomite is located between 75 and 78 mbsf (Sections 167-1020B-9H-1, 55–65 cm, and 167-1020C-9H-6, 60–70 cm) sur-

**Table 1. Coring summary for Site 1020.**

| Core | Date (June 1996) | Time | Top (mbsf) | Bottom (mbsf) | Length cored (m) | Length recovered (m) | Recovery (%) |
|---|---|---|---|---|---|---|---|
| 167-1020A- | | | | | | | |
| 1H | 02 | 0345 | 0.0 | 10.0 | 10.0 | 10.02 | 100.2 |
| 167-1020B- | | | | | | | |
| 1H | 02 | 0440 | 0.0 | 7.8 | 7.8 | 7.82 | 100.0 |
| 2H | 02 | 0510 | 7.8 | 17.3 | 9.5 | 8.85 | 93.1 |
| 3H | 02 | 0555 | 17.3 | 26.8 | 9.5 | 10.00 | 105.2 |
| 4H | 02 | 0700 | 26.8 | 36.3 | 9.5 | 10.07 | 106.0 |
| 5H | 02 | 0755 | 36.3 | 45.8 | 9.5 | 10.14 | 106.7 |
| 6H | 02 | 0900 | 45.8 | 55.3 | 9.5 | 10.17 | 107.0 |
| 7H | 02 | 0945 | 55.3 | 64.8 | 9.5 | 10.17 | 107.0 |
| 8H | 02 | 1055 | 64.8 | 74.3 | 9.5 | 10.11 | 106.4 |
| 9H | 02 | 1150 | 74.3 | 83.8 | 9.5 | 10.10 | 106.3 |
| 10H | 02 | 1250 | 83.8 | 93.3 | 9.5 | 9.95 | 105.0 |
| 11H | 02 | 1350 | 93.3 | 102.8 | 9.5 | 10.13 | 106.6 |
| 12H | 02 | 1450 | 102.8 | 112.3 | 9.5 | 9.99 | 105.0 |
| 13H | 02 | 1545 | 112.3 | 121.8 | 9.5 | 10.07 | 106.0 |
| 14H | 02 | 1640 | 121.8 | 131.3 | 9.5 | 9.93 | 104.0 |
| 15H | 02 | 1735 | 131.3 | 140.8 | 9.5 | 9.98 | 105.0 |
| 16H | 02 | 1830 | 140.8 | 150.3 | 9.5 | 10.07 | 106.0 |
| 17H | 02 | 1925 | 150.3 | 159.8 | 9.5 | 10.20 | 107.3 |
| 18H | 02 | 2005 | 159.8 | 169.3 | 9.5 | 10.18 | 107.1 |
| 19X | 02 | 2130 | 169.3 | 178.9 | 9.6 | 9.63 | 100.0 |
| 20X | 03 | 0220 | 178.9 | 188.5 | 9.6 | 1.37 | 14.3 |
| 21X | 03 | 0310 | 188.5 | 198.1 | 9.6 | 9.75 | 101.0 |
| 22X | 03 | 0355 | 198.1 | 207.7 | 9.6 | 9.83 | 102.0 |
| 23X | 03 | 0440 | 207.7 | 217.3 | 9.6 | 9.81 | 102.0 |
| 24X | 03 | 0545 | 217.3 | 227.0 | 9.7 | 0.00 | 0.0 |
| 25X | 03 | 0630 | 227.0 | 236.6 | 9.6 | 9.74 | 101.0 |
| 26X | 03 | 0755 | 236.6 | 246.3 | 9.7 | 9.67 | 99.7 |
| 27X | 03 | 0915 | 246.3 | 255.9 | 9.6 | 9.96 | 104.0 |
| 28X | 03 | 1045 | 255.9 | 265.3 | 9.4 | 9.88 | 105.0 |
| 29X | 03 | 1245 | 265.3 | 274.7 | 9.4 | 4.12 | 43.8 |
| 30X | 03 | 1505 | 274.7 | 278.8 | 4.1 | 3.31 | 80.7 |
| 167-1020C- | | | | | | | |
| 1H | 04 | 1300 | 0.0 | 4.3 | 4.3 | 4.31 | 100.0 |
| 2H | 04 | 1355 | 4.3 | 13.8 | 9.5 | 9.10 | 95.8 |
| 3H | 04 | 1505 | 13.8 | 23.3 | 9.5 | 10.11 | 106.4 |
| 4H | 04 | 1610 | 23.3 | 32.8 | 9.5 | 10.15 | 106.8 |
| 5H | 04 | 1705 | 32.8 | 42.3 | 9.5 | 10.15 | 106.8 |
| 6H | 04 | 1800 | 42.3 | 51.8 | 9.5 | 10.08 | 106.1 |
| 7H | 04 | 1855 | 51.8 | 61.3 | 9.5 | 9.88 | 104.0 |
| 8H | 04 | 1935 | 61.3 | 70.8 | 9.5 | 9.84 | 103.0 |
| 9H | 04 | 2020 | 70.8 | 80.3 | 9.5 | 9.99 | 105.0 |
| 10H | 04 | 2100 | 80.3 | 89.8 | 9.5 | 10.16 | 106.9 |
| 11H | 04 | 2200 | 89.8 | 99.3 | 9.5 | 9.99 | 105.0 |
| 12H | 04 | 2300 | 99.3 | 108.8 | 9.5 | 9.92 | 104.0 |
| 13H | 04 | 2350 | 108.8 | 118.3 | 9.5 | 10.05 | 105.8 |
| 14H | 05 | 0045 | 118.3 | 127.8 | 9.5 | 9.73 | 102.0 |
| 15H | 05 | 0130 | 127.8 | 137.3 | 9.5 | 9.11 | 95.9 |
| 16H | 05 | 0225 | 137.3 | 146.8 | 9.5 | 10.05 | 105.8 |
| 17X | 05 | 0345 | 146.8 | 156.3 | 9.5 | 9.87 | 104.0 |
| 18X | 05 | 0440 | 156.3 | 165.9 | 9.6 | 9.80 | 102.0 |
| 19X | 05 | 0530 | 165.9 | 175.5 | 9.6 | 9.89 | 103.0 |
| 20X | 05 | 0615 | 175.5 | 185.1 | 9.6 | 8.58 | 89.4 |
| 21X | 05 | 0735 | 185.1 | 194.7 | 9.6 | 9.71 | 101.0 |
| 22X | 05 | 0850 | 194.7 | 204.3 | 9.6 | 9.80 | 102.0 |
| 23X | 05 | 0945 | 204.3 | 213.9 | 9.6 | 9.80 | 102.0 |
| 24X | 05 | 1045 | 213.9 | 223.5 | 9.6 | 9.73 | 101.0 |
| 25X | 05 | 1145 | 223.5 | 233.2 | 9.7 | 9.69 | 99.9 |
| 167-1020D- | | | | | | | |
| 1H | 05 | 1425 | 0.0 | 9.4 | 9.4 | 9.43 | 100.0 |
| 2H | 05 | 1520 | 9.4 | 18.9 | 9.5 | 10.04 | 105.7 |
| 3H | 05 | 1605 | 18.9 | 28.4 | 9.5 | 10.02 | 105.5 |
| 4H | 05 | 1700 | 28.4 | 37.9 | 9.5 | 9.96 | 105.0 |
| 5H | 05 | 1745 | 37.9 | 47.4 | 9.5 | 10.04 | 105.7 |
| 6H | 05 | 1830 | 47.4 | 56.9 | 9.5 | 10.08 | 106.1 |
| 7H | 05 | 1915 | 56.9 | 66.4 | 9.5 | 10.11 | 106.4 |
| 8H | 05 | 2015 | 66.4 | 75.9 | 9.5 | 9.97 | 105.0 |
| 9H | 05 | 2050 | 75.9 | 85.4 | 9.5 | 10.17 | 107.0 |
| 10H | 05 | 2135 | 85.4 | 94.9 | 9.5 | 10.14 | 106.7 |
| 11H | 05 | 2215 | 94.9 | 104.4 | 9.5 | 9.98 | 105.0 |
| 12H | 05 | 2300 | 104.4 | 113.9 | 9.5 | 9.98 | 105.0 |
| 13H | 05 | 2345 | 113.9 | 118.2 | 4.3 | 4.29 | 99.7 |
| 14H | 06 | 0040 | 118.2 | 127.7 | 9.5 | 9.67 | 102.0 |
| 15H | 06 | 0130 | 127.7 | 137.2 | 9.5 | 10.10 | 106.3 |
| 16H | 06 | 0215 | 137.2 | 146.7 | 9.5 | 9.81 | 103.0 |
| 17H | 06 | 0310 | 146.7 | 156.2 | 9.5 | 9.95 | 105.0 |

Note: Table 2, on the CD-ROM in the back pocket, this volume, is a more detailed coring summary.

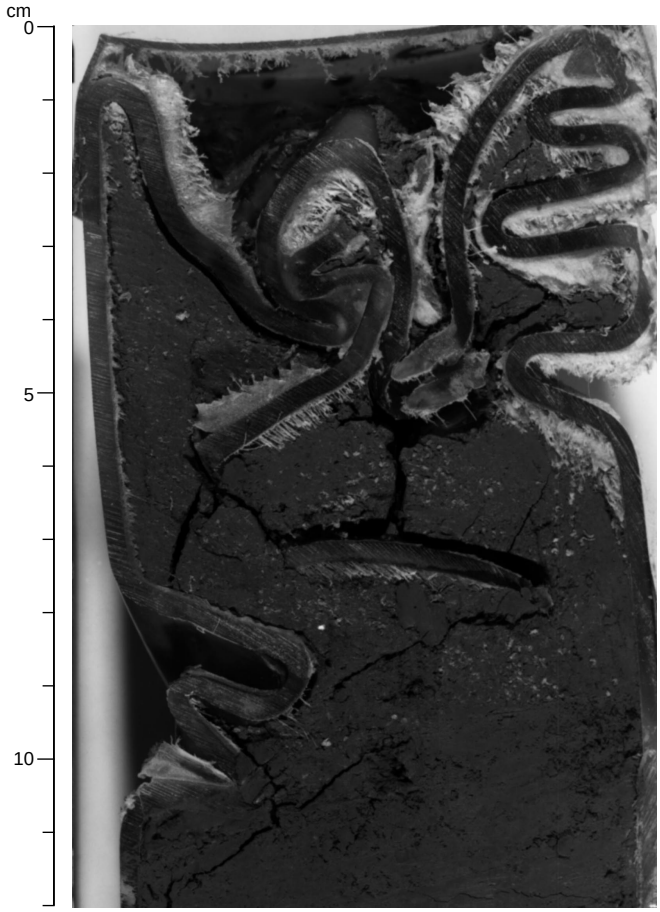


Figure 4. Deformed core liner at top of Section 137-1020C-15H-2, 0–12 cm.

rounded by a ~1 m interval of dolomite clay. Pyrite occurs regularly throughout this subunit as centimeter-sized nodules/concretions and finely disseminated grains in dark gray (N4) patches and color bands.

*Subunit IB*

Hole 1020B, interval 167-1020B-13H-CC through 25X-1; 121.8–228.5 mbsf;
Hole 1020C, interval 167-1020C-14H-2, 70 cm, through 25X-3; 120.5–226.8 mbsf;
Hole 1020D, interval 167-1020D-14H-2, 30 cm, through 17H-CC; 120.0–156.2 mbsf (base of hole).
Age: Quaternary to late Pliocene; 1.3–2.9 Ma.

The contact of Subunit IA with Subunit IB is gradational and defined by an increase in diatom content with depth (Fig. 5). This subunit consists of grayish olive to dark gray (10Y 4/1 to 5Y 4/1) clay and diatom clay. The diatom content ranges from 5% to 40%, whereas content of calcareous microfossils is generally low, ranging from 0% to 20% based on smear-slide estimates, except for a few meter-scale beds of nannofossil-rich sediments at about 170–180 mbsf (see also "Organic Geochemistry" section, this chapter). A 6-cm-thick medium to very light gray (N5 to N8) layer of vitric ash with pyrite occurs in Section 167-1020C-20X-5, 55–61 cm. A submeter bed of dolomite clay occurs at about 188 mbsf in Hole 1020C (not recovered in other holes). Large pyrite concretions and nodules are also common in these sediments. The sediments are moderately to heavily bioturbated with abundant *Zoophycos* and *Planolites* trace fossils throughout this subunit.

***Unit II***

Hole 1020B, interval 167-1020B-25X-2 through 30X-3; 228.5–278.8 mbsf (base of hole);
Hole 1020C, interval 167-1020C-25X-3, 30 cm, through 25X-CC; 226.8–233.2 mbsf (base of hole).
Age: late Pliocene to early Pliocene; 2.9–3.8 Ma.

The upper boundary of Unit II is marked by an increase of nannofossils. Unit II consists of light yellowish gray to light olive gray (10Y 7/1 to 5Y 6/2) nannofossil chalk gradationally interbedded with meter-scale intervals of grayish olive to light grayish olive (10Y 4/1 to 10Y 5/1) nannofossil clay. Nannofossil content decreases with depth. Sediments below ~260 mbsf are predominantly very dark gray to dark gray (5Y 3/1 to 5Y 4/1) claystone with or without minor nannofossils. As in Unit I, large pyrite nodules and concretions are distributed throughout the sediments. *Chondrites*, *Zoophycos*, and *Planolites* trace fossils are abundant throughout Unit II.

***Unit III***

Basement was reached at 278.9 mbsf and 5 cm of brecciated dark gray (N3) amygdaloidal basalt was recovered.

## Depositional History

The sedimentary sequence at Site 1020 consists of fine-grained siliciclastic clays with small to moderate amounts of siliceous and calcareous biogenic components. Initial deposition of clay-rich sediments on basaltic crust (lower Unit II) took place during the early Pliocene at lower middle bathyal water depths, which subsequently deepened to lower bathyal depths (see "Biostratigraphy" section, this chapter). During the late early Pliocene to early late Pliocene, nannofossils dominated sedimentation, which is similar to the pattern recorded at other sites drilled during this leg (Sites 1010 through 1014, 1016, and 1018). During the late Pliocene to early Quaternary, diatoms and siliciclastic clays dominated sedimentation. After ~1.2 Ma, fine-grained sedimentation alternated between nannofossil-rich and clay-rich intervals. Although turbidite deposition (identified as normally graded, coarse-grained sediments) is relatively unimportant at this site, sedimentation rates remain fairly high and constant throughout the Quaternary (see "Biostratigraphy" section, this chapter), suggesting increased input of siliciclastic material during this time.

## BIOSTRATIGRAPHY

The sedimentary sequence recovered from the four holes at Site 1020 consists of a well-dated, apparently continuous 279-m-thick interval of upper lower Pliocene to Quaternary sediments. A well-constrained biostratigraphy and chronology for all holes at Site 1020 is provided by a combination of calcareous nannofossil, planktonic foraminifer, radiolarian, and diatom datums and paleomagnetic reversals for the upper lower Pliocene and Quaternary. Calcareous nannofossils indicate that the base of Hole 1020B is 3.79 Ma in age. An age/depth plot for Hole 1020B (Fig. 6) suggests a slight upward increase in sedimentation rate beginning in the latest Pliocene (1.9 Ma).

Most of the sequence contains common radiolarians and mostly common to abundant diatoms. Diatoms and radiolarians are more abundant below the lowest Quaternary (>140 mbsf), except in the lower Pliocene below 255 mbsf where they are absent. Radiolarians are generally well preserved, and diatoms exhibit moderate to poor preservation throughout. Calcareous nannofossils are generally common and are moderately well preserved, except in sediments immediately overlying basement where they are absent. Planktonic foraminifers are generally common to abundant throughout and are mod-

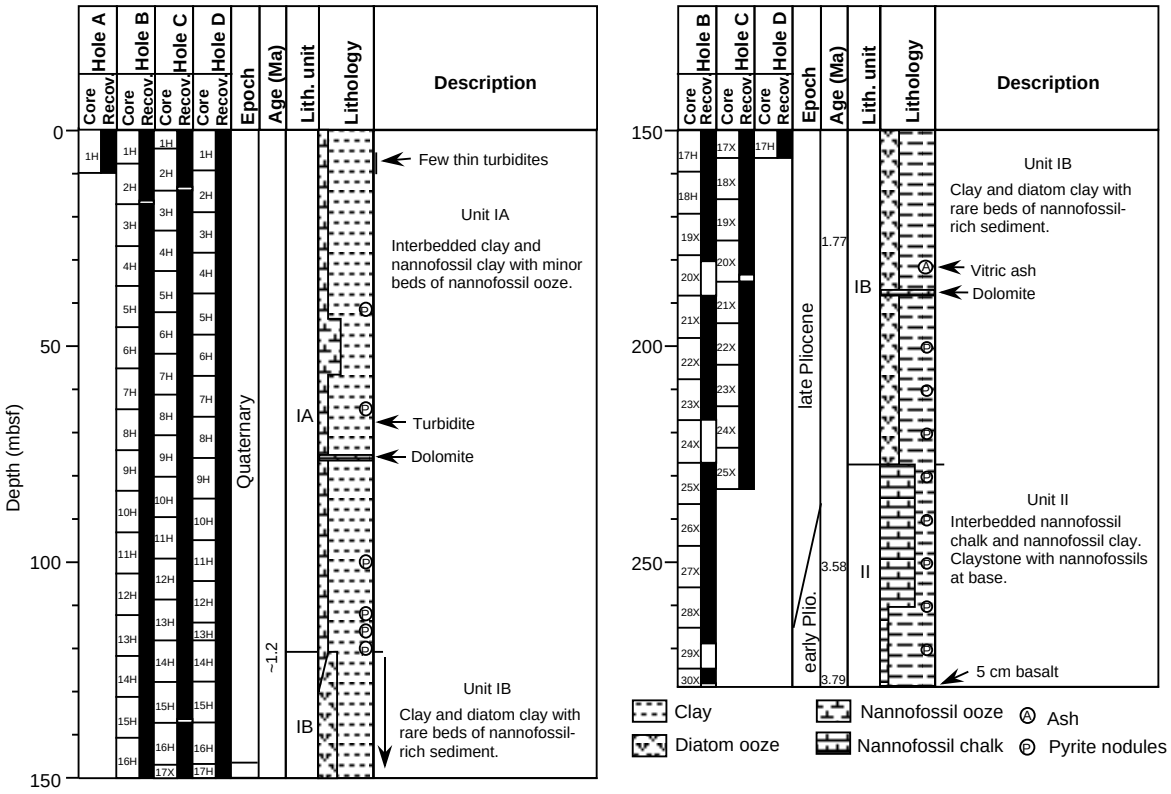


Figure 5. Site 1020 lithostratigraphic summary (0–278.8 mbsf).

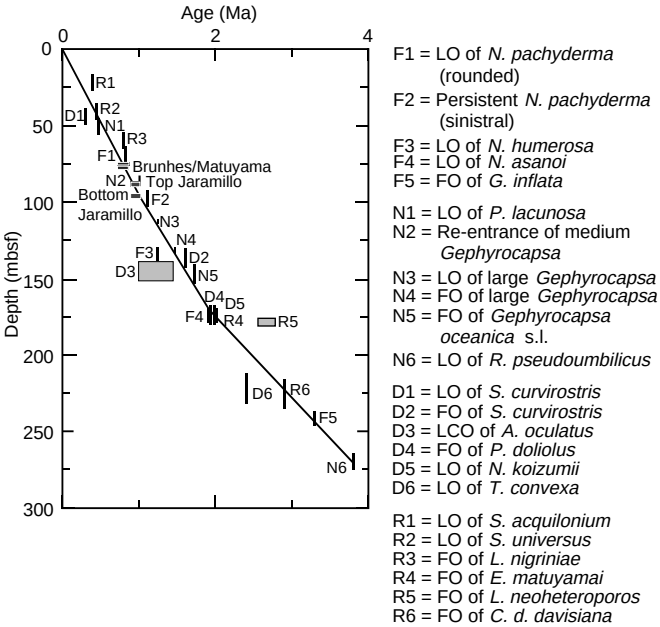


Figure 6. Age/depth plot for Hole 1020B.

erately to well preserved. Benthic foraminifers are essentially continuous in the section and especially well preserved in the Quaternary and uppermost Pliocene.

All of the microfossil groups at Site 1020 are clearly dominated by cool, high-latitude elements throughout the late Neogene. Radiolarians are entirely represented by subarctic forms and the assemblages exhibit noticeably lower diversity than at all other sites cored during Leg 167. Diatoms are dominated by North Pacific subarctic assemblages in addition to rare temperate elements. Discoasters are absent above the middle upper Pliocene (younger than 2.7 Ma) and rare when present. Relative high abundances of *Gephyrocapsa caribbeanica* may indicate cooler episodes within the Quaternary. Planktonic foraminifer assemblages are dominated by subarctic to cool temperate forms, with subtropical elements absent. Throughout the entire sequence, radiolarians are represented by forms not characteristic of upwelling regions. Likewise, diatoms are represented by open-ocean forms not characteristic of coastal upwelling regions, except during the early late Pliocene when upwelling forms are present in relatively low frequencies.

Planktonic foraminifer assemblages are made up entirely of cool temperate to subarctic taxa. The assemblages are distinctly cool throughout, and the diversity within the faunas is generally low. Distinct changes in planktonic foraminifer assemblages in the latest Pliocene and Quaternary (above ~170 mbsf) clearly reflect glacial to interglacial oscillations, whereas radiolarians do not. At greater depths in the section, short-term, climatically related faunal changes are much less conspicuous. During the Quaternary, interglacial planktonic foraminifer assemblages exhibit the effects of significant dissolution compared with assemblages of glacial episodes, which are well preserved.

Upper lower Pliocene planktonic foraminifers (~3.8 Ma) exhibit the highest diversity in the sequence and are considered to reflect the warmest surface-water temperatures. The first consistent occurrence of mostly common to abundant populations of sinistrally coiled *Neogloboquadrina pachyderma* marks a distinct cooling step at ~1.14 Ma.

Benthic foraminifers in the upper Pliocene and Quaternary are typical lower bathyal, deep-sea assemblages indicative of well-oxygenated bottom waters. The faunas exhibit little change throughout the entire upper Pliocene and Quaternary and exhibit no clear oscil-

lations associated with glacial/interglacial change, as reflected in the planktonic foraminifer assemblages. Well-oxygenated bottom waters bathed Site 1020 throughout the entire late Neogene. In the lowermost part of the section (~256 mbsf to basement depth of 279 mbsf) the benthic foraminifer assemblages may represent deposition in lower middle bathyal water depths as compared with lower bathyal depths in the sequence above. The changes in benthic foraminifer assemblages represent evidence for rapid tectonic subsidence in the lower ~30 m of the sequence at Site 1020. According to the scheme of Ingle (1967) the changes in benthic foraminifers would indicate subsidence of 500 to 1000 m during this interval. No evidence for paleodepth change is evident from benthic foraminifers above ~256 mbsf during the late early Pliocene through Quaternary.

## Planktonic Foraminifers

Site 1020 contains a moderately good and apparently continuous sequence of planktonic and benthic foraminifers of late early Pliocene (~3.8 Ma) through Quaternary age (Table 3). The base of Hole 1020B (Sample 167-1020B-29X-CC) is around the lower/upper Pliocene boundary, based on the FO of *Globorotalia inflata* in Sample 167-1020B-25X-CC, and within the uppermost part of the range zone of *Globigerina decoraperta*. Planktonic foraminifers are generally common to abundant throughout (Table 3) and are moderately to well preserved. A number of barren intervals occur in the sequence.

The planktonic foraminifer sequence at Site 1020 is similar to that found in the upper lower Pliocene through Quaternary of Site 1018 except that the bottom of the sequence is slightly older. In Hole 1020B we arbitrarily place the base of the Quaternary at 150 mbsf (between Samples 167-1020B-17H-CC and 16H-CC) between the LO of *Neogloboquadrina asanoi* and before the LO of *Neogloboquadrina humerosa*. We recognized a sequence of five datum levels in the Quaternary through upper Pliocene as follows: (1) the LO of *N. pachyderma* sp. (rounded form) at 0.8 Ma (Samples 167-1020B-8H-CC, 167-1020C-8H-CC, and 167-1020D-7H-CC); (2) the FCO of mostly abundant populations of sinistral *N. pachyderma* at 1.15 Ma (Samples 167-1020B-11H-CC and 167-1020C-11H-CC); (3) the LO of *N. humerosa* at 1.2 Ma (Samples 167-1020B-15H-CC and 167-1020C-15H-CC); (4) the LO of *N. asanoi* at 1.9 Ma (Samples 167-1020B-19X-CC and 167-1020C-19X-CC); and (5) the FO of *G. inflata* at 3.3 Ma (Samples 167-1020B-25X-CC and 167-1020C-23X-CC). The LO of *Neogloboquadrina* sp. (rounded) at 2.25 Ma was observed in Samples 167-1020B-25X-CC and 167-1020C-25X-CC. This is a useful datum in the late Pliocene in other Leg 167 sites, but not in Holes 1020B or 1020C because of barren intervals and coring gaps in the immediately overlying sequence (Table 3).

Planktonic foraminifer assemblages at Site 1020 are made up entirely of cool temperate to subarctic taxa. The assemblages are distinctly cool throughout, and the diversity within the faunas is generally low. Distinct changes in planktonic foraminifer assemblages in

**Table 3. Distribution and relative abundances of planktonic foraminifers in Hole 1020B.**

| Zone | Core, section, interval | Depth (mbsf) | Abundance | Preservation | *Globorotalia hirsuta* | *Globorotalia inflata* | *Globorotalia scitula* | *Globorotalia crassaformis* | *Globorotalia crassula* | *Globorotalia punticulata* | *Globorotalia decoraperta* | *Globorotalia* cf. *continuosa* | *Neogloboquadrina asanoi* | *Neogloboquadrina humerosa* | *Neogloboquadrina* sp. "rounded" | *Neogloboquadrina pachyderma* "rounded" | *Neogloboquadrina pachyderma* 5 chambers | *Neogloboquadrina pachyderma* dex. | *Neogloboquadrina pachyderma* sin. | *Globigerina bulloides* | *Globigerina umbilicata* | *Globigerina apertura* | *Globigerina quinqueloba* | *Globigerina falconensis* | *Globigerinita glutinata* | *Globorotaloides hexagona* | *Orbulina universa* |
|---|---|---|---|---|---|---|---|---|---|---|---|---|---|---|---|---|---|---|---|---|---|---|---|---|---|---|---|
| | 167-1020B- | | | | | | | | | | | | | | | | | | | | | | | | | | |
| | 1H-CC | 8 | A | G | | | C | | | | | | | | | | | | A | A | A | | A | | F | | |
| | 2H-CC | 17 | A | G | | | F | | | | | | | | | | | | A | A | A | | A | | | R | R |
| | 3H-CC | 27 | C | G | | | F | | | | | | | | | | | A | A | A | A | | | | F | | |
| | 4H-CC | 36 | C | G | | | R | | | | | | | | | | | | A | A | | | A | | | | |
| | 5H-CC | 46 | C | M | | | R | | | | | | | | | | | | A | A | | | | | | | R |
| | 6H-CC | 55 | A | G | | R | | | | | | | | | | | C | A | A | A | | | | | | | F |
| | 7H-CC | 65 | R | P | | | R | | | | | | | | | | | | R | R | | | | | R | | |
| N22/23 | 8H-CC | 74 | A | G | | | | | | | | | | | | A | C | | A | A | | | A | | | | |
| | 9H-CC | 84 | A | G | | | | | | | | | | | | A | | | A | A | | | C | | | | |
| | 10H-CC | 93 | A | G | | | | | | | | | | | | A | | | A | A | | | A | | | | |
| | 11H-CC | 102 | R | P | | | | | | | | | | | | R | | R | R | R | | | | | | | |
| | 12H-CC | 112 | R | P/M | | | | | | | | | | | | R | | R | | R | | | | | | | |
| | 13H-CC | 122 | B | | | | | | | | | | | | | | | | | | | | | | | | |
| | 14H-CC | 131 | C | M | | R | | | | | | | | | | C | | C | | C | | R | | | | | |
| | 15H-CC | 141 | R | M | | | | | | | | | | R | | F | | F | | C | | | | | | | |
| | 16H-CC | 150 | C | M | | F | | | | | | | | C | | C | | A | | A | | | C | | R | | |
| | 17H-CC | 160 | C | M | | | | | | | | | | | | C | | C | | A | | | | | | | F |
| | 18H-CC | 170 | C | M | | | | | | | | | | R | | C | | C | A | A | | | | | | | R |
| | 19X-CC | 179 | R | M | | | | | | | | | C | F | | | | R | | R | | | | | | | R |
| | 20X-CC | 189 | A | G | | | | | | | | | A | C | | | | A | | A | | | A | | | | |
| N21 | 21X-CC | 198 | A | G | | | | | | | | | A | F | | | | A | | A | | | | | | | |
| | 22X-CC | 208 | R | M | | | | | | R | | | R | | | | | | | R | | | | R | | | |
| | 23X-CC | 217 | B | | | | | | | | | | | | | | | | | | | | | | | | |
| | 24X-CC | 227 | NCC | | | | | | | | | | | | | | | | | | | | | | | | |
| | 25X-CC | 237 | C | M | | C | | | | | | | C | F | C | | | | | F | | R | R | | | | |
| | 26X-CC | 246 | F | M | R | | | | | | | | C | | A | | | | | A | | | | | | | F |
| | 27X-CC | 256 | B | | | | | | | | | | | | | | | | | | | | | | | | |
| N20 | 28X-CC | 265 | A | M | | | F | A | F | A | F | A | | C | | | | A | | A | | F | | | F | | C |
| | 29X-CC | 275 | A | M | | | | | | A | A | A | | | | | | | | A | | | | R | | | C |

Note: NCC = no core catcher. See "Explanatory Notes" chapter for abbreviations.

the latest Pliocene and Quaternary (above ~170 mbsf) clearly reflect glacial to interglacial oscillations. At greater depths in the section, short-term climatically related faunal changes are much less conspicuous. During the Quaternary, interglacial planktonic foraminifer assemblages exhibit evidence for significant dissolution compared with those of glacial episodes, which are well preserved.

Benthic foraminifers in the upper Pliocene and Quaternary (above Sample 167-1020B-28X-CC) are typical lower bathyal, deep-sea assemblages indicative of well-oxygenated bottom waters. Faunas above ~256 mbsf (Sample 167-1020-28X-CC) usually contain, in varying proportions, forms such as *Uvigerina proboscidea, U. juncea, Cibicidoides wuellerstorfi, Globobulimina affinis, Gyroidina soldani, Melonis pompilioides, Pyrgo murrhina, Oridorsalis umbonatus, Hoeglundina elegans, Chilostomella ovoidea, Pullenia bulloides,* and various nodosariids. The faunas exhibit little change throughout the entire upper Pliocene and Quaternary and exhibit no clear oscillations associated with glacial/interglacial change as reflected in the planktonic foraminifer assemblages. Well-oxygenated bottom waters bathed Site 1020 throughout the entire late Neogene. In the lowermost part of the section (~256 mbsf to basement depth of 279 mbsf), the benthic foraminifer assemblages distinctly differ from those above. Assemblages within this interval are dominated by nodosariids such as *Dentalina, Nodosaria,* and *Lenticulina,* and contain abundant *Stilostomella,* and *Melonis parkerae, Eggerella, Karreriella,* and different species of *Cibicidoides* and *Cassidulina.* This assemblage appears to represent deposition in lower middle bathyal water depths compared with lower bathyal depths in the sequence above. We suggest that the changes in benthic foraminifer assemblages represent evidence for rapid tectonic subsidence in the lower ~30 mbsf of the sequence at Site 1020. According to the scheme of Ingle (1967), the changes in benthic foraminifers would indicate subsidence of 500 to 1000 m. No evidence for paleodepth change is inferred from benthic foraminifers above ~256 mbsf during the late early Pliocene through Quaternary.

## Calcareous Nannofossils

Calcareous nannofossils are generally common and moderately well preserved through the Quaternary and upper lower Pliocene in Holes 1020B, 1020C, and 1020D (Table 4). Discoasters in the upper upper Pliocene are rare or absent, because of the cooler conditions at this higher latitude location. Below this interval (~2.7 Ma), they are few. The higher relative abundance of *Gephyrocapsa caribbeanica* in some samples may be associated with cooler conditions. Hole 1020B spans the early Pliocene Zone CN11 to the late Pleistocene Zone CN15. Hole 1020C is dated from the late Pliocene Zone CN12 to the late Pleistocene Zone CN15. Hole 1020D spans from the latest Pliocene Zone CN13a to the late Pleistocene Zone CN15-CN14b. Datums recognized within the Quaternary are the LO of *P. lacunosa,* the FO and the LO of large *Gephyrocapsa,* and the LO of *Gephyrocapsa oceanica* s.l. In the Quaternary, calcareous nannofossil assemblages are marked by the presence of *Emiliania huxleyi, Pseudoemiliania lacunosa, Calcidiscus leptoporus, Helicosphaera carteri, H. sellii,* and several morphotypes of *Gephyrocapsa* spp.

The FO of *G. oceanica* s.l. places the Pliocene/Pleistocene boundary at 140.8 mbsf (Sample 167-1020B-15H-CC) in Hole 1020B, at 146.8 mbsf (Sample 167-1020C-16H-CC) in Hole 1020C, and at 146.7 mbsf (Sample 167-1020D-16H-CC) in Hole 1020D. The lower/upper Pliocene boundary is placed at 265 mbsf (Sample 167-1020-29X-CC) by the LO of *Reticulofenestra pseudoumbilicus,* which marks the base of Zone CN12a. Pliocene nannofossil assemblages are marked by an association of *Helicosphaera carteri, H. sellii, Discoaster tamalis, D. pentaradiatus, D. surculus, Reticulofenestra pseudoumbilicus, Ceratolithus* spp., and several morphotypes of *Reticulofenestra.*

## Diatoms

Except for a barren interval immediately above basaltic basement, all samples from Site 1020 were readily placed within the subarctic diatom zonation of the North Pacific (Tables 5, 6). Sparse occurrences of temperate taxa, such as *Hemidiscus cuneiformis, Nitzschia reinholdii, N. marina,* and *Thalassiosira convexa,* indicate the influence of temperate water masses from the south during the late Pliocene through early Quaternary.

In spite of the location of Site 1020 in relatively deep water (>3000 m depth), diatom assemblages in the sequence above 140 mbsf are not typical of hemipelagic environments, but show considerable resemblance to the assemblages encountered at nearshore Site 1019. Diatoms are few to common and poorly to moderately well preserved throughout the late Quaternary section recovered at Site 1020. Abundant clay diluted the diatoms, and almost all are strongly etched and fragmented by dissolution, except for robust forms of *Stephanophyxis turris.* In contrast, the early Quaternary through late Pliocene interval below 140 mbsf is diatomaceous, and diatoms in this interval are common to abundant and generally moderately to well preserved.

The boundary between the late Quaternary *Neodenticula seminae* and *Simonseniella curvirostris* Zones (NPD 12/11) is indicated by the LO of *S. curvirostris* in Samples 167-1020B-5H-CC and 167-1020C-6H-CC, respectively. The LCO of *Actinocyclus oculatus* in Samples 167-1020B-16H-CC and 167-1020C-15H-CC marks the boundary between the *S. curvirostris* and *A. oculatus* Zones (NPD 11/10) in these holes. This boundary is estimated to be between 1.00 and 1.44 Ma in the subarctic region. The FO of *S. curvirostris* with an age of 1.58 Ma is recognized between Samples 167-1020B-14H-CC and 15H-CC.

The normal-polarity Jaramillo Subchron (0.99 to 1.07 Ma) at about 89 to 98 mbsf in Hole 1020B supports an age older than 1 Ma for the LCO of *A. oculatus* at Site 1020. Koizumi (1992) proposed that the LO of *Neodenticula koizumii* clearly defines the base of the *A. oculatus* Zone (NPD 10) and top of the underlying *N. koizumii* Zone (NPD 9). This latest Pliocene event at approximately 2.0 Ma falls between Samples 167-1020B-18H-CC and 19X-CC, and between Samples 167-1020C-19X-CC and 20X-CC, respectively. The occurrence of *Pseudoeunotia doliolus* in Samples 167-1020B-18H-CC and 167-1020C-19X-CC supports the recognition of the NPD 10/9 boundary, because the FO of that species has an estimated age of 1.9 Ma in the eastern equatorial Pacific (Baldauf and Iwai, 1995). Continuous common occurrences of *Neodenticula kamtschatica,* which verify the underlying *N. koizumii-N. kamtschatica* Zone (NPD 8), were not found at Site 1020.

## Radiolarians

Most of the sequence contains radiolarians except in the early Pliocene below 255 mbsf where they are absent. They are common to abundant and well preserved in the upper Pliocene and the upper Quaternary. They are rare and poorly preserved in the early Quaternary (Table 7). For this reason, the Pliocene/Quaternary boundary could not be placed. The FO of *Cycladophora davisiana* between 217.3 and 236.6 mbsf in Hole 1020B and between 223.5 and 233.2 mbsf in Hole 1020C gives an age of 2.9 Ma to the oldest radiolarian assemblages. The main radiolarian events are summarized in Table 8.

All assemblages are indicative of cold subarctic conditions and diversity is lower than in previous sites. Species characteristic of upwelling conditions are very rare, suggesting that vertical advection of deep waters was weak at this site during most of the upper Pliocene and Quaternary. Representatives of the *Lamprocyrtis heteroporos – L. neoheteroporos – L. nigriniae* are, thus, exceptionally rare, and the transition from *L. heteroporos* to *L. neoheteroporos* is not a reliable event at this site (Fig. 6).

**Table 4. Distribution and relative abundances of calcareous nannofossils in Holes 1020A, 1020B, 1020C, and 1020D.**

| Zone | Core, section, interval (cm)) | Depth (mbsf) | Preservation | Abundance | *Emiliania huxleyi* | *Pseudoemiliania lacunosa* | *Helicosphaera carteri* | *Helicosphaera sellii* | *Gephyrocapsa oceanica* s.l. | *Gephyrocapsa caribbeanica* | *Gephyrocapsa* small | *Gephyrocapsa* large | *Discoaster brouweri* | *Discoaster triradiatus* | *Discoaster pentaradiatus* | *Discoaster surculus* | *Discoaster tamalis* | *Discoaster asymmetricus* | *Reticulofenestra pseudoumbilicus* | *Amaurolithus* spp. | *Coccolithus pelagicus* | *Calcidiscus macintyrei* >11 µm | *Calcidiscus leptoporus* | *Braarudosphaera* spp. |
|---|---|---|---|---|---|---|---|---|---|---|---|---|---|---|---|---|---|---|---|---|---|---|---|---|
| CN15 | 167-1020A-<br>1H-CC | 10.0 | G | F/C | P | | | | P | | | | | | | | | | | | F | | | |
| CN15 | 167-1020B-<br>1H-CC | 7.8 | G | F/C | P | | | | P | | | | | | | | | | | | F | | | |
| CN15–CN14b | 2H-CC | 17.3 | G | A | | | R | | C | | A | | | | | | | | | | | | | R |
| CN15–CN14b | 3H-CC | 26.8 | M/P | F | | | | | C | | P | | | | | | | | | | C | | | |
| CN15–CN14b | 4H-CC | 36.3 | M | F/C | | | | | R/F | P | A | | | | | | | | | | F | | | |
| CN14a? | 5H-CC | 45.8 | M | R | | R | | | R/F | P | C | | | | | | | | | | | | | |
| CN14a–CN13b | 6H-CC | 55.3 | G | A | | C | | | R | | A | | | | | | | | | | | | R | |
| | 7H-CC | 64.8 | | B | | | | | | | | | | | | | | | | | | | | |
| CN14a–CN13b | 8H-CC | 74.3 | M | F/C | | P | | | | | A | | | | | | | | | | R | | | |
| CN14a–CN13b | 9H-CC | 83.8 | G | F/C | | | | | RR | | A | | | | | | | | | | R | | | |
| | 10H-CC | 93.3 | P | RR | | | | | | | R | | | | | | | | | | | | F | |
| | 11H-CC | 101.8 | P | RR | | R | | | | | | | | | | | | | | | | | | |
| | 12H-CC | 112.3 | P | RR | | P | | | | | | | | | | | | | | | P | | | |
| CN13b | 13H-3, 20 | 115.5 | M/G | C | | C | | C | A | C | | R | | | | | | | | | | | R | R |
| CN13b | 13H-5, 21 | 118.5 | M | F/C | | C | | | C | C | | P | | | | | | | | | F | | F | |
| CN13b | 13H-CC | 121.8 | P/M | F | | C | | | R | C | | | | | | | | | | | R | | R/F | |
| CN13b | 14H-3, 20 | 125.0 | P/M | C | | R | | | C | C | P | | | | | | | | | | | | P | |
| CN13b | 14H-5, 20 | 128.0 | P/M | F | | | | | P | C | | | | | | | | | | | P | | R | |
| CN13b | 14H-CC | 131.3 | P/M | A | | | | R | C | | | RR | | | | | | | | | P | | P | |
| CN13b | 15H-3, 21 | 134.5 | P/M | C | | C | | | P | C | C | | | | | | | | | | | | R | |
| CN13b | 15H-5, 21 | 137.5 | M | F/C | | R | | | P | C | | | | | | | | | | | | | R | |
| CN13b | 15H-CC | 140.8 | P | R | | | | | R | P | | | | | | | | | | | | | P | |
| CN13a–CN12 | 16H-CC | 150.3 | P/M | A | | A | | | | | | | | | | | | | | | C | | F | |
| CN13a–CN12 | 17H-CC | 159.8 | P | R | | P | | P | | | | | | | | | | | | | | | R | P |
| CN13a–CN12 | 18H-CC | 169.3 | P/M | C | | C | | R/F | | | P | | | | | | | | | | C | | C | |
| CN13a–CN12 | 19X-CC | 178.9 | P/M | F | | C | R | C/F | | | | | | | | | | | | | C | | | |
| CN13a–CN12 | 20X-CC | 188.5 | P/M | C/A | | | | P | | | | | | | | | | | | | C | | C | |
| CN13a–CN12 | 21X-CC | 198.5 | P | R/F | | | | | | | | | | | | | | | | | P | | P | |
| | 22X-CC | 207.7 | | B | | | | | | | | | | | | | | | | | | | | |
| | 23X-CC | 217.3 | | B | | | | | | | | | | | | | | | | | | | | |
| CN12a | 25X-CC | 236.6 | G | A | | | | | | | | | | | R | P | R | R | | | F | | P | |
| CN12a | 26X-CC | 246.2 | G | A | | | | | | | | | | | R | R | R | | | | | R | C | |
| CN12a | 27X-CC | 255.9 | P | C/A | | R | | | | | | | | | | R | | | | | F | | R | |
| CN12a | 28X-CC | 265.3 | G | A | | | | F | | | | | R | | | F | | | | | C | R/F | C | |
| CN11 | 29X-CC | 274.7 | M | C/A | | | | R/F | | | | | | | F | R | | | F | RR | | C | F | |
| CN15 | 167-1020C-<br>1H-CC | 4.3 | M/G | F/C | P | | | | P | | C | | | | | | | | | | F | | | |
| CN15? | 2H-CC | 13.8 | M | R | P | | | | | | P | | | | | | | | | | | | RR | |
| CN15–CN14b | 3H-CC | 23.3 | P | RR | | | | | | | P | | | | | | | | | | | | | |
| CN15–CN14b | 4H-CC | 32.8 | M | F | | | F/C | | C | P | P | | | | | | | | | | C | | | |
| CN15–CN14b | 5H-CC | 42.3 | G | A | | | | | C | P | A | | | | | | | | | | C | | | |
| CN15–CN14b | 6H-CC | 51.8 | G | A | | | | | P | | A | | | | | | | | | | F | | | |
| CN14a? | 7H-CC | 61.3 | G | A | | RR | | | R | | A | | | | | | | | | | C | | | |
| | 8H-CC | 70.8 | | B | | | | | | | | | | | | | | | | | | | | |
| CN14a | 9H-CC | 80.3 | P | RR | | R | | | | | R | | | | | | | | | | | | R | |
| | 10H-CC | 89.8 | | B | | | | | | | | | | | | | | | | | | | | |
| | 11H-CC | 99.3 | | B | | | | | | | | | | | | | | | | | | | | |
| CN14a–CN13b | 12H-CC | 108.8 | M/G | C | | F | | | | | A | | | | | | | | | | | | R/F | |
| CN13b | 13H-CC | 118.3 | G | C/A | | C | | | P | C | P | P | | | | | | | | | C | | R | |
| CN13b | 14H-CC | 127.8 | P | RR | | | | | R | P | | RR | | | | | | | | | | | | |
| CN13b | 15H-CC | 137.3 | P | RR | | | | | R | P | R | | | | | | | | | | | | | |
| CN13b | 16H-CC | 146.8 | P/M | R | | | | | R | P | P | | | | | | | | | | F | | P | |
| | 17X-CC | 156.3 | P | RR | | | | R | | | R | | | | | | | | | | R | | R | |
| | 18X-CC | 165.9 | | B | | | | | | | | | | | | | | | | | | | | |
| CN13a–CN12 | 19X-CC | 175.5 | P/M | F | | P | | R | | | | | | | | | | | | | R | | F | |
| CN13a–CN12 | 20X-CC | 185.1 | G | C/A | | C | | | | | | | | | | | | | | | F | P | R/F | |
| CN13a–CN12 | 21X-CC | 194.7 | P | RR | | R | | R | | | | | | | | | | | | | | | | |
| | 22X-CC | 204.3 | | B | | | | | | | | | | | | | | | | | | | | |
| CN13a–CN12 | 23X-CC | 213.9 | M | F | | R | | | | | | | | | | | | | | | R | | R | |
| CN12a–CN12b | 24X-CC | 223.5 | P | RR | | | | | | | | | | | | R | | | | | R | | | |
| CN12a–CN12b | 25X-CC | 233.2 | G | A | | C | | | | | | | | | R | P | | | | | | | R | |
| CN15–CN14b | 167-1020D-<br>1H-CC | 9.4 | G | A | | | | | F/C | | A | | | | | | | | | | R | | | |
| CN15–CN14b | 2H-CC | 18.9 | P | R | | | | | | | P | | | | | | | | | | R | | | |
| | 3H-CC | 28.4 | | B | | | | | | | | | | | | | | | | | | | | |
| CN15–CN14b | 4H-CC | 37.9 | P | R | | | | | | | P | | | | | | | | | | | | | |
| CN14a | 5H-CC | 47.4 | G | A | | C | | | P | | A | | | | | | | | | | | | R | |
| CN14a | 6H-CC | 56.9 | M | F/C | | RR | | | | | A | | | | | | | | | | | | | |
| | 7H-CC | 66.4 | | B | | | | | | | | | | | | | | | | | | | | |
| CN14a | 8H-CC | 75.9 | M/G | A | | RR | R | | R | | A | | | | | | | | | | C | | R | P |
| CN14a–CN13b | 9H-CC | 85.4 | G | A | | R | | | | | A | | | | | | | | | | F | | R/F | |
| CN14a–CN13b | 10H-CC | 94.9 | P | RR | | | | | | | P | | | | | | | | | | | | | |
| CN14a–CN13b | 11H-CC | 104.4 | M | R/F | | | | | | | P | | | | | | | | | | R | | | |
| | 12H-CC | 113.9 | P | RR | | R | | | | | | | | | | | | | | | | | R | |

**Table 4 (continued).**

| Zone | Core, section, interval (cm)) | Depth (mbsf) | Preservation | Abundance | *Emiliania huxleyi* | *Pseudoemiliania lacunosa* | *Helicosphaera carteri* | *Helicosphaera sellii* | *Gephyrocapsa oceanica* s.l. | *Gephyrocapsa caribbeanica* | *Gephyrocapsa* small | *Gephyrocapsa* large | *Discoaster brouweri* | *Discoaster triradiatus* | *Discoaster pentaradiatus* | *Discoaster surculus* | *Discoaster tamalis* | *Discoaster asymmetricus* | *Reticulofenestra pseudoumbilicus* | *Amaurolithus* spp. | *Coccolithus pelagicus* | *Calcidiscus macintyrei* >11 µm | *Calcidiscus leptoporus* | *Braarudosphaera* spp. |
|---|---|---|---|---|---|---|---|---|---|---|---|---|---|---|---|---|---|---|---|---|---|---|---|---|
| CN13b | 13H-CC | 118.2 | P/M | R/F | | P | | | P | P | | R | | | | | | | | | | | R | |
| CN13b | 14H-CC | 127.7 | M | R/F | | R | | | R | P | | R | | | | | | | | | | | | |
| CN13b | 15H-CC | 137.2 | P/M | RR | | R | | | R | P | | | | | | | | | | | | | R | |
| CN13b | 16H-CC | 146.7 | M | F | | P | | | P | | | | | | | | | | | | | | R | |
| CN13a? | 17H-CC | 156.2 | P/M | R | | R | | | | | P | | | | | | | | | | F | | F | |

## PALEOMAGNETISM

We made magnetic measurements with the pass-through cryogenic magnetometer on the archive halves of 18 APC cores from Hole 1020B. After measuring the natural remanent magnetization (NRM), the sections were demagnetized with a peak alternating field (AF) of 20 mT. At Hole 1020C, the working halves of the top 13 APC cores were measured after demagnetization at 20 mT without measurement of the NRM. At both holes, the intensity of NRM fluctuates strongly in the upper 50 mbsf (Figs. 7, 8), depending on the amount of magnetic minerals in the sediment. A similar variation with depth was observed for the magnetic susceptibility of these cores (see "Physical Properties" section, this chapter). Between 50 and 100 mbsf the NRM intensity varies little around 10 mA/m, and the intensity and direction after AF demagnetization can be determined reliably in this interval for both holes.

The positive inclinations above 78 mbsf in Holes 1020B and 1020C represent Chron C1n (Brunhes). The Brunhes/Matuyama (B/M) transition is not as clearly defined in Hole 1020B (Fig. 7) as it is in Hole 1020C (Fig. 8), where it occurs over a short interval at 78 mbsf. Assuming an age of 0.78 Ma for the B/M transition gives a sedimentation rate of exactly 100 m/m.y. The reversed polarity interval of Subchron C1r.1r is easily identified, based on the negative inclination between 79 and 89 mbsf in Hole 1020B. In the inclination record from Hole 1020C, this reversed polarity interval is not as well represented because of the core disturbance at the top of Core 167-1020C-10H and the very low intensity of magnetization around 83 mbsf. The top and bottom boundaries of Subchron C1r.1n (Jaramillo) are resolved in detail in Holes 1020B and 1020C.

After orientation of the APC cores with the Tensor tool, the corrected declinations of Cores 167-1020B-3H to 11H and Cores 167-1021C-3H to 12H (open circles in Figs. 7, 8) are distributed around 30° in the normal polarity intervals and around 220° in the reversed polarity intervals. The declination data support the interpretation of magnetic polarity zonation based on the inclination data. Our assignments of the magnetostratigraphic datums (Table 9) are consistent with biostratigraphic data from Hole 1020B (see "Biostratigraphy" section, this chapter). The considerable offset of the corrected declinations from the geographic north-south direction (Dec = 0°) by about 40° and more could be caused by a clockwise rotation of the Gorda Plate. This speculation must be substantiated by comparison with stable directions from stepwise demagnetized single samples. A more likely explanation for the offset could be a directional bias in the Tensor tool measurement.

As shown in the enlarged section of the declination and inclination records from Hole 1020C (Fig. 9), the inclination change at the top and bottom of the Jaramillo magnetozone occurs approximately over a 2-m interval. The 8-m depth extent of the Jaramillo magnetozone translates into a 20 k.y. duration for the inclination change during each of the two reversals, which is substantially longer than the 2 k.y. reported for the B/M transition (Kent and Schneider, 1995). Stepwise AF demagnetization of single samples and of U-channels across the reversals will show whether the long duration of the reversal is caused by insufficient removal of a normal magnetic overprint. The high-resolution reversal records represent an excellent opportunity to study the behavior of the Earth's magnetic field during a transition.

The remanent magnetization after AF treatment falls below the sensitivity limit of the magnetometer in the interval from 100 to 130 mbsf (Figs. 7, 8). The higher but rapidly varying intensity below 130 mbsf does not permit an interpretation of the inclination record. The high intensities occur at intervals of 1 to 2 m in Cores 167-1020B-15H to 18H, corresponding to spikes of the whole-core susceptibility data (Fig. 10; see "Physical Properties" section, this chapter). These intervals of high intensity of magnetization probably correspond to diagenetic formation of iron sulfide associated with pyrite nodules in diatom clay of the lithostratigraphic Subunit IB (see "Lithostratigraphy" section, this chapter).

## COMPOSITE DEPTHS AND SEDIMENTATION RATES

Multisensor track (MST) data collected at 4-cm intervals from Holes 1020A through 1020D and color reflectance data collected at 6-cm intervals from Holes 1020B, 1020C, and 1020D were used to determine depth offsets in the composite section. On the composite depth scale (expressed as mcd, meters composite depth), features of the plotted MST and color reflectance data present in adjacent holes are aligned so that they occur at approximately the same depth. Working from the top of the sedimentary sequence, a constant was added to the mbsf (meters below sea floor) depth for each core in each hole to arrive at a mcd depth for that core. The depths offsets that compose the composite depth section are given in Table 10, also on CD-ROM, back pocket. The continuity of the sedimentary sequence was documented for the upper 126 mcd. Between 126 and 242 mcd, there is continuity of the sedimentary sequence with the exception of core gaps at 137 and 200 mcd.

Color reflectance, magnetic susceptibility, and GRAPE density measurement were the primary parameters used for interhole correlation purposes. Natural gamma-ray activity measurements were made throughout the entire section in Holes 1020A, 1020B, 1020C, and 1020D, but the sampling interval of 12 cm was insufficient for interhole correlation.

The color reflectance, magnetic susceptibility, and GRAPE records used to verify core overlap for Site 1020 are shown on a composite depth scale in Figures 11, 12, and 13, respectively. The GRAPE data were used to identify intervals of voids and highly disturbed sediments (values less than 1.50 g/cm$^3$), and all MST and color

**Table 5. Distribution and relative abundances of diatoms in Hole 1020B.**

| Geologic age | North Pacific diatom zone | Numeric age (Ma) | Core, section, interval | Sample depth (mbsf) | Abundance | Preservation | Environment | *Actinocyclus curvatulus* | *Actinocyclus oculatus* | *Actinocyclus* cf. *oculatus* | *Actinoptychus senarius* | *Aulacosira granulata* | *Biddulphia aurita* | *Cocconeis costata* | *Cocconeis* sp. | *Coscinodiscus marginatus* | *Coscinodiscus radiatus* | *Denticulopsis lauta* s.l. | *Gomphonema* sp. | *Grammatophora* sp. | *Hemidiscus cuneiformis* | *Neodenticula kamtschatica* | *Neodenticula koizumii* | *Neodenticula* cf. *koizumii* | *Neodenticula seminae* | *Neodenticula seminae* (sensu Akiba) | *Nitzschia marina* | *Nitzschia reinholdii* | *Paralia sulcata* | *Pseudoeunotia doliolus* | *Rhaphoneis* sp. | *Rhizosolenia barboi* | *Simonseniella (Rhizosolenia) curvirostris* | *Simonseniella (R.)* cf. *curvirostris* | *Stephanopyxis turris* |
|---|---|---|---|---|---|---|---|---|---|---|---|---|---|---|---|---|---|---|---|---|---|---|---|---|---|---|---|---|---|---|---|---|---|---|---|
| | | | 167-1020B- | | | | | | | | | | | | | | | | | | | | | | | | | | | | | | | | |
| | | | 1H-CC | 7.8 | F | P | | F | | | R | | | | R | | | | | | | | | | | | | | | | R | | | | A |
| | NPD 12 | | 2H-CC | 17.3 | R | P | | | | | R | | | | | | | | | | | | | | | | | | R | | | | | | F |
| | | | 3H-CC | 26.8 | T | P | | | | | | | | | | | | | | | | | | R | | | | | | | | | | | F |
| | | | 4H-CC | 36.3 | T | P | | | | | | | | | | | | | | | | | | P | | | | | | | | | | | |
| | | 0.30 | 5H-CC | 45.8 | F | P/M | | | | | | | | | | | | | | | | | | F | | | | | | | R | | F | | F |
| | | | 6H-CC | 55.3 | T | P | | | | | | | | | | | | T | | | | | | R | | | | | | | | T | | | R |
| | | | 7H-CC | 64.8 | C | P/M | | | | | | | | | | | | | T | R | | | | T | | | | | | | | T | | | C |
| | | | 8H-CC | 74.3 | F | P/M | Coastal | | | | R | R | | R | | | R | | | | | | R | | | | | | | | | | | | C |
| Quaternary | NPD 11 | | 9H-CC | 83.8 | F | P | | | | | F | R | | | | R | | | | | | | R | | | | | | | | | | | | C |
| | | | 10H-CC | 93.3 | C | P/M | | R | | | | | R | | | | | | | | | | | R | | | | | | | | | | R | | C |
| | | | 11H-CC | 101.8 | F | P | | | | | | | | | | | | | | R | | | | R | | | | | | | | | | R | | F |
| | | | 12H-CC | 112.3 | C | P/M | | | | | | | | | | | | | | | | | | R | | | | | | | | | R | R | | C |
| | | | 13H-CC | 121.8 | T | P | | | | | | | | | | | | | | | | | | T | | | | | | | | | | | | |
| | | | 14H-CC | 131.3 | R | P | | | | R | | | | | | | | | | | | | | F | | | | | | | | | | R | | R |
| | | 1.58 | 15H-CC | 140.8 | A | P/M | | F | | | | | | | | | F | | | | | | | F | | | | R | | | | | | P | C |
| | | | 16H-CC | 150.3 | A | M | | R | R | | | | | | | | | | | | F | | | F | F | R | | | | | R | | | | C |
| | NPD 10 | | 17H-CC | 159.8 | F | P/M | | | R | | | | | | | R | | | | | R | | R | | R | | R | | | | R | | R | | |
| | | 1.90 | 18H-CC | 169.3 | C | P/M | | R | R | | | | | | | R | R | | | | | | | R | R | | R | | | R | R | | | | |
| | | 2.00 | 19X-CC | 178.9 | A | M | | R | | | | | | | | C | | | | | | | R | F | F | | R | | | | A | | | | |
| Pliocene | | | 20X-CC | 181.5 | C | P/M | | | R | | | | | | | | | | | | R | | | F | R | | | | | | C | | | | F |
| | NPD 9 | | 21X-CC | 198.1 | A | P/M | Upwelling | F | R | | | | | | | | | | | | | | R | | | | | | | | A | | | | A |
| | | | 22X-CC | 207.7 | A | M/G | Upwelling | R | | | | | | | | C | | | | | | | F | | R | | | | | | C | | | | A |
| | | | 23X-CC | 217.3 | C | P/M | | | R | | | | | | | C | | | | | | R | R | | | | | | | | C | | | | F |
| | | 2.40 | 25X-CC | 236.6 | A | M | Upwelling | | | | | | | | | C | | | | | | | R | | R | | | | | | A | | | | F |
| | | | 26X-CC | 246.2 | R | P | | | | | | | | | | C | | R | | | | | | | | | | | | | | F | | | | |
| | Barren | | 27X-CC | 255.9 | B | | | | | | | | | | | | | | | | | | | | | | | | | | | | | | |
| | | | 28X-CC | 265.3 | B | | | | | | | | | | | | | | | | | | | | | | | | | | | | | | |
| | | | 29X-CC | 274.7 | B | | | | | | | | | | | | | | | | | | | | | | | | | | | | | | |

Note: See “Explanatory Notes” chapter for abbreviations.

**Table 5 (continued).**

| Geologic age | North Pacific diatom zone | Numeric age (Ma) | Core, section, interval | Sample depth (mbsf) | Abundance | Preservation | Environment | *Simonseniella (R.)* cf. *curvirostris* | *Stephanopyxis turris* | *Stephanopyxis* sp. | *Synedra* sp. | *Thalassionema nitzschioides* | *Thalassiosira antiqua* | *Thalassiosira convexa* | *Thalassiosira eccentrica* | *Thalassiosira oestrupii* | *Thalassiosira* sp. | *Thalassiosira* spp. (*nativa* type) | *Thalassiothrix longissima* | *Thalassiothrix* spp. | Diatom fragments (girdle bands) | Diatom fragments | Resting spores |
|---|---|---|---|---|---|---|---|---|---|---|---|---|---|---|---|---|---|---|---|---|---|---|---|
| Quaternary | NPD 12 | 0.30 | 167-1020B- | | | | | | | | | | | | | | | | | | | | |
| | | | 1H-CC | 7.8 | F | P | | | A | | | R | | | | | | R | R | | | | |
| | | | 2H-CC | 17.3 | R | P | | | F | | | | | | | | | R | R | | | | |
| | | | 3H-CC | 26.8 | T | P | | | F | | R | | | | | | R | | | | | | |
| | | | 4H-CC | 36.3 | T | P | | | | P | | | | | | | | | P | | | | |
| | | | 5H-CC | 45.8 | F | P/M | | | F | | | R | | | | | | | | | | | |
| | NPD 11 | | 6H-CC | 55.3 | T | P | | | R | | | | | | | | | | T | | | | |
| | | | 7H-CC | 64.8 | C | P/M | | | C | | | | | | F | | T | | | | | | R |
| | | | 8H-CC | 74.3 | F | P/M | Coastal | | C | | | | | | R | | | R | | | | | |
| | | | 9H-CC | 83.8 | F | P | | | C | | | | | | | | | R | | | | | |
| | | | 10H-CC | 93.3 | C | P/M | | | C | | | | | | | | | | F | | | | |
| | | 1.58 | 11H-CC | 101.8 | F | P | | | F | | | | | | | | | | | | F | | |
| | | | 12H-CC | 112.3 | C | P/M | | | C | | | | | | | | | | R | | | | |
| | | | 13H-CC | 121.8 | T | P | | | | | | | | | | | | | | | | R | |
| | | | 14H-CC | 131.3 | R | P | | | R | | | | | | | | | | | | | | |
| | | | 15H-CC | 140.8 | A | P/M | | P | C | | | | | | | | | | F | A | | | |
| | NPD 10 | 1.90 | 16H-CC | 150.3 | A | M | | | C | | | | | | | | | | R | A | | | |
| | | | 17H-CC | 159.8 | F | P/M | | R | | | | R | | | | | | | R | | | | |
| | | | 18H-CC | 169.3 | C | P/M | | | | | | R | | | | | | | | | | | |
| | | 2.00 | 19X-CC | 178.9 | A | M | | | | | | | R | | | R | | | | C | | | |
| | | | 20X-CC | 181.5 | C | P/M | | | F | | | | | | | | | | | | | | |
| Pliocene | NPD 9 | 2.40 | 21X-CC | 198.1 | A | P/M | Upwelling | | A | | | R | | | | | | | | A | | | |
| | | | 22X-CC | 207.7 | A | M/G | Upwelling | | A | | | | | | | | | | F | A | | | |
| | | | 23X-CC | 217.3 | C | P/M | | | F | | | | | | | | | | R | | | | |
| | | | 25X-CC | 236.6 | A | M | Upwelling | | F | | | | | F | | | | | R | | | | |
| | | | 26X-CC | 246.2 | R | P | | | | | | | | F | | | | | | | | | |
| | Barren | | 27X-CC | 255.9 | B | | | | | | | | | | | | | | | | | | |
| | | | 28X-CC | 265.3 | B | | | | | | | | | | | | | | | | | | |
| | | | 29X-CC | 274.7 | B | | | | | | | | | | | | | | | | | | |

**Table 6. Distribution and relative abundances of diatoms in Hole 1020C.**

| Geologic age | North Pacific diatom zone | Depth (mbsf) | Numeric age (Ma) | Core, section, interval | Abundance | Preservation | Comments | *Actinocyclus curvatulus* | *Actinocyclus* cf. *curvatulus* | *Actinocyclus oculatus* | *Actinocyclus* cf. *oculatus* | *Actinoptychus senarius* | *Aulacosira granulata* | *Aulacosira* cf. *italica* | *Biddulphia aurita* | *Cocconeis scutellum* | *Coscinodiscus marginatus* | *Coscinodiscus radiatus* | *Cymbella* sp. | *Grammatophora* sp. | *Hemidiscus cuneiformis* | *Neodenticula kamtschatica* | *Neodenticula koizumii* | *Neodenticula* cf. *koizumii* | *Neodenticula seminae* | *Neodenticula seminae* (sensu Akiba) | *Nitzschia marina* | *Nitzschia reinholdii* | *Paralia sulcata* | *Pseudoeunotia doliolus* |
|---|---|---|---|---|---|---|---|---|---|---|---|---|---|---|---|---|---|---|---|---|---|---|---|---|---|---|---|---|---|
| | | | 167-1020C- | | | | | | | | | | | | | | | | | | | | | | | | | | |
| | | | 1H-CC | 4.3 | R | P/M | | T | | | | | T | | | | T | T | | | | | | | T | | | | | T |
| | | | 2H-CC | 13.8 | T | P | Clay | | | | | | | | | | | | | | | | | | | | | | | |
| | NPD 12 | | 3H-CC | 23.3 | T | P | Clay + silt | | | | | | | | | | | | | | | | | | T | | | | | |
| | | | 4H-CC | 32.8 | T | P | Clay | | | | | | | | | | | | | | | | | | T | | | | T | |
| | | 0.30 | 5H-CC | 42.3 | T | P | Clay | | | | | | | T | | | | | | T | | | | | | | | | | |
| | | | 6H-CC | 51.8 | C | M | Clay | | | | | | | | | | | | | | | | | | C | | | | | |
| | | | 7H-CC | 61.3 | R | P | Dissolution | | | | | | | | | | | | | | | | | | R | | | | | |
| | | | 8H-CC | 70.8 | F | P | Clay | | | | | | | | | R | R | | | | | | | | C | | | | | |
| | | | 9H-CC | 80.3 | C | P | Clay | | | | | | | | | | | | | | | | | | F | | | | R | |
| Quaternary | NPD 11 | | 10H-CC | 89.8 | F | P | Clay | | | | | | | | | | | | | | | | | | F | | | | | |
| | | | 11H-CC | 99.3 | F | P | Clay | | | | | | | | | | | | | | | | | | R | | | | | |
| | | | 12H-CC | 108.8 | F | P | Clay | | | | | | | | | | | | | | | | | | R | | | | | |
| | | | 13H-CC | 118.3 | R | P | Clay | | | | | | T | | | | | | | | | | | | R | | R | R | | |
| | | 1.00 | 14H-CC | 127.8 | C | P | Dissolution | R | R | | | R | | | | | | | T | | | | | | R | | | | | |
| | | | 15H-CC | 137.3 | F | P | Clay | | R | R | | | | | | | | | | R | | | | | R | | | | | |
| | | | 16H-CC | 146.8 | C | P | Dissolution | R | | | | | | | R | | | | | | | | | | R | | | R | | |
| | NPD 10 | | 17X-CC | 156.3 | R | P | Warm, littoral element | | | | R | R | R | | | R | | | | | | | | | R | | R | | | |
| | | | 18X-CC | 165.9 | R | P | Warm, coastal, clay | | | R | | | | | | | | | | | R | | | | R | | | | | |
| | | 1.90 | 19X-CC | 175.5 | A | P | Clay + diatomaceous | | | R | | | | | | | | | | | R | | | | R | R | R | R | | R |
| | | 2.00 | 20X-CC | 185.1 | A | P | Clay + diatomaceous | R | | R | | | | | | | | | | | | T | T | | R | | | | | |
| | | | 21X-CC | 194.7 | A | P | Upwelling | | | R | | | | | | | C | | | | | | R | | R | R | | R | R | |
| late Pliocene | NPD 9 | | 22X-CC | 204.3 | C | P | | | | | | R | | | | | C | | | | | | R | | | R | | | | |
| | | 2.40 | 23X-CC | 213.9 | R | P | | R | | | | | | | | | C | | | | | | R | | | | | | | |
| | | | 24X-CC | 223.5 | F | P | | | | | | | | | | | C | | | | | | | | | R | | | | |
| | | <2.63 | 25X-CC | 233.2 | A | M | Coastal upwelling | | | | | | | | | | A | | | | | R | R | | | R | | | | |

Note: See “Explanatory Notes” chapter for abbreviations.

**Table 6 (continued).**

| Geologic age | North Pacific diatom zone | Depth (mbsf) | Numeric age (Ma) | Core, section, interval | Abundance | Preservation | Comments | *Rhaphoneis* sp. | *Rhaphoneis surirella* | *Rhizosolenia barboi* | *Simonseniella (Rhizosolenia) curvirostris* | *Simonseniella (R.)* cf. *curvirostris* | *Rhopalodia gibba* | *Stephanopyxis turris* | *Thalassionema nitzschioides* | *Thalassiosira convexa* | *Thalassiosira* cf. *convexa* | *Thalassiosira eccentrica* | *Thalassiosira leptopus* | *Thalassiosira oestrupii* | *Thalassiothrix longissima* | Diatom fragments (girdle bands) | Resting spores |
|---|---|---|---|---|---|---|---|---|---|---|---|---|---|---|---|---|---|---|---|---|---|---|---|
| | | | 167-1020C- | | | | | | | | | | | | | | | | | | | | |
| | | | | 1H-CC | 4.3 | R | P/M | | T | | | | | F | T | | | | | | | | |
| | | | | 2H-CC | 13.8 | T | P | Clay | | | | | | T | | | | | | | | C | |
| | NPD 12 | | | 3H-CC | 23.3 | T | P | Clay + silt | | | | | | F | | | | | | | | | |
| | | | | 4H-CC | 32.8 | T | P | Clay | | | | | | | | | | | | | | C | |
| | | 0.30 | | 5H-CC | 42.3 | T | P | Clay | | | | | | T | | | | | | | | | |
| | | | | 6H-CC | 51.8 | C | M | Clay | | | | C | | A | | | | R | | | | | |
| | | | | 7H-CC | 61.3 | R | P | Dissolution | | | | | | F | | | | | | | | | |
| | | | | 8H-CC | 70.8 | F | P | Clay | | | | | | C | | | | | | | | C | C |
| | | | | 9H-CC | 80.3 | C | P | Clay | | | | F | | C | | | | | | | | F | F |
| Quaternary | NPD 11 | | | 10H-CC | 89.8 | F | P | Clay | | | R | R | | C | | | | | | | | | |
| | | | | 11H-CC | 99.3 | F | P | Clay | | | | | | R | | | | | | | | R | |
| | | | | 12H-CC | 108.8 | F | P | Clay | | | | T | | R | | | | | | | | C | |
| | | | | 13H-CC | 118.3 | R | P | Clay | | | | | | R | | | | | | | T | F | |
| | | 1.00 | | 14H-CC | 127.8 | C | P | Dissolution | | R | | R | | F | | | | | | | | C | |
| | | | | 15H-CC | 137.3 | F | P | Clay | | | R | | | R | | | | | | | | F | F |
| | | | | 16H-CC | 146.8 | C | P | Dissolution | | | R | | | R | | | | | R | | | A | |
| | NPD 10 | | | 17X-CC | 156.3 | R | P | Warm, littoral element | | | R | | | R | R | | | | | R | | | |
| | | | | 18X-CC | 165.9 | R | P | Warm, coastal, clay | | | R | | R | | | | | R | | | | | |
| | | 1.90 | | 19X-CC | 175.5 | A | P | Clay + diatomaceous | | | | | R | | | | R | | | | R | A | |
| late Pliocene | NPD 9 | 2.00 | | 20X-CC | 185.1 | A | P | Clay + diatomaceous | | | R | | | | | | | | | | | A | A |
| | | | | 21X-CC | 194.7 | A | P | Upwelling | | | A | | | C | | | | | | | | | |
| | | | | 22X-CC | 204.3 | C | P | | | | C | | | C | | | | | | | | | |
| | | 2.40 | | 23X-CC | 213.9 | R | P | | | | C | | | C | | R | | | | | R | | |
| | | | | 24X-CC | 223.5 | F | P | | | | C | | | C | | | | | | | | | |
| | | <2.63 | | 25X-CC | 233.2 | A | M | Coastal upwelling | | | C | | | F | | | | | | | R | | |

**Table 7. Distribution and relative abundance of radiolarians in Holes 1020A and 1020B.**

| Zone | Core, section, interval | Depth (mbsf) | Abundance | Preservation | *Acrosphaera murrayana* | *Actinoma delicatulum* | *Actinomma popofski* | *Amphimelissa setosa* | *Botryostrobus aquilonaris* | *Botryostrobus praetumidulus* | *Botryostrobus tumidulus* | *Ceratospyris hyperborea* | *Circodiscus ellipticus* | *Clathrocyclas bicornis* | *Cycladophora bicincta* | *Cycladophora craspedota* | *Cycladophora davisiana davisiana* | *Dictyophimus crisiae* | *Eucyrtidium acuminatum* | *Eucyrtidium calvertense* | *Eucyrtidium matuyamai* | *Eucyrtidium teuscheri* | *Gondwanaria dogeli* | *Lamprocyclas hannai* | *Lamprocyclas junonis* | *Lamprocyrtis daniellae* | *Lamprocyrtis heteroporos* |
|---|---|---|---|---|---|---|---|---|---|---|---|---|---|---|---|---|---|---|---|---|---|---|---|---|---|---|---|
| *B. aquilonaris* | 167-1020A-<br>1H-CC | 10.0 | A | G | | | A | R | A | | R | A | | | A | A | A | F | R | F | | R | R | | | | |
| *B. aquilonaris* | 167-1020B-<br>1H-CC | 7.8 | A | G | R | F | A | R | A | | R | A | | | A | A | A | F | R | | | T | R | | R | | |
| | 2H-CC | 17.3 | C | G | | C | C | | C | | | A | | | A | | A | R | | | | | T | | | | |
| | 3H-CC | 26.8 | C | G | | F | A | T | A | | | A | | | A | R | A | R | | R | | T | T | | R | | |
| | 4H-CC | 36.3 | F | M | | | A | | | | | A | | | C | | A | R | | | | | | | | | |
| *S. universus* | 5H-CC | 45.8 | A | G | | R | F | | F | | | A | | | A | | A | R | | R | | | | | | | |
| | 6H-CC | 55.3 | A | G | | R | F | | F | | | A | | | A | | A | R | | R | | | | | | | |
| | 7H-CC | 64.8 | R | M | | | P | P | P | | P | | | | P | P | P | P | | | | P | | | | | |
| | 8H-CC | 74.3 | A | G | | R | R | | C | | R | A | | | A | R | A | R | | | | R | T | | | | |
| | 9H-CC | 83.8 | F | G | | R | R | | R | | T | F | | | | R | A | R | | | | | R | | | | |
| | 10H-CC | 93.3 | F | M | | | | P | P | | | P | | P | | P | P | | | | | | | | | | |
| Unzoned | 11H-CC | 101.8 | R | P | | | | | | | | P | | P | | | P | | | | | | | | | | |
| | 12H-CC | 112.3 | R | P | | | | | | | | P | | P | | | P | | | | | | | | | | |
| | 13H-CC | 121.8 | R | P | | | | | | | | | | | | | | | | | | | | | | | |
| | 14H-CC | 131.3 | R | P | | | | | | | | | | | | | | | | | | | | | | | |
| *E. matuyamai* | 15H-CC | 140.8 | A | G | | | A | | | | A | C | | A | | | A | | | | R | R | | | | | R |
| | 16H-CC | 150.3 | C | G | | | R | | | | | C | | C | R | | A | R | | | | | | | | | A |
| | 17H-CC | 159.0 | A | G | | | | | | R | | | | A | | | A | R | | R | C | R | | | | | A |
| | 18H-CC | 169.3 | A | G | | | | | A | | | | | F | | | A | | | | R | R | | | | | A |
| *S. langii* | 19X-CC | 178.9 | A | G | | | | | | A | F | C | | A | | | C | R | | | | R | | T | | | A |
| | 20X-CC | 181.5 | A | G | | | | | | | | C | | F | | | A | R | | | | R | | | | | A |
| | 21X-CC | 198.1 | C | G | | | | | | | | | | C | | | C | | T | R | | | | | T | | A |
| | 22X-CC | 207.7 | C | G | | | | | | | | | | C | | | | | | | | | | | | | C |
| | 23X-CC | 217.3 | C | G | | | | | | | | | | C | | | T | | | | | | | | | | A |
| | 25X-CC | 236.6 | C | G | | | | | | | | | | C | | | | R | | | | | T | | | | A |
| | 26X-CC | 246.2 | C | G | | | R | | | C | | | | C | | | | R | T | | | | | | | R | C |
| | 27X-CC | 255.9 | R | P | | | | | | | | | | | | | | | | | | | | | | | |
| | 28X-CC | 265.3 | B | | | | | | | | | | | | | | | | | | | | | | | | |
| | 29X-CC | 274.7 | B | | | | | | | | | | | | | | | | | | | | | | | | |

Notes: P = present; more detailed abundance information not available. See “Explanatory Notes” chapter for other abbreviations.

reflectance data were culled from these intervals. The cores from Holes 1020A through 1020D provide nearly continuous overlap to about 242 mcd. Core gaps occur at 126 mcd at the bottom of Cores 167-1020B-12H, 1020C-13H, and 1020D-13H; 137 mcd at the bottom of Cores 167-1020B-13H, 1020C-14H, and 1020D-13H; and 200 mcd at the bottom of Cores 167-1020B-20X and 1020C-20X. The composite records suggest that up to 3 m of material may be missing between cores down to about 242 mcd, although the average gap is 1–2 m. As there are no data to fill possible core gaps below 242 mcd, an assessment of core gap length below this depth is not possible.

Following construction of the composite depth section for Site 1020, a single spliced record was assembled from the aligned cores mainly using magnetic susceptibility and GRAPE data and, in some cases, color reflectance data. Cores from Hole 1020C were used as the backbone of the sampling splice. Cores from Holes 1020D were used to splice across core gaps in Hole 1020C in the upper 127 m of the sedimentary section. Below approximately 127 mcd, cores from Hole 1020B were used to splice across core gaps in Hole 1020C. The composite depths were aligned so that tie points between adjacent holes occurred at exactly the same depths in meters composite depth. The Site 1020 splice (Table 11, also on CD-ROM, back pocket) can be used as a sampling guide to recover a single sedimentary sequence that is nearly continuous down to 242 mcd. Intervals having significant disturbance or distortion were avoided if possible.

A preliminary age model (Table 12) was constructed to estimate sedimentation rates (Fig. 14). The age model was applied to the spliced records of color reflectance, magnetic susceptibility, and GRAPE shown in Figure 15.

## INORGANIC GEOCHEMISTRY

We collected 13 interstitial water samples from Hole 1020B at depths ranging from 4.45 to 260.30 mbsf, with samples covering the two lithostratigraphic units defined at this site (see “Lithostratigraphy” section, this chapter). Chemical gradients in the interstitial waters at this site (Table 13) reflect organic matter diagenesis, the dissolution of biogenic opal and calcium carbonate, the influence of authigenic mineral precipitation reactions, and the diffusive influence of reactions in the underlying basalt.

Chlorinity increases by 3.3% from 550 mM at 4.45 mbsf to 568 mM at 50.25 mbsf, then decreases with increasing depth to 556–557 mM from 164.25 to 231.40 mbsf (Fig. 16). Salinity, measured refractively as total dissolved solids, ranges from 32.0–35.0. Sodium concentrations measured by flame emission spectrophotometry were on average <1.0% lower than those estimated by charge balance (Table 13).

Alkalinity increases to ≥20 mM from 31.25 to 135.75 mbsf, then decreases with depth to 6.2 mM at 231.40 mbsf (Fig. 16). Sulfate concentrations decrease with depth, reaching values less than the detection limit (~0.2 mM) by 107.25 mbsf. The deepest sample at 260.30 mbsf has a measurable sulfate concentration, but this may reflect contamination (~10%) by seawater drilling fluid in this harder material.

**Table 7 (continued).**

| Zone | Core, section, interval | Depth (mbsf) | Abundance | Preservation | *Lamprocyrtis neoheteroporos* | *Lamprocyrtis nigriniae* | *Lipmanella virchowii* | *Lychnocanoma nipponica sakai* | *Phormostichoartus crustula* | *Phormostichoartus multiseriatum* | *Plectacantha cresmatoplegma* | *Pseudocubus warreni* | *Pterocanium auritum* | *Pterocanium korotnevi* | *Pterocorys clausus* | *Rhizosphaera antarctica* | *Siphostichoartus scalaris* | *Sphaeropyle langii* | *Spongatrochus glacialis* | *Stylacontarium acquilonium* | *Stylatractus universus* | *Stylodictya validispina* |
|---|---|---|---|---|---|---|---|---|---|---|---|---|---|---|---|---|---|---|---|---|---|---|
| *B. aquilonaris* | 167-1020A-<br>1H-CC | 10.0 | A | G | | A | | C | | | T | | R | C | A | F | R | | C | | | R |
| *B. aquilonaris* | 167-1020B-<br>1H-CC | 7.8 | A | G | | F | T | C | | | | | | C | A | R | R | F | C | | | |
| | 2H-CC | 17.3 | C | G | | T | | F | | | | | | C | A | F | | C | C | | | |
| | 3H-CC | 26.8 | C | G | | T | | T | | | | | R | C | F | R | T | | F | R | | R |
| | 4H-CC | 36.3 | F | M | | | | | | | | | | R | | | | | F | F | | R |
| *S. universus* | 5H-CC | 45.8 | A | G | | A | | C | | | | | | C | A | R | R | C | | C | F | |
| | 6H-CC | 55.3 | A | G | | A | | R | | | | | | C | A | R | R | C | | R | F | |
| | 7H-CC | 64.8 | R | M | | | | P | | | | | P | | | | P | P | P | P | | |
| | 8H-CC | 74.3 | A | G | | | | R | | | | | | F | C | R | | | R | R | C | |
| | 9H-CC | 83.8 | F | G | | | | R | | | | | | R | F | | | R | R | | F | |
| | 10H-CC | 93.3 | F | M | | | | | | | | | | | P | | | P | P | P | P | P |
| Unzoned | 11H-CC | 101.8 | R | P | | | | | | | | | | | | | | | | | P | |
| | 12H-CC | 112.3 | R | P | | | | | | | | | | | | | | | | | P | |
| | 13H-CC | 121.8 | R | P | | | | | | | | | | | | | | | | | | |
| | 14H-CC | 131.3 | R | P | | | | | | | | | | | | | | | | | | |
| *E. matuyamai* | 15H-CC | 140.8 | A | G | F | | | | | R | | | | | | | | C | R | | C | R |
| | 16H-CC | 150.3 | C | G | | | | | | R | | | | | | | | | | | | |
| | 17H-CC | 159.0 | A | G | C | | | R | | | | R | | | | R | | | | | F | F |
| | 18H-CC | 169.3 | A | G | C | | | | | | | C | | | | R | | R | | | | R |
| *S. langii* | 19X-CC | 178.9 | A | G | R | | T | R | R | C | | C | R | | | R | | R | | R | | F |
| | 20X-CC | 181.5 | A | G | | | T | | | | | A | | | | | | R | | | R | R |
| | 21X-CC | 198.1 | C | G | | | | | | C | | C | T | | | R | | R | R | | R | R |
| | 22X-CC | 207.7 | C | G | | | T | | R | C | | C | | | | C | | R | | | | |
| | 23X-CC | 217.3 | C | G | | | | R | | | | | | | | R | | | | | | |
| | 25X-CC | 236.6 | C | G | | | | R | | | | C | | | | | | | | | C | |
| | 26X-CC | 246.2 | C | G | | | | | | | | R | | R | | | | | | | F | |
| | 27X-CC | 255.9 | R | P | | | | | | | | | | | | | | | | | | |
| | 28X-CC | 265.3 | B | | | | | | | | | | | | | | | | | | | |
| | 29X-CC | 274.7 | B | | | | | | | | | | | | | | | | | | | |

**Table 8. Radiolarian events for Holes 1020B and 1020C.**

| Event | Hole 1020B Top (mbsf) | Hole 1020B Base (mbsf) | Hole 1020C Top (mbsf) | Hole 1020C Base (mbsf) |
|---|---|---|---|---|
| LO *S. acquilonium* | 17.3 | 26.8 | 23.8 | 32.8 |
| LO *S. universus* | 36.3 | 45.8 | 32.8 | 42.3 |
| FO *L. nigriniae* | 55.3 | 64.8 | 51.8 | 61.3 |
| FO *E. matuyamai* | 159.0 | 169.3 | 146.8 | 156.3 |
| FO *L. neoheteroporos* | 178.9 | 181.5 | 175.5 | 185.1 |
| FO *C. d. davisiana* | 217.3 | 236.6 | 223.5 | 233.2 |

Note: LO = last occurrenece, FO = first occurrence.

Phosphate concentrations increase steeply to ≥55 µM from 12.25 to 50.25 mbsf, then decrease with increasing depth to 2–4 µM from 192.95 to 260.30 mbsf. Ammonium concentrations increase with increasing depth to >3 mM from 164.25 to 192.95 mbsf, then decrease slightly in the two deepest samples. Manganese concentrations are >50 µM from 4.45 to 31.25 mbsf, then decrease sharply to values <15 µM from 50.25 to 260.30 mbsf, consistent with suboxic diagenesis shallow in the sediments.

Dissolved silicate concentrations increase steadily with depth to 1550 µM at 231.40 mbsf (Fig. 16), indicative of the dissolution of biogenic opal. The dissolved silicate concentration in the deepest sample at 260.30 mbsf is substantially lower than in shallower samples, even when the effects of the contamination by seawater drilling fluid indicated by the sulfate data are taken into consideration. No discrete silica-rich diagenetic phases were observed in the sediments from this site (see "Lithostratigraphy" section, this chapter). Strontium concentrations are approximately seawater values from 4.45 to 50.25 mbsf, then increase with depth to 233 µM at 260.30 mbsf.

Calcium concentrations decrease to a minimum of 5.2 mM at 50.25 mbsf, then increase with increasing depth to 26.3 mM in the deepest sample at 260.30 mbsf (Fig. 16). The average calcium gradient below the calcium minimum is +11.4 mM/100 m. Magnesium concentrations decrease throughout to 19.6 mM at 260.30 mbsf, with an average gradient below the depth of the calcium minimum of –11.8 mM/100 m. The decrease in dissolved calcium in the upper sediment indicates that authigenic mineral precipitation may be significant in influencing this profile in this depth range, while both profiles apparently reflect the diffusive influence of reactions in underlying basalt at deeper depths. At depths ≥78.75 mbsf, the calcium increase is linearly correlated to the magnesium decrease, with $\Delta Ca/\Delta Mg$ of –0.82 ($R^2$ = 0.94). Potassium concentrations generally decrease with increasing depth to 4 mM at 260.30 mbsf (Fig. 16). Lithium concentrations are at or below typical seawater values from 4.45 to 31.25 mbsf, then increase with increasing depth to 202 µM at 260.30 mbsf (Fig. 16).

## ORGANIC GEOCHEMISTRY

Organic geochemical analyses performed at Site 1020 include measurements of elemental composition and volatile hydrocarbons (for methods see "Organic Geochemistry" section, "Explanatory Notes" chapter, this volume).

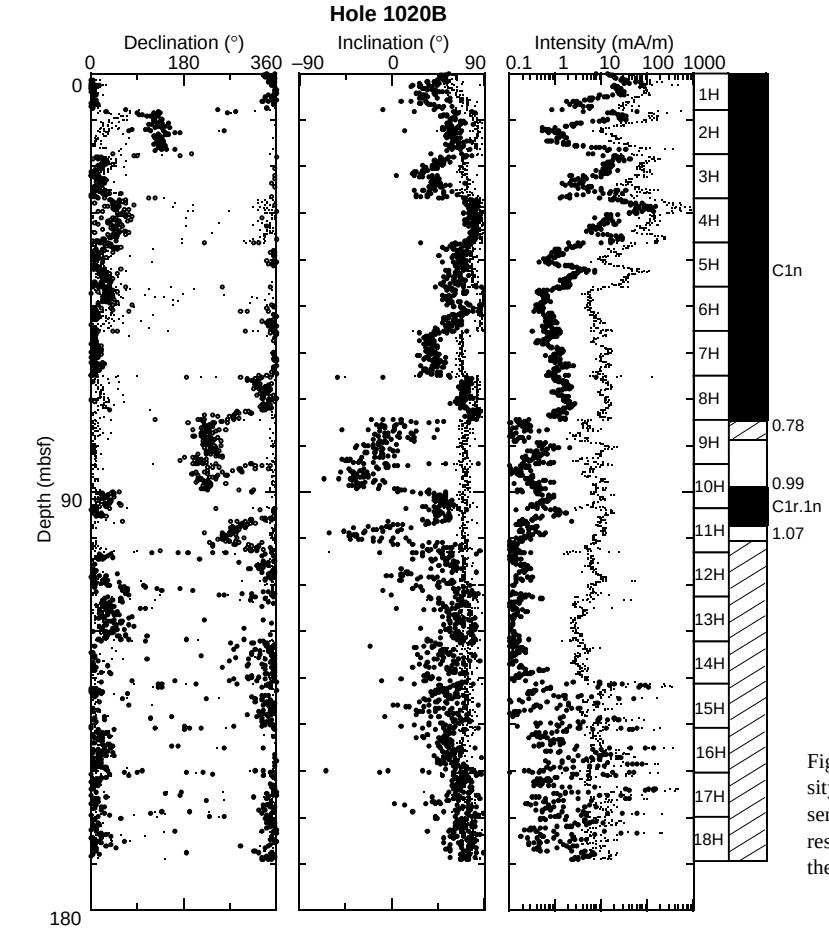


Figure 7. Plots of magnetic declination, inclination, and intensity of APC cores from Hole 1020B. Small and large dots represent the data before and after AF demagnetization at 20 mT, respectively. Open symbols in the declination plots represent the values corrected for orientation with the Tensor tool.

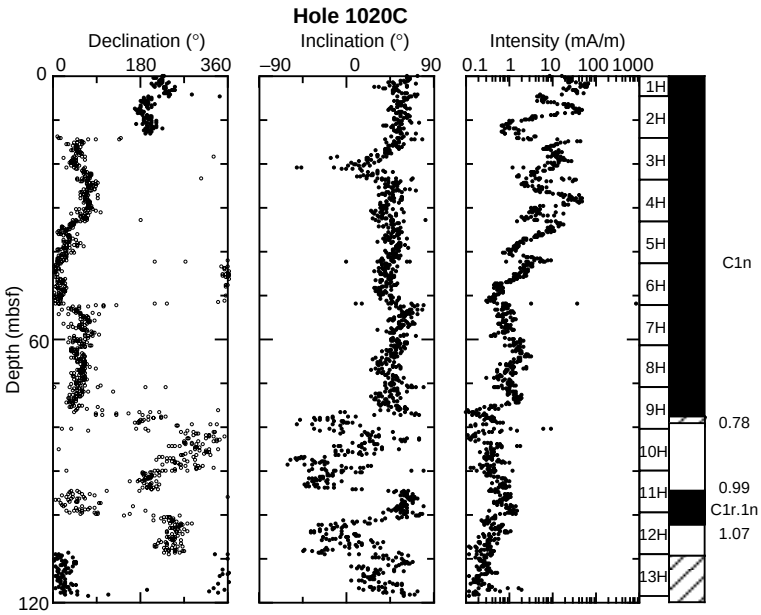


Figure 8. Plots of magnetic declination, inclination, and intensity of APC cores from Hole 1020C obtained after AF demagnetization at 20 mT (solid symbols). Open symbols in the declination plots represent the values corrected for orientation with the Tensor tool.

**Table 9. Magnetostratigraphic datum levels in Holes 1020B and 1020C.**

| Chronozone boundary | Age (Ma) | Upper limit | | | Lower limit | | |
|---|---|---|---|---|---|---|---|
| | | Core, section | Level (cm) | Depth (mbsf) | Core, section | Level (cm) | Depth (mbsf) |
| | | 167-1020B- | | | | | |
| C1n Brunhes (o) | 0.780 | 9H-1 | 5 | 74.35 | 9H-4 | 25 | 79.05 |
| C1r.1n Jaramillo (t) | 0.990 | 10H-4 | 85 | 89.15 | 10H-4 | 145 | 89.75 |
| C1r.1n Jaramillo (o) | 1.070 | 11H-3 | 65 | 96.95 | 11H-4 | 75 | 98.55 |
| | | 167-1020C- | | | | | |
| C1n Brunhes (o) | 0.780 | 9H-5 | 75 | 77.55 | 9H-5 | 135 | 78.15 |
| C1r.1n Jaramillo (t) | 0.990 | 11H-3 | 115 | 93.95 | 11H-4 | 5 | 94.35 |
| C1r.1n Jaramillo (o) | 1.070 | 12H-2 | 115 | 101.95 | 12H-3 | 25 | 102.55 |

Notes: o = onset; t = termination; the assigned ages of the reversal boundaries are according to the time scale of Cande and Kent (1995). The upper and lower limits define the range within which a reversal occurs.

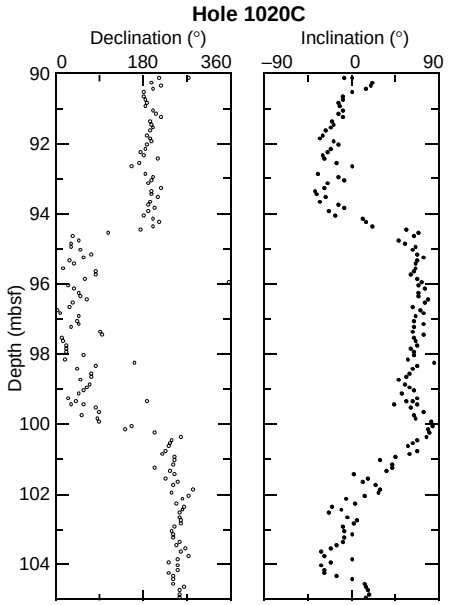


Figure 9. Plots of magnetic declination and inclination for the top and bottom of the Jaramillo Subchron in Hole 1020C obtained after AF demagnetization at 20 mT. Declination values were rotated to their in situ coordinates using the Tensor tool data.

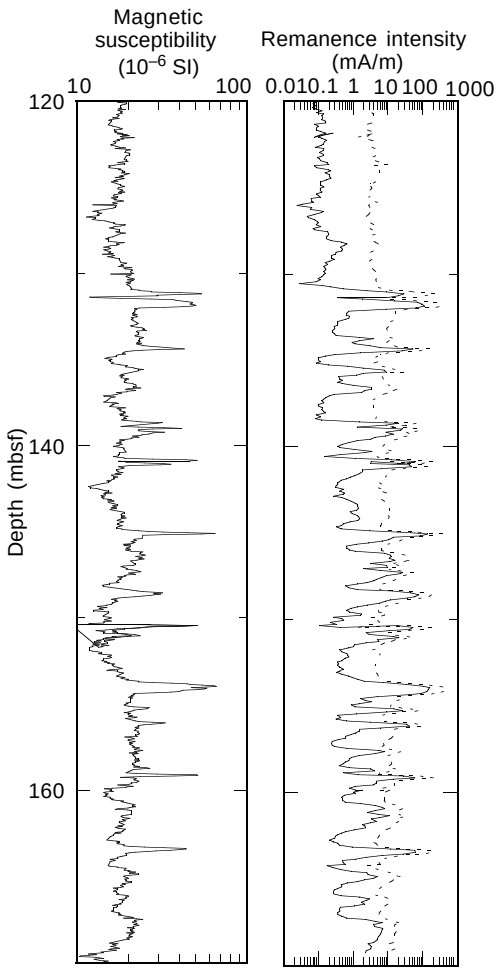


Figure 10. Whole-core magnetic susceptibility and intensity of remanent magnetization before (dashed line) and after (solid line) AF demagnetization at 20 mT for the interval between 120 and 170 mbsf in Hole 1020B. The high peaks could represent horizons of diagenetic iron-sulfide formation that may contain pyrrhotite.

## Volatile Hydrocarbons

As a part of the shipboard safety and pollution program, volatile hydrocarbons (methane, ethane, and propane) in the sediments at Site 1020 were routinely measured by gas chromatography. Results are presented in Table 14 and Figure 17. Headspace methane concentrations were at low values near the detection limit within the uppermost 68 mbsf. Methane content increased gradually to a maximum of about 8900 ppm around 150 mbsf, then gradually decreased to the bottom of hole. Ethane and propane were detected only in traces. Higher weight molecular hydrocarbon gases were not observed. High methane/ethane ratios suggest that the methane is of biogenic origin.

## Elemental Analysis

At Site 1020, 92 sediment samples were analyzed for total carbon, inorganic carbon, total nitrogen, and total sulfur (Table 15, also on CD-ROM, back pocket; Fig. 18).

The percentage of calcium carbonate ($CaCO_3$) was calculated from inorganic carbon concentrations by assuming that all carbonate occurs in the form of calcite. $CaCO_3$ content varies between ~1 and 58 wt%, and shows a good correlation to lithology (see "Lithostratigraphy" section, this chapter; Fig. 18). Lithostratigraphic Unit I (0–229 mbsf) is characterized by low $CaCO_3$ content, ranging between 1 and 10 wt%. Some single spikes of up to 20 wt% occur in this interval. The poor preservation of nannofossils (see "Biostratigraphy" section, this chapter) suggests that the low $CaCO_3$ content in the interval between 60 and 220 mbsf is probably caused by carbonate dissolution. In lithostratigraphic Unit II (229–279 mbsf), the carbonate

**Table 10. Site 1020 composite depth section.**

| Hole, core, section | Depth (mbsf) | Offset (m) | Depth (mcd) |
|---|---|---|---|
| 167-1020A- | | | |
| 1H-1 | 0 | 4.14 | 4.14 |
| 167-1020B- | | | |
| 1H-1 | 0 | 0.08 | 0.08 |
| 2H-1 | 7.8 | –0.14 | 7.66 |
| 3H-1 | 17.3 | 0.26 | 17.56 |
| 4H-1 | 26.8 | 2.08 | 28.88 |
| 5H-1 | 36.3 | 3.16 | 39.46 |
| 6H-1 | 45.8 | 4.92 | 50.72 |
| 7H-1 | 55.3 | 5.92 | 61.22 |
| 8H-1 | 64.8 | 7.71 | 72.51 |
| 9H-1 | 74.3 | 10.19 | 84.49 |
| 10H-1 | 83.8 | 12.05 | 95.85 |
| 11H-1 | 93.3 | 11.27 | 104.57 |
| 12H-1 | 102.8 | 12.44 | 115.24 |
| 13H-1 | 112.3 | 14.88 | 127.18 |
| 14H-1 | 121.8 | 14.98 | 136.78 |
| 15H-1 | 131.3 | 14.98 | 146.28 |
| 16H-1 | 140.8 | 14.93 | 155.73 |
| 17H-1 | 150.3 | 15.81 | 166.11 |
| 18H-1 | 159.8 | 17.13 | 176.93 |
| 19X-1 | 169.3 | 17.89 | 187.19 |
| 20X-1 | 178.9 | 17.89 | 196.79 |
| 21X-1 | 188.5 | 19.81 | 208.31 |
| 22X-1 | 198.1 | 20.19 | 218.29 |
| 23X-1 | 207.7 | 22.03 | 229.73 |
| 25X-1 | 227 | 19.07 | 246.07 |
| 26X-1 | 236.6 | 19.07 | 255.67 |
| 27X-1 | 246.3 | 19.07 | 265.37 |
| 28X-1 | 255.9 | 19.07 | 274.97 |
| 29X-1 | 265.3 | 19.07 | 284.37 |
| 30X-1 | 274.7 | 19.07 | 293.77 |
| 167-1020C- | | | |
| 1H-1 | 0 | 0 | 0 |
| 2H-1 | 4.3 | 1.3 | 5.6 |
| 3H-1 | 13.8 | 1.16 | 14.96 |
| 4H-1 | 23.3 | 2.72 | 26.02 |
| 5H-1 | 32.8 | 3.82 | 36.62 |
| 6H-1 | 42.3 | 4.82 | 47.12 |
| 7H-1 | 51.8 | 4.68 | 56.48 |
| 8H-1 | 61.3 | 4.29 | 65.59 |
| 9H-1 | 70.8 | 4.91 | 75.71 |
| 10H-1 | 80.3 | 4.55 | 84.85 |
| 11H-1 | 89.8 | 5.71 | 95.51 |
| 12H-1 | 99.3 | 6.35 | 105.65 |
| 13H-1 | 108.8 | 7.88 | 116.68 |
| 14H-1 | 118.3 | 7.88 | 126.18 |
| 15H-1 | 127.8 | 10.21 | 138.01 |
| 16H-1 | 137.3 | 11.92 | 149.22 |
| 17X-1 | 146.8 | 13.67 | 160.47 |
| 18X-1 | 156.3 | 14.37 | 170.67 |
| 19X-1 | 165.9 | 14.37 | 180.27 |
| 20X-1 | 175.5 | 15.99 | 191.49 |
| 21X-1 | 185.1 | 15.99 | 201.09 |
| 22X-1 | 194.7 | 17.91 | 212.61 |
| 23X-1 | 204.3 | 18.45 | 222.75 |
| 24X-1 | 213.9 | 19.01 | 232.91 |
| 25X-1 | 223.5 | 19.01 | 242.51 |
| 167-1020D- | | | |
| 1H-1 | 0 | –0.04 | –0.04 |
| 2H-1 | 9.4 | 1.98 | 11.38 |
| 3H-1 | 18.9 | 2.18 | 21.08 |
| 4H-1 | 28.4 | 3.76 | 32.16 |
| 5H-1 | 37.9 | 4.48 | 42.38 |
| 6H-1 | 47.4 | 5.18 | 52.58 |
| 7H-1 | 56.9 | 5.68 | 62.58 |
| 8H-1 | 66.4 | 5.6 | 72 |
| 9H-1 | 75.9 | 5.96 | 81.86 |
| 10H-1 | 85.4 | 5.83 | 91.23 |
| 11H-1 | 94.9 | 6.69 | 101.59 |
| 12H-1 | 104.4 | 8.05 | 112.45 |
| 13H-1 | 113.9 | 8.77 | 122.67 |
| 14H-1 | 118.2 | 8.78 | 126.98 |
| 15H-1 | 127.7 | 10.97 | 138.67 |
| 16H-1 | 137.2 | 12.05 | 149.25 |
| 17H-1 | 146.7 | 14.13 | 160.83 |

Note: This table is also on CD-ROM, back pocket, this volume.

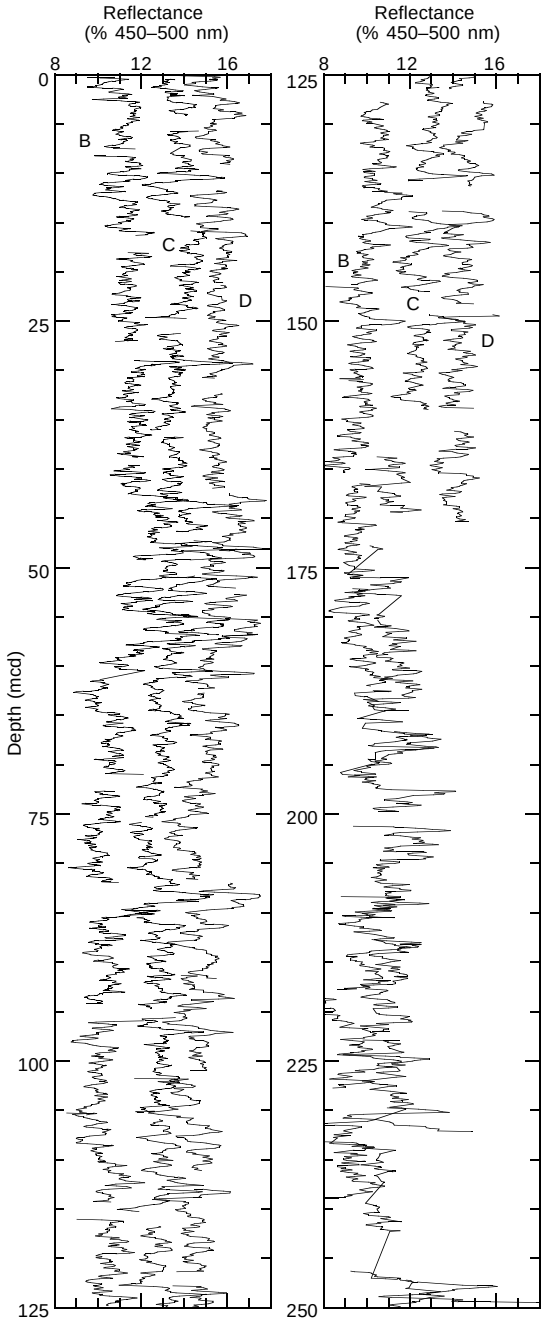


Figure 11. Smoothed (15-cm Gaussian) color reflectance (% 450–500 nm band) data for the upper 250 m from Site 1020 on the mcd scale. Holes 1020B, 1020C, and 1020D are offset from each other by a constant (3%).

record shows rapidly increasing values between 18 and 58 wt%. In this interval, the nannofossil preservation is very good, which may indicate that the carbonate fluctuation is caused by of changes in primary productivity.

The total organic carbon (TOC) content at Site 1020 varies between 0.32 and 1.28 wt% (Table 15; Fig. 18). Again, a dependency on the lithology is apparent. In Unit I, the TOC content varies consistently around an average value of 0.75 wt%. In lithostratigraphic Unit II, organic matter concentration decreases downcore. The correlation with the carbonate-rich interval points to dilution as the reason for decreased TOC content.

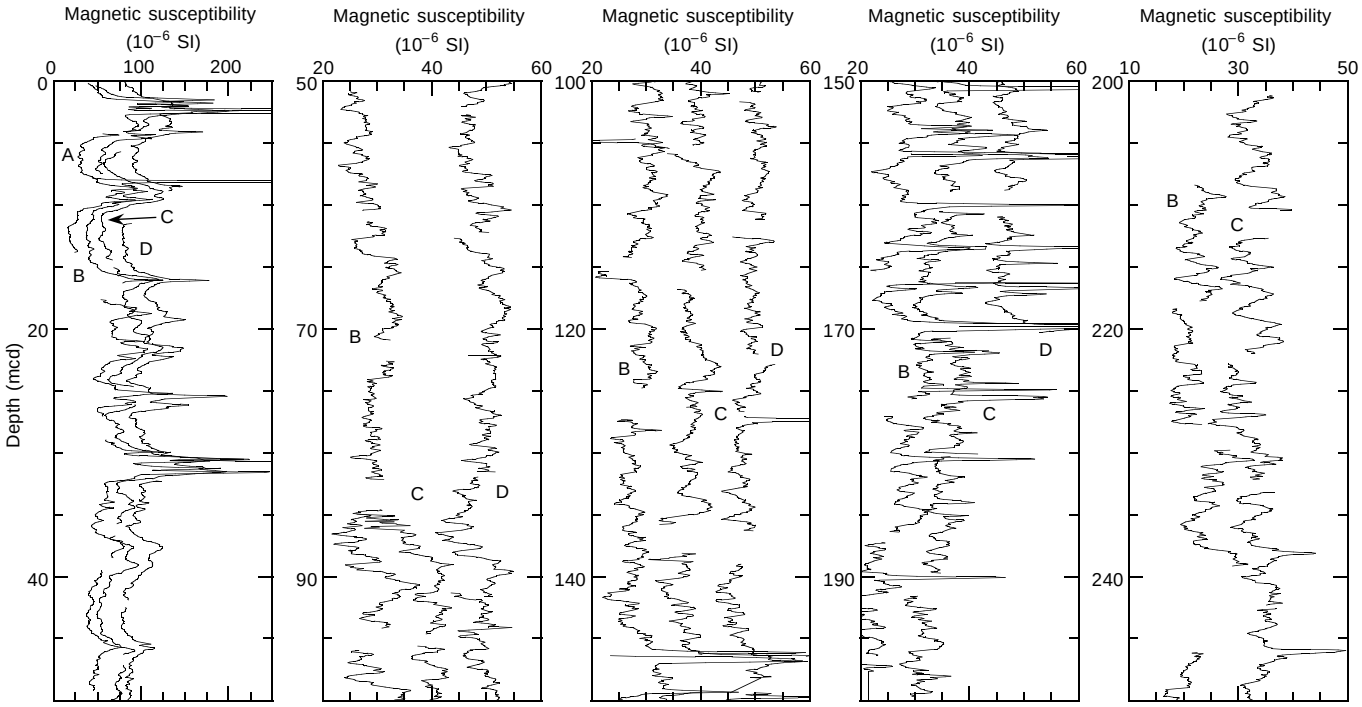


Figure 12. Smoothed (15-cm Gaussian) magnetic susceptibility data for the upper 250 m from Site 1020 on the mcd scale. Holes 1020A, 1020B, 1020C, and 1020D are offset from each other by a constant ($20 \times 10^{-6}$ on 0–50 mcd panel and $10 \times 10^{-6}$ on other panels). Note the different scale used for the 0–50 mcd panel. Susceptibility data for Hole 1012C were not plotted for the interval from 50 to 85 mcd, because the data were affected by intermittent noise that seriously degraded the quality of the signal.

Total nitrogen content varies between 0.1 and 0.4 wt%, and total sulfur content ranges from 0 to ~2 wt% (Table 15). To characterize the type of organic matter in the sediments, total organic carbon/total nitrogen (TOC/TN) ratios were used. Most of the TOC/TN ratios range between 4 and 8, which indicates a predominantly marine origin of the organic material (Bordovskiy, 1965; Emerson and Hedges, 1988).

## PHYSICAL PROPERTIES

### Multisensor Track Measurements

The shipboard physical properties program at Site 1020 included nondestructive measurements of bulk density, magnetic susceptibility, *P*-wave velocity, and natural gamma-ray activity on whole sections of all cores using the MST (Fig. 19). Magnetic susceptibility was measured at 4-cm intervals at low sensitivity (1-s measuring time). GRAPE bulk density measurements were made at 4-cm intervals on all Site 1020 cores. PWL velocity measurements were made at 4-cm intervals on Cores 167-1020A-1H, 167-1020B-1H through 19X, 167-1020C-1H through 19X, and 167-1020D-1H through 17H. Natural gamma-ray activity was measured with a 15-s count every 12 cm on cores from Holes 1020A, 1020B, and 1020C.

### Index Properties

Index properties measurements were made at one sample per working section on all cores from Hole 1020B. Values of bulk density and the index properties void ratio, porosity, water content, dry-bulk density, and grain density (Fig. 20) were determined using gravimetric Method C (Table 16 on CD-ROM in the back pocket of this volume).

### Compressional-Wave Velocity

Sonic velocity was measured with the Hamilton Frame (pair T3, in the x-direction) at an average of one per core in Hole 1020B (Table 17 on CD-ROM in the back pocket of this volume).

### Heat Flow

Thermal conductivity was measured to 82.55 mbsf in Hole 1020B (Table 18 on CD-ROM in the back pocket of this volume). Three downhole temperature measurements were taken with the APC Adara temperature tool in Hole 1020B: 8.4°C at 36.3 mbsf, 11.7°C at 55.3 mbsf, and 15.5°C at 74.3 mbsf in Cores 167-1020B-4H, 6H, and 8H, respectively (Fig. 21). Bottom-water temperature was measured on all runs, indicating a bottom-water temperature of 1.4°C ± 0.1°C. The four data points yield a thermal gradient of 189°C/km (Fig. 22). Using an average measured thermal conductivity of 0.899 W/(m·K) provides a heat-flow estimate of 170 mW/m$^2$ at Site 1020.

### Color Reflectance

Color reflectance measurements were taken at 4- to 6-cm intervals on cores from Holes 1020B, 1020C, and 1020D. The reflectance data are consistent with the major lithostratigraphic units at this site. A summary for the blue band (450–500 nm) and the near infrared (850–900 nm) to blue ratio is given in Figure 23. Data from Hole 1020C are used for the near infrared/blue ratio because instrumental noise was lower than at Hole 1020B.

In lithostratigraphic Unit I, which is composed of clay mixed with nannofossil clay (Subunit IA) and diatom clay (Subunit IB), color reflectance is consistently low for the 450–500-nm band (average =

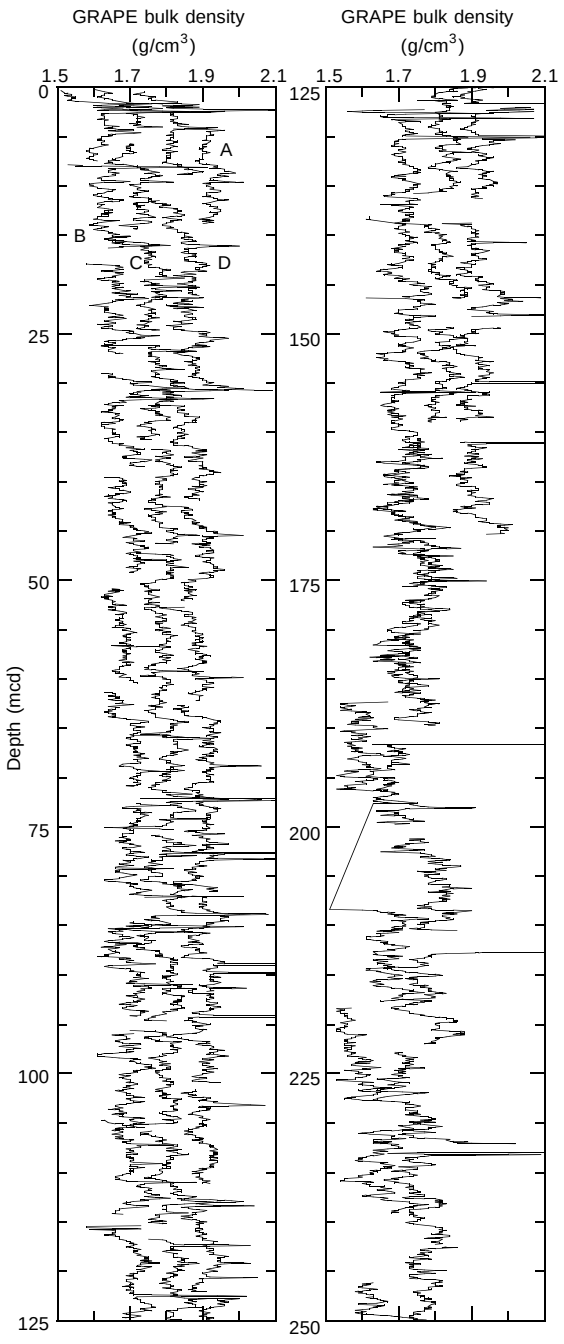


Figure 13. Smoothed (15-cm Gaussian) GRAPE bulk density data for the upper 250 m from Site 1020 on the mcd scale. Holes 1020B, 1020C, 1020D, and 1020A are offset from each other by a constant (0.1 g/cm$^3$).

10.6%, standard deviation = 1.2%). The peak in reflectance from 40 to 55 mbsf coincides with the relatively high nannofossil content of this interval. Lithostratigraphic Unit II, which is predominantly nannofossil chalk mixed with clay, shows greater and more variable color reflectance than lithostratigraphic Unit I (average = 13.9%, standard deviation = 3.7%). The high reflectance values in lithostratigraphic Unit II generally match nannofossil-rich layers.

The near infrared/blue ratio is analogous to the near infrared over red (650–700 nm) ratio used to detect diatomaceous sediments in the eastern equatorial Pacific (Mix et al., 1992). We chose to use near infrared/blue at Site 1020 because it shows greater variance (mean = 1.0, standard deviation = 0.07) than near infrared/red (mean = 0.99, standard deviation = 0.03). This ratio is also sensitive to diatom content at Site 1016 (see "Physical Properties" section, "Site 1016" chapter, this volume). In lithostratigraphic Subunit IA at Site 1020, where clay predominates, near infrared/blue is low. As lithostratigraphic Subunit IA grades into Subunit IB, the proportion of diatoms increases, as does the mean value and variability of the near infrared/blue ratio.

### Digital Color Video

Cores from all Site 1020 holes were imaged with the ODP color digital imaging system at 20-cm intervals downcore, providing a 0.25-mm pixel. Intensity of color CIELAB L* from the digital color video system from Holes 1020B, 1020C, and 1020D is shown in Figure 24.

## DOWNHOLE MEASUREMENTS

### Logging Operations and Log Quality

Hole 1020B was logged with the density-porosity combination, sonic-FMS, and GHMT tool strings after the hole was flushed of debris and the drill pipe was set at 56 mbsf (Table 19). Two full passes of the density-porosity combination tool string (pass 1: 95–275 mbsf; pass 2: 90–275 mbsf), two full passes of the FMS-sonic tool string (pass 1: 100–275, with one pause at 200 mbsf; pass 2: 100–275 mbsf), and two passes of the GHMT tool string (pass 1: 75–260 mbsf; pass 2: 60–272 mbsf) were conducted. Sea-state conditions were calm (<1-m swells), and the wireline heave compensator was used on all passes.

Borehole caliper measurements conducted during the density-porosity combination and sonic-FMS passes indicate that the borehole was moderately washed out from the bottom of the hole to 170 mbsf and significantly washed out from 170 mbsf to the base of the pipe at 56 mbsf (Fig. 25). Overall log quality at this site is excellent to very good below 170 mbsf and fair in the washed-out section above 170 mbsf.

The TLT was run during both passes of the density-porosity combination tool. The temperature logs were linked to the actual logging depths using the time-depth log recorded at the logging unit. The raw TLT results show a minimum thermal gradient of 56°C/km (Fig. 26); this is an underestimate because of the cooling by seawater circulation. In situ temperature measurements using the Adara probe indicate a thermal gradient near 189°C/km at this site (see "Physical Properties" section, this chapter).

One way that log quality can be assessed is by comparing separate log passes to determine how well measurements are reproduced. The high-resolution photoelectric effect can be related to variation in the calcium carbonate percentage (see "Downhole Measurements" section, "Explanatory Notes" chapter, this volume, for an explanation of the photoelectric factor). Both passes in Hole 1020B, where hole conditions are very good, reproduced the photoelectric effect in detail (Fig. 27), suggesting that the photoelectric factor can be a reliable lithologic proxy if quantitative calibrations to lithologic composition are calculated. High-resolution conductivity records from the FMS tool string are clearly reproduced both on the meter to decimeter scale and on the centimeter scale (Fig. 28). The quality of the FMS data is poor above 170 mbsf, where the caliper reaches its maximum extension at 15 cm. However, detailed comparisons of the interval below 170 mbsf (example given in Fig. 28) demonstrate that the data are of excellent quality. Comparison of the magnetic susceptibility logs

**Table 11. Site 1020 splice tie points.**

| Hole, core, section, interval (cm) | Depth (mbsf) | Depth (mcd) | | Hole, core, section, interval (cm) | Depth (mbsf) | Depth (mcd) |
|---|---|---|---|---|---|---|
| 1020C-1H-2, 135 | 2.85 | 2.85 | tie to | 1020D-1H-2, 139 | 2.89 | 2.85 |
| 1020D-1H-5, 35 | 6.35 | 6.31 | tie to | 1020C-2H-1, 71 | 5.01 | 6.31 |
| 1020C-2H-5, 59 | 10.89 | 12.19 | tie to | 1020D-2H-1, 81 | 10.21 | 12.19 |
| 1020D-2H-3, 135 | 13.75 | 15.73 | tie to | 1020C-3H-1, 77 | 14.57 | 15.73 |
| 1020C-3H-7, 39 | 23.19 | 24.35 | tie to | 1020D-3H-3, 27 | 22.17 | 24.35 |
| 1020D-3H-5, 11 | 25.01 | 27.19 | tie to | 1020C-4H-1, 117 | 24.47 | 27.19 |
| 1020C-4H-6, 67 | 31.47 | 34.19 | tie to | 1020D-4H-2, 53 | 30.43 | 34.19 |
| 1020D-4H-4, 59 | 33.49 | 37.25 | tie to | 1020C-5H-1, 63 | 33.43 | 37.25 |
| 1020C-5H-6, 135 | 41.65 | 45.47 | tie to | 1020D-5H-3, 19 | 41.09 | 45.57 |
| 1020D-5H-4, 75 | 43.15 | 47.63 | tie to | 1020C-6H-1, 51 | 42.81 | 47.63 |
| 1020C-6H-7, 7 | 51.37 | 56.19 | tie to | 1020D-6H-3, 61 | 51.01 | 56.19 |
| 1020D-6H-4, 51 | 52.41 | 57.59 | tie to | 1020C-7H-1, 111 | 52.91 | 57.59 |
| 1020C-7H-6, 139 | 60.69 | 65.37 | tie to | 1020D-7H-2, 129 | 59.69 | 65.37 |
| 1020D-7H-3, 123 | 61.13 | 66.81 | tie to | 1020C-8H-1, 122 | 62.52 | 66.81 |
| 1020C-8H-7, 39 | 70.69 | 74.98 | tie to | 1020D-8H-2, 148 | 69.38 | 74.98 |
| 1020D-8H-3, 139 | 70.79 | 76.39 | tie to | 1020C-9H-1, 68 | 71.48 | 76.39 |
| 1020C-9H-6, 47 | 78.77 | 83.68 | tie to | 1020D-9H-2, 32 | 77.72 | 83.68 |
| 1020D-9H-3, 123 | 80.13 | 86.09 | tie to | 1020C-10H-1, 24 | 81.54 | 86.09 |
| 1020C-10H-6, 139 | 89.19 | 93.74 | tie to | 1020D-10H-2, 101 | 87.91 | 93.74 |
| 1020D-10H-4, 99 | 90.89 | 96.72 | tie to | 1020C-11H-1, 121 | 91.01 | 96.72 |
| 1020C-11H-6, 99 | 98.29 | 104 | tie to | 1020D-11H-2, 91 | 97.31 | 104 |
| 1020D-11H-4, 27 | 99.67 | 106.36 | tie to | 1020C-12H-1, 71 | 100.01 | 106.36 |
| 1020C-12H-6, 115 | 107.95 | 114.3 | tie to | 1020D-12H-2, 35 | 106.25 | 114.3 |
| 1020D-12H-4, 91 | 109.81 | 117.86 | tie to | 1020C-13H-1, 118 | 109.98 | 117.86 |
| 1020C-13H-7, 63 | 118.43 | 126.31 | tie to | 1020C-14H-1, 15 | 118.45 | 126.31 |
| 1020C-14H-7, 59 | 127.89 | 135.75 | tie to | 1020B-13H-7, 47 | 121.77 | 136.75 |
| 1020B-14H-6, 59 | 129.89 | 144.87 | tie to | 1020D-15H-5, 20 | 133.90 | 144.87 |
| 1020D-15H-6, 95 | 136.15 | 147.12 | tie to | 1020B-15H-1, 84 | 132.14 | 147.12 |
| 1020B-15H-3, 35 | 134.65 | 149.63 | tie to | 1020C-16H-1, 41 | 137.71 | 149.63 |
| 1020C-16H-6, 75 | 145.58 | 157.5 | tie to | 1020B-16H-2, 27 | 142.57 | 157.5 |
| 1020B-16H-6, 55 | 148.85 | 163.78 | tie to | 1020C-17X-3, 31 | 150.11 | 163.78 |
| 1020C-17X-7, 11 | 155.91 | 169.58 | tie to | 1020B-17H-3, 47 | 153.77 | 169.58 |
| 1020B-17H-5, 7 | 155.97 | 171.78 | tie to | 1020C-18X-1, 111 | 157.41 | 171.78 |
| 1020C-18X-6, 111 | 164.91 | 179.28 | tie to | 1020B-18H-2, 85 | 162.15 | 179.28 |
| 1020B-18H-4, 47 | 164.77 | 181.9 | tie to | 1020C-19X-2, 13 | 167.53 | 181.90 |
| 1020C-19X-6, 23 | 173.63 | 188 | tie to | 1020B-19X-1, 81 | 170.11 | 188.00 |
| 1020B-19X-4, 99 | 174.79 | 192.68 | tie to | 1020C-20X-1, 119 | 176.69 | 192.68 |
| 1020C-20X-5, 74 | 182.31 | 198.30 | tie to | 1020C-20X-6, 31 | 183.31 | 198.30 |
| 1020C-21X-6, 83 | 193.43 | 209.42 | tie to | 1020B-21X-1, 111 | 189.61 | 209.42 |
| 1020B-21X-4, 67 | 193.67 | 213.48 | tie to | 1020C-22X-1, 87 | 195.57 | 213.48 |
| 1020C-22X-6, 127 | 203.47 | 221.38 | tie to | 1020B-22X-3, 9 | 201.19 | 221.38 |
| 1020B-22X-5, 15 | 204.25 | 224.44 | tie to | 1020C-23X-2, 19 | 205.99 | 224.44 |
| 1020C-23X-6, 75 | 212.55 | 231 | tie to | 1020B-23X-1, 127 | 208.97 | 231 |
| 1020B-23X-6, 47 | 215.67 | 237.7 | tie to | 1020C-24X-4, 31 | 218.71 | 237.72 |
| 1020C-24X-7, 39 | 223.29 | 242.3 | tie to | 1020C-25X-1, 7 | 223.57 | 242.58 |
| 1020C-25X-6, 111 | 232.11 | 251.12 | tie to | 1020B-25X-4, 55 | 232.05 | 251.12 |
| 1020B-25X-7, 79 | 236.29 | 255.36 | tie to | 1020C-23X-2, 19 | 205.99 | 224.44 |

Note: This table is also on CD-ROM, back pocket, this volume.

**Table 12. Site 1020 sedimentation rate age control points.**

| Event | Depth (mcd) | Age (Ma) |
|---|---|---|
| T *P. lacunosa* | 51.30 | 0.46 |
| B Brunhes | 84.83 | 0.78 |
| T Jaramillo | 100.68 | 0.99 |
| B Jaramillo | 108.81 | 1.07 |
| T large *Gephyrocapsa* spp. | 125.01 | 1.24 |
| B large *Gephyrocapsa* spp. | 144.69 | 1.44 |
| B *G. oceanica* | 160.48 | 1.69 |
| T *T. convexa* | 238.27 | 2.40 |
| B *C. davisiana* | 248.17 | 2.80 |
| T *R. pseudoumbilicus* | 289.07 | 3.79 |

Note: T = top, B = bottom.

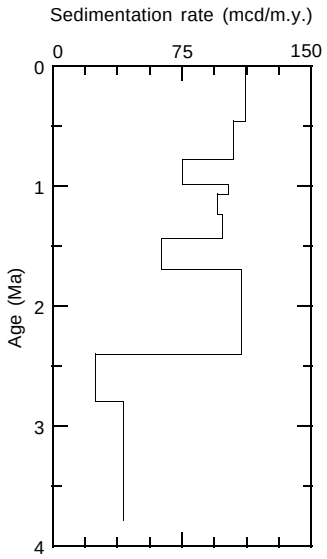


Figure 14. Sedimentation rate vs. age based on the age control points from Table 12.

from the two separate passes of the GHMT tool string also demonstrates that the data are reproduced in detail with the exception of the interval above 170 mbsf (Fig. 29).

## Lithology

The transition from interbedded clays and nannofossil clays to sediment with more siliceous components (lithostratigraphic Subunit IA/Subunit IB transition) at about 120 mbsf is not marked by a significant change in the logging data (Fig. 25). There is a gradual de-

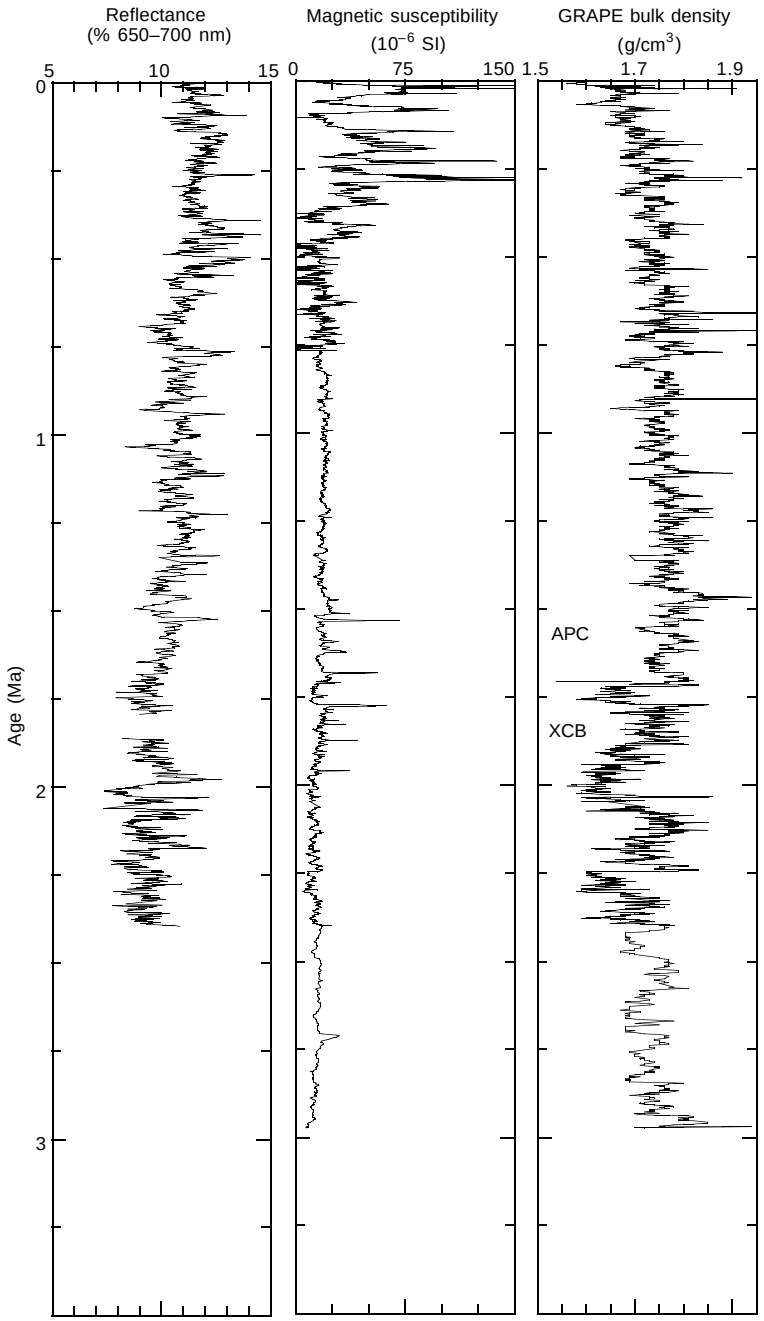


Figure 15. Spliced records of Site 1020 color reflectance, magnetic susceptibility, and GRAPE bulk density vs. age based on age control points from Table 12. High-frequency, relatively high-amplitude variations between 0.45 and 0.75 Ma are caused by high instrument noise in Hole 1020C data.

crease in porosity and resistivity and an increase in density and gamma-ray activity from 80 to 170 mbsf that may reflect changes in borehole conditions from a larger diameter above 170 mbsf to a narrower borehole below 170 mbsf. There is a transition to higher density, resistivity, and gamma-ray activity values and to lower porosity values from 210 mbsf toward the bottom of the hole. This transition reflects the observed small increase in lithification and in carbonate content near the bottom of lithostratigraphic Subunit IB (see "Lithostratigraphy" section, this chapter). A more distinctive decrease in porosity and increase in density and resistivity mark the transition from lithostratigraphic Subunit IB, a diatom clay with nannofossils, to lithostratigraphic Unit II, a nannofossil chalk. The relatively large peak in the gamma-ray log at about 187 mbsf (Fig. 25) reflects a 5-cm-thick layer of ash. A sub-meter-thick dolomitic clay at 190 mbsf is recorded as a peak in resistivity and density and as lower porosity.

## Comparison of Core and Log Data

The core and log measurements of sediment bulk density are similar over their common interval. The largest deviations between the log and core data occur above 170 mbsf in intervals where the borehole is washed out (Fig. 30). Between 170 and 210 mbsf the core density measurement is slightly lower than the log (neutron) measurements, in part because of core disturbance during XCB drilling. As observed at Holes 1014A and 1016A, the log (neutron) porosity data are also higher than the core density measurements because the neutron log porosity data tend to overestimate porosity in very clay-rich formations such as at Hole 1020B.

Comparison between the log natural gamma-ray and the core natural gamma-ray data, between the log density and the core GRAPE density data, and between the log magnetic susceptibility and the core

**Table 13. Interstitial water geochemical data, Hole 1020B.**

| Core, section, interval (cm) | Depth (mbsf) | pH | Alkalinity (mM) | Salinity | $Cl^-$ (mM) | $Na^+$ (mM) | $SO_4^{2-}$ (mM) | $HPO_4^{2-}$ (μM) | $NH_4^+$ (mM) | $Mn^{2+}$ (μM) | $H_4SiO_4$ (μM) | $Ca^{2+}$ (mM) | $Mg^{2+}$ (mM) | $Sr^{2+}$ (μM) | $Li^+$ (μM) | $K^+$ (mM) |
|---|---|---|---|---|---|---|---|---|---|---|---|---|---|---|---|---|
| 167-1020B- | | | | | | | | | | | | | | | | |
| 1H-3, 145–150 | 4.45 | 7.50 | 9.29 | 35.0 | 550 | 474 | 23.6 | 50 | 0.13 | 59 | 688 | 9.72 | 50.8 | 85 | 19 | 11.0 |
| 2H-3, 145–150 | 12.25 | 7.42 | 15.4 | 35.0 | 555 | 480 | 18.4 | 74 | 0.71 | 54 | 775 | 8.92 | 49.4 | 85 | 20 | 10.7 |
| 3H-3, 145–150 | 21.75 | 7.34 | 19.0 | 35.0 | 562 | 487 | 15.9 | 66 | 1.28 | 63 | 775 | 8.37 | 49.1 | 85 | 24 | 11.0 |
| 4H-3, 145–150 | 31.25 | 7.32 | 20.7 | 35.0 | 566 | 489 | 13.2 | 59 | 1.52 | 53 | 838 | 7.73 | 49.0 | 85 | 28 | 10.7 |
| 5H-3, 145–150 | 40.75 | 7.26 | 21.1 | 34.5 | 566 | 489 | 10.5 | 56 | 1.82 | 28 | 927 | 6.43 | 47.9 | 85 | 35 | 10.5 |
| 6H-3, 145–150 | 50.25 | 7.13 | 21.2 | 34.0 | 568 | 489 | 8.1 | 55 | 2.04 | 8 | 959 | 5.18 | 47.7 | 89 | 41 | 10.1 |
| 9H-3, 145–150 | 78.75 | 7.22 | 20.3 | 33.0 | 563 | 486 | 2.5 | 38 | 2.53 | 13 | 1161 | 5.50 | 41.1 | 111 | 58 | 9.3 |
| 12H-3, 145–150 | 107.25 | 7.31 | ND | 33.0 | 560 | ND | <0.2 | 38 | 2.76 | 19 | 1280 | 6.09 | 41.3 | 133 | 69 | 8.6 |
| 15H-3, 145–150 | 135.75 | 7.25 | 21.9 | 33.0 | 563 | 483 | <0.2 | 21 | 2.87 | 12 | 1409 | 7.88 | 39.0 | 152 | 105 | 8.0 |
| 18H-3, 145–150 | 164.25 | 7.17 | 18.3 | 33.0 | 556 | 478 | <0.2 | 16 | 3.12 | 12 | 1452 | 10.2 | 34.0 | 174 | 145 | 7.7 |
| 21X-3, 145–150 | 192.95 | 7.30 | 12.9 | 32.0 | 556 | 477 | <0.2 | 4 | 3.07 | 9 | 1394 | 13.6 | 28.8 | 196 | 183 | 7.2 |
| 25X-3, 140–150 | 231.40 | 7.18 | 6.17 | 32.0 | 557 | 476 | <0.2 | 3 | 2.84 | 7 | 1549 | 18.8 | 22.1 | 215 | 205 | 5.8 |
| 28X-3, 140–150 | 260.30 | ND | ND | ND | 550 | ND | 2.8 | 2 | 1.95 | 15 | 789 | 26.3 | 19.6 | 233 | 202 | 4.0 |

Note: ND = value not determined.

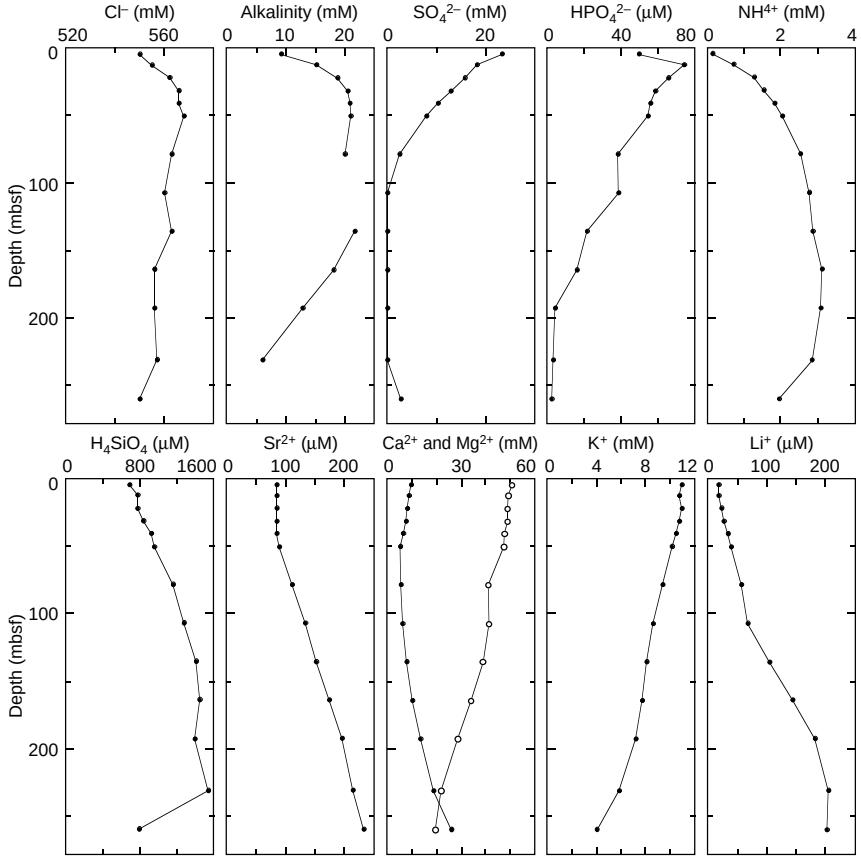


Figure 16. Interstitial water geochemical data, Site 1020. Solid circles = Ca, open circles = Mg.

magnetic susceptibility data demonstrates that the logs can reliably reproduce first-order features of the records generated from measurements of the sediments on the MST track, particularly in the interval below 170 mbsf, where hole conditions are very good. The magnetic susceptibility log (Fig. 29) is particularly useful in determining the zone of pyritization at 135–165 mbsf and in providing a detailed record of variation in the interval below 170 mbsf, where the core magnetic susceptibility and GRAPE data are noisy because of disturbances during XCB drilling. Comparison of the core magnetic susceptibility splice record and the logging data suggests that there is about 10% expansion of the recovered sediment, and therefore the mcd scale, relative to the drilled mbsf depth scale (Fig. 29).

## SUMMARY

Site 1020 is the high-resolution offshore site on the eastern flank of the Gorda Ridge (Fig. 31) drilled to complement Sites 1019 (Eel River Basin) and 1022 (Delgada Slope). The Gorda Transect is completed by Site 1021 on the Delgada Fan, which provides a longer but lower resolution sedimentary section. Besides a missed mudline core, Site 1020 was triple cored to 156 mbsf (~1.8 Ma) and double cored to 233 mbsf (~2.8 Ma). A continuous spliced section was demonstrated to a depth of 118 mbsf (~1.2 Ma), and only three core gaps exist between 118 mbsf and 223 mbsf (~2.6 Ma). The deepest hole touched basement that had a paleomagnetic age of 5.1 Ma, and ~5 cm of basalt

**Table 14. Concentrations of methane ($C_1$), ethene ($C_{2=}$), ethane ($C_2$), propene ($C_{3=}$), and propane ($C_3$) obtained by the headspace technique from Hole 1020B.**

| Core, section, interval (cm) | Depth (mbsf) | $C_1$ (ppm) | $C_{2=}$ (ppm) | $C_2$ (ppm) | $C_{3=}$ (ppm) | $C_3$ (ppm) | $C_1/C_2$ |
|---|---|---|---|---|---|---|---|
| 167-1020B- | | | | | | | |
| 1H-4, 0–5 | 4.53 | 64 | 2 | 4 | 2 | 5 | 16 |
| 2H-4, 0–5 | 12.33 | 11 | | | | | |
| 3H-4, 0–5 | 21.83 | 13 | | | | | |
| 4H-4, 0–5 | 31.33 | 9 | | | | | |
| 5H-4, 0–5 | 40.83 | 9 | | | | | |
| 6H-4, 0–5 | 50.33 | 13 | | | | | |
| 7H-3, 0–5 | 58.33 | 7 | | | | | |
| 8H-3, 0–5 | 67.83 | 36 | | | | | |
| 9H-4, 0–5 | 78.83 | 113 | | | | | |
| 10H-7, 0–5 | 92.83 | 213 | | | | | |
| 11H-6, 145–150 | 102.28 | 325 | | | | | |
| 12H-4, 0–5 | 107.33 | 633 | | | | | |
| 13H-6, 145–150 | 121.28 | 4891 | | | | | |
| 14H-6, 145–150 | 130.78 | 3892 | | | | | |
| 15H-4, 0–5 | 135.83 | 4497 | | | | | |
| 16H-6, 0–5 | 149.78 | 8879 | | 2 | | 1 | 4440 |
| 17H-7, 145–150 | 159.33 | 5242 | | 2 | | | 2621 |
| 18H-4, 0–5 | 164.33 | 8889 | | 2 | | 2 | 4445 |
| 19X-4, 0–5 | 173.83 | 4808 | | 2 | | 1 | 2404 |
| 21X-4, 0–5 | 193.03 | 3040 | | | | | |
| 22X-4, 0–5 | 202.63 | 5412 | | 2 | | | 2706 |
| 23X-4, 0–5 | 212.23 | 2687 | | | | | |
| 25X-4, 0–5 | 231.53 | 1316 | | | | | |
| 26X-4, 0–5 | 241.13 | 654 | | | | | |
| 27X-4, 0–5 | 250.83 | 470 | | | | | |
| 28X-4, 0–5 | 260.43 | 398 | | | | | |
| 29X-2, 0–5 | 266.83 | 120 | | | | | |

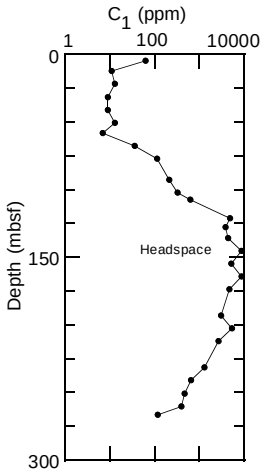


Figure 17. Depth variation of methane ($C_1$) concentration obtained by the headspace technique from Hole 1020B.

was collected. A significant hiatus exists just above basement, and the basal sediments have an age of 3.8 Ma. Age control at the site was provided by excellent paleomagnetics to a depth of ~105 mbsf and by biostratigraphy from all microfossil groups. The sediment column is primarily aluminosilicates, with variable but usually low nannofossil and foraminifer contents in the upper Pleistocene section. Diatom contents are higher downsection, whereas calcareous microfossil contents are lower, especially in the lower Pleistocene and upper Pliocene sediments. Lower Pliocene sediments are marked by a strong enrichment in calcium carbonate compared to the rest of the sediment column and also are more lithified. Site 1020 has the highest heat flow of any of the Leg 167 sites and, unsurprisingly, lies above the youngest oceanic basement. Both the transition from ooze to chalk marking lithostratigraphic Unit II (228 mbsf) and the disappearance of siliceous microfossils below 255 mbsf are probably caused by diagenesis resulting from the high heat flow.

## REFERENCES


Atwater, T., and Severinghaus, J., 1989. Tectonic map of the northeast Pacific Ocean. *In* Winterer, E.L., Hussong, D.M., and Decker, R.W. (Eds.) *The Eastern Pacific Ocean and Hawaii.* Geol. Soc. Am., Decade of North Am. Geol., Vol. N.

Baldauf, J.G., and Iwai, M., 1995. Neogene diatom biostratigraphy for the eastern equatorial Pacific Ocean, Leg 138. *In* Pisias, N.G., Mayer, L.A., Janecek, T.R., Palmer-Julson, A., and van Andel, T.H. (Eds.), *Proc. ODP, Sci. Res.*, 138: College Station, TX (Ocean Drilling Program), 105–128.

Bordovskiy, O.K., 1965. Accumulation and transformation of organic substances in marine sediment, 2. Sources of organic matter in marine basins. *Mar. Geol.*, 3:5–31.

Cande, S.C., and Kent, D.V., 1995. Revised calibration of the geomagnetic polarity timescale for the Late Cretaceous and Cenozoic. *J. Geophys. Res.*, 100:6093–6095.

Emerson, S., and Hedges, J.I., 1988. Processes controlling the organic carbon content of open ocean sediments. *Paleoceanography*, 3:621–634.

Ingle, J.C., Jr., 1967. Foraminiferal biofacies variation and the Miocene-Pliocene boundary in Southern California. *Bull. Am. Paleontol.*, 52:217–394.

Kent, D.V., and Schneider, D.A., 1995. Correlation of paleointensity variation records in the Brunhes/Matuyama polarity transition interval. *Earth Planet. Sci. Lett.*, 129:135–144.

Koizumi, I., 1992. Diatom biostratigraphy of the Japan Sea: Leg 127. *In* Pisciotto, K.A., Ingle, J.C., Jr., von Breymann, M.T., Barron, J., et al., *Proc. ODP, Sci. Results*, 127/128 (Pt. 1): College Station, TX (Ocean Drilling Program), 249–289.

Lyle, M., Gallaway, P.J., Liberty, L.M., Mix, A., Stott, L., Hammond, D., Gardner, J., Dean, W., and the EW9504 Scientific Party, 1995a. Data submission. W9406 and EW9504 site surveys of the California margin proposed drillsites, Leg 167 (Vol. 1): Site maps and descriptions. Boise State Univ., *CGISS Tech. Rep.*, 95–11.

————, 1995b. Data submission. W9406 and EW9504 site surveys of the California margin proposed drillsites, Leg 167 (Vol. 2): Seismic profiles. Boise State Univ., *CGISS Tech. Rep.*, 95–12.

Mix, A.C., Rugh, W., Pisias, N.G., Veirs, S., Leg 138 Shipboard Sedimentologists (Hagelberg, T., Hovan, S., Kemp, A., Leinen, M., Levitan, M., Ravelo, C.), and Leg 138 Scientific Party, 1992. Color reflectance spectroscopy: a tool for rapid characterization of deep-sea sediments. *In* Mayer, L., Pisias, N., Janecek, T., et al., *Proc. ODP, Init. Repts.*, 138 (Pt. 1): College Station, TX (Ocean Drilling Program), 67–77.

Riddihough, R.P., 1980. Gorda Plate motions from magnetic anomaly analysis. *Earth Planet. Sci. Lett.*, 51:163–170.

Wilson, D.S., 1989. Deformation of the so-called Gorda Plate. *J. Geophys. Res.*, 94:3065–3075.

**Ms 167IR-114**

**NOTE: For all sites drilled, core-description forms ("barrel sheets") and core photographs can be found in Section 3, beginning on page 499. Smear-slide data can be found in Section 4, beginning on page 1327. See Table of Contents for material contained on CD-ROM.**

**Table 15. Concentrations of inorganic carbon, calcium carbonate, total carbon, total organic carbon, total nitrogen, and total sulfur in weight percent (wt%) in Hole 1020B.**

| Core | Depth (mbsf) | Inorganic carbon (wt%) | $CaCO_3$ (wt%) | Total carbon (wt%) | Total organic carbon (wt%) | Total nitrogen (wt%) | Total sulfur (wt%) | Total organic carbon/ Total nitrogen |
|---|---|---|---|---|---|---|---|---|
| 167B-1020- | | | | | | | | |
| 1H-3, 29–30 | 3.29 | 0.49 | 4.1 | 1.18 | 0.69 | 0.14 | 0.00 | 4.93 |
| 1H-5, 29–30 | 6.29 | 0.40 | 3.3 | 1.19 | 0.79 | 0.14 | 0.00 | 5.64 |
| 2H-2, 29–30 | 9.59 | 0.39 | 3.2 | 1.23 | 0.84 | 0.16 | 0.00 | 5.25 |
| 2H-4, 29–30 | 12.59 | 0.14 | 1.2 | 1.42 | 1.28 | 0.19 | 0.00 | 6.74 |
| 2H-6, 29–30 | 15.59 | 0.49 | 4.1 | 1.51 | 1.02 | 0.16 | 0.00 | 6.38 |
| 3H-2, 30–31 | 19.10 | 0.41 | 3.4 | 1.13 | 0.72 | 0.10 | 0.00 | 7.20 |
| 3H-4, 30–31 | 22.10 | 0.11 | 0.9 | 0.66 | 0.55 | 0.10 | 0.30 | 5.50 |
| 3H-6, 30–31 | 25.10 | 0.28 | 2.3 | 0.69 | 0.41 | 0.08 | 0.00 | 5.13 |
| 4H-1, 29–30 | 27.09 | 2.32 | 19.3 | 2.95 | 0.63 | 0.13 | 0.00 | 4.85 |
| 4H-3, 28–29 | 30.08 | 0.11 | 0.9 | 0.69 | 0.58 | 0.11 | 0.00 | 5.27 |

**Only part of this table is reproduced here. The entire table appears on CD-ROM (back pocket).**

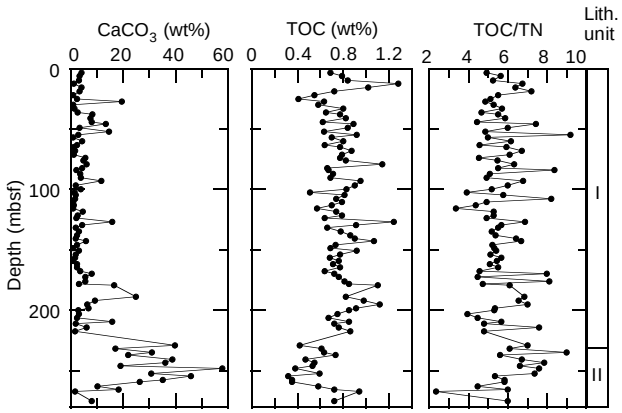


Figure 18. Depth variation of calcium carbonate, total organic carbon (TOC), and total organic carbon/total nitrogen (TOC/TN) in sediments of Hole 1020B.

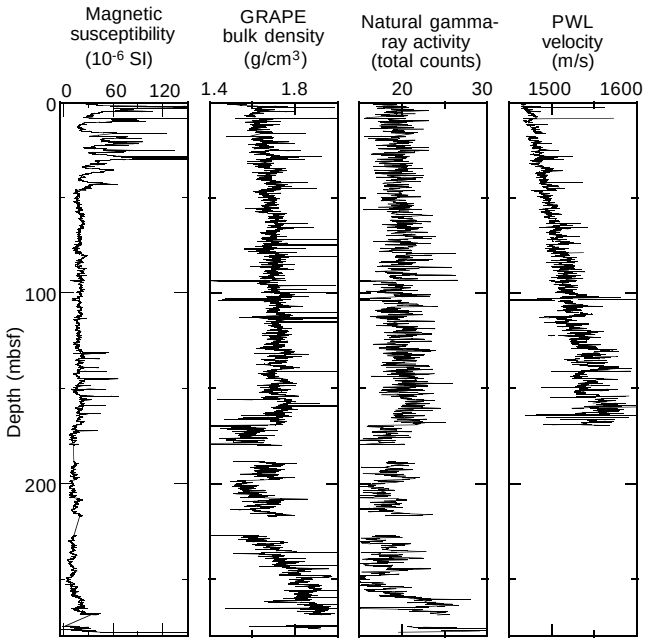


Figure 19. MST data from Hole 1020B.

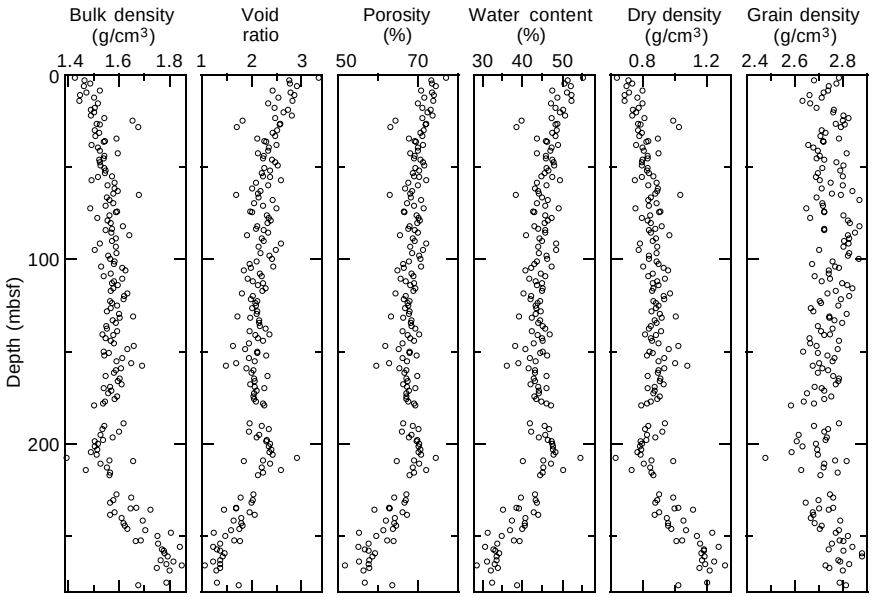


Figure 20. Index property data from Hole 1020B.

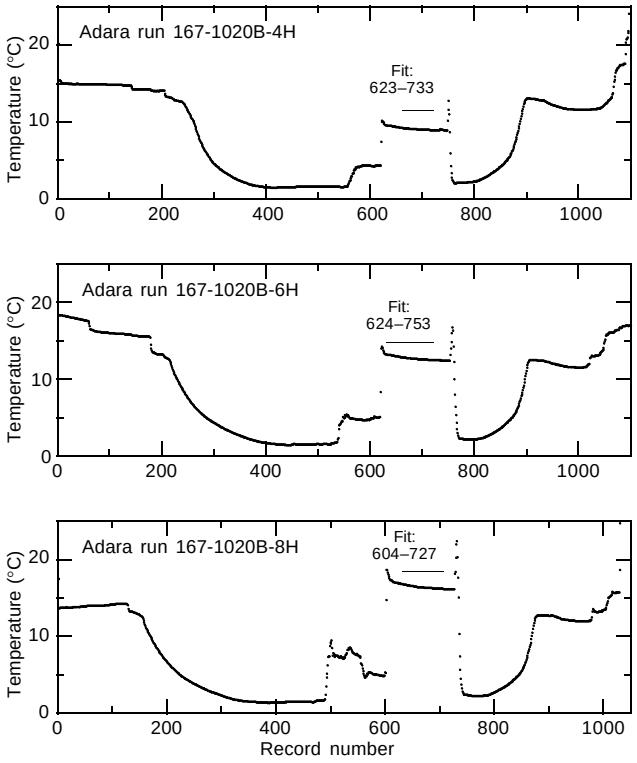


Figure 21. Hole 1020B downhole temperature vs. record number (5-s recording frequency) for each measurement run, showing the intervals fitted to determine the downhole temperature.

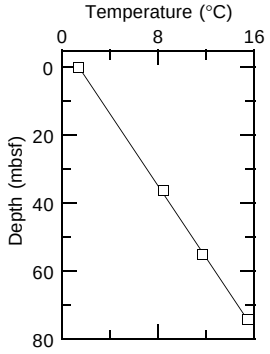


Figure 22. Downhole temperature gradient for Hole 1020B.

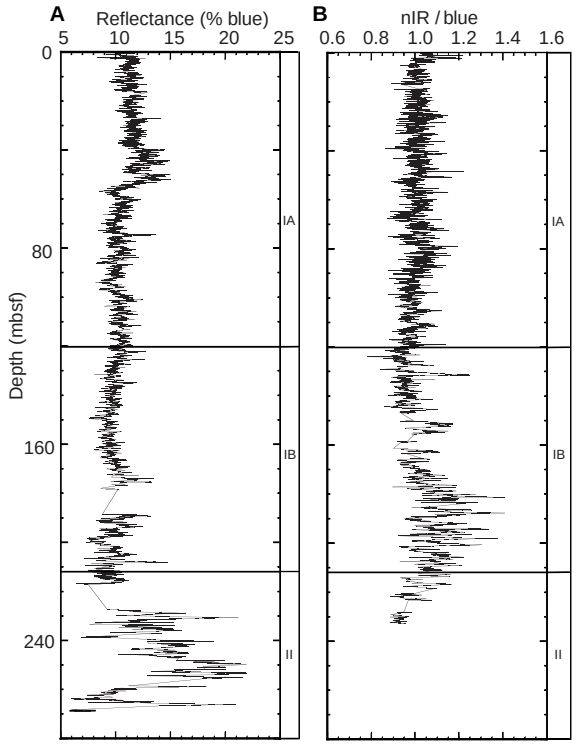


Figure 23. Summary of color reflectance data for Site 1020. **A.** Percent reflectance for 450–500-nm band average (blue) of Hole 1020B compared to major lithostratigraphic units. **B.** Ratio of 850–900-nm band average (near infrared) to blue for Hole 1020C.

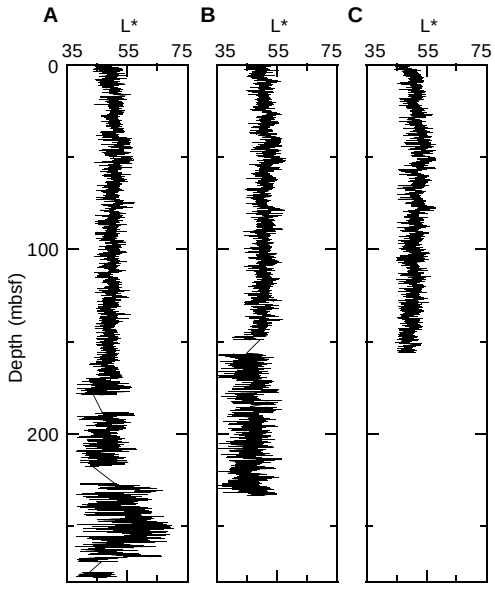


Figure 24. Digital color video data for CIELAB L* from Holes (**A**) 1020B, (**B**) 1020C, and (**C**) 1020D. Data were decimated at 2-cm intervals.

**Table 19. Downhole measurements in Hole 1020B.**

| Date, time | Description |
|---|---|
| 3 June 1996 | |
| 1100 | Set pipe at 56 mbsf, rig up wireline, rig up density-porosity combination tool string, sea state calm. |
| 1200 | RIH density-porosity, wireline heave compensator on. |
| 1310 | At TD, begin density-porosity pass 1 at 300 m/hr (275–95 mbsf). |
| 1400 | At TD, begin density-porosity pass 2 (275–90 mbsf), continue logging to mudline. |
| 1500 | POOH, rig down density-porosity, rig up sonic-FMS tool string, RIH. |
| 1845 | At TD, begin sonic-FMS pass 1 at 300 m/hr (275−100 mbsf), pause at 200 mbsf because of winch problem, close/reopen calipers. |
| 2000 | At TD, begin sonic-FMS pass 2 (275–100 mbsf). |
| 2200 | POOH sonic-FMS, rig down, rig up GHMT tool string, RIH. |
| 4 June 1996 | |
| 0000 | At TD, begin GHMT pass 1 at 1000 m/hr (260–75 mbsf). |
| 0040 | At TD, begin GHMT pass 2 (272−60 mbsf). |
| 0200 | POOH GHMT, rig down, end logging operations. |

Note: RIH = run in hole, TD = total depth, FMS = Formation MicroScanner, POOH = pull out of hole, GHMT = geological high-sensitivity magnetic tool.

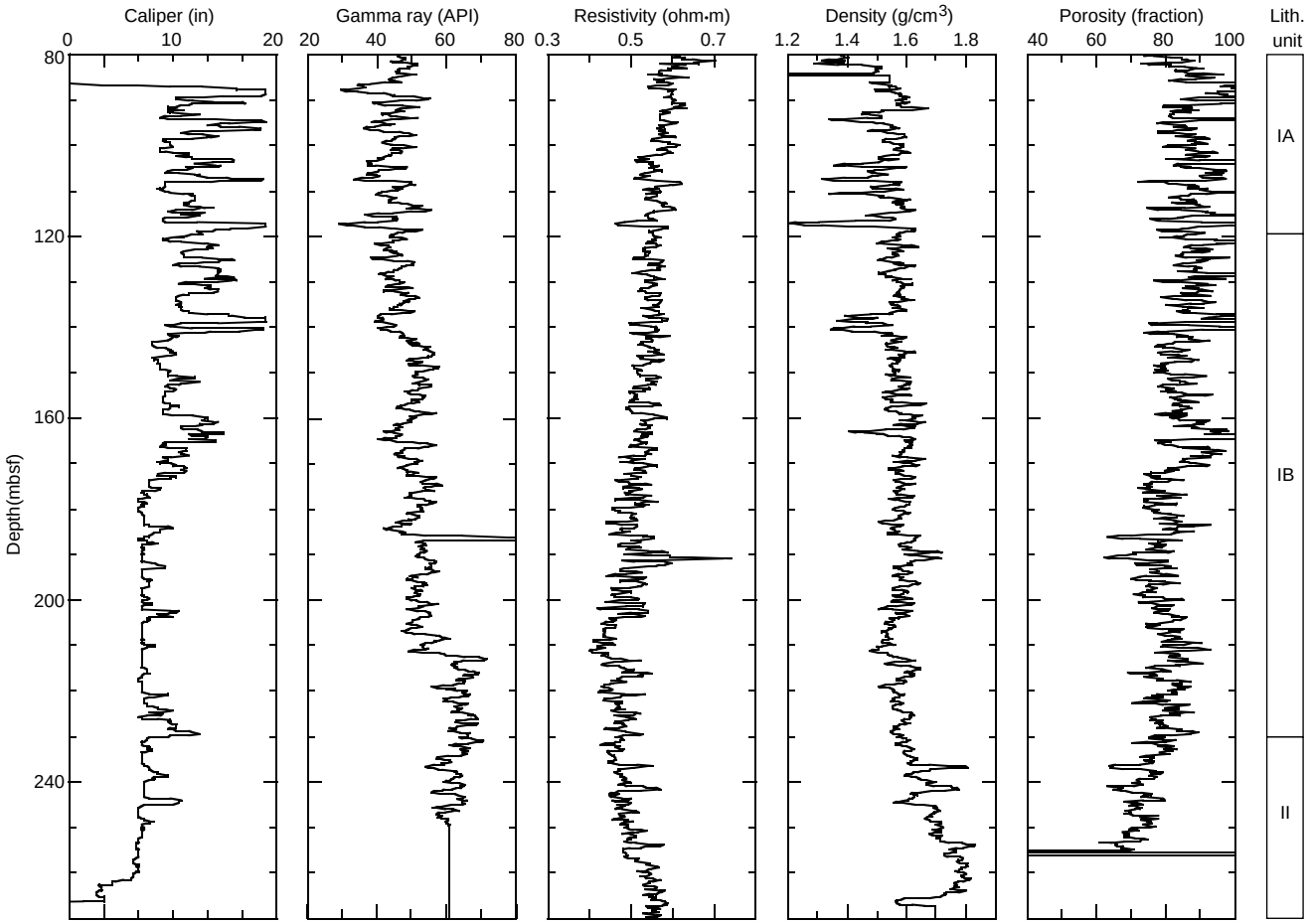


Figure 25. Downhole log data from the density-porosity combination tool string (pass 1) and a lithostratigraphic summary column of Hole 1020B (see “Lithostratigraphy” section, this chapter).

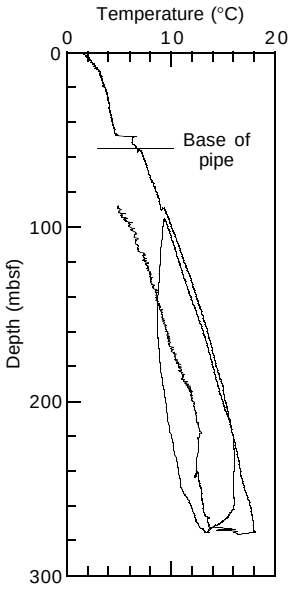


Figure 26. Borehole temperature measurements from the Lamont-Doherty temperature logging tool. The results suggest a downhole temperature gradient of 56°C/km.

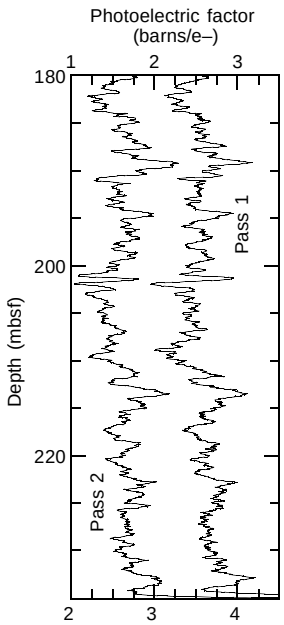


Figure 27. Hole 1020B photoelectric factor from pass 1 and pass 2 of the density-porosity combination tool string.

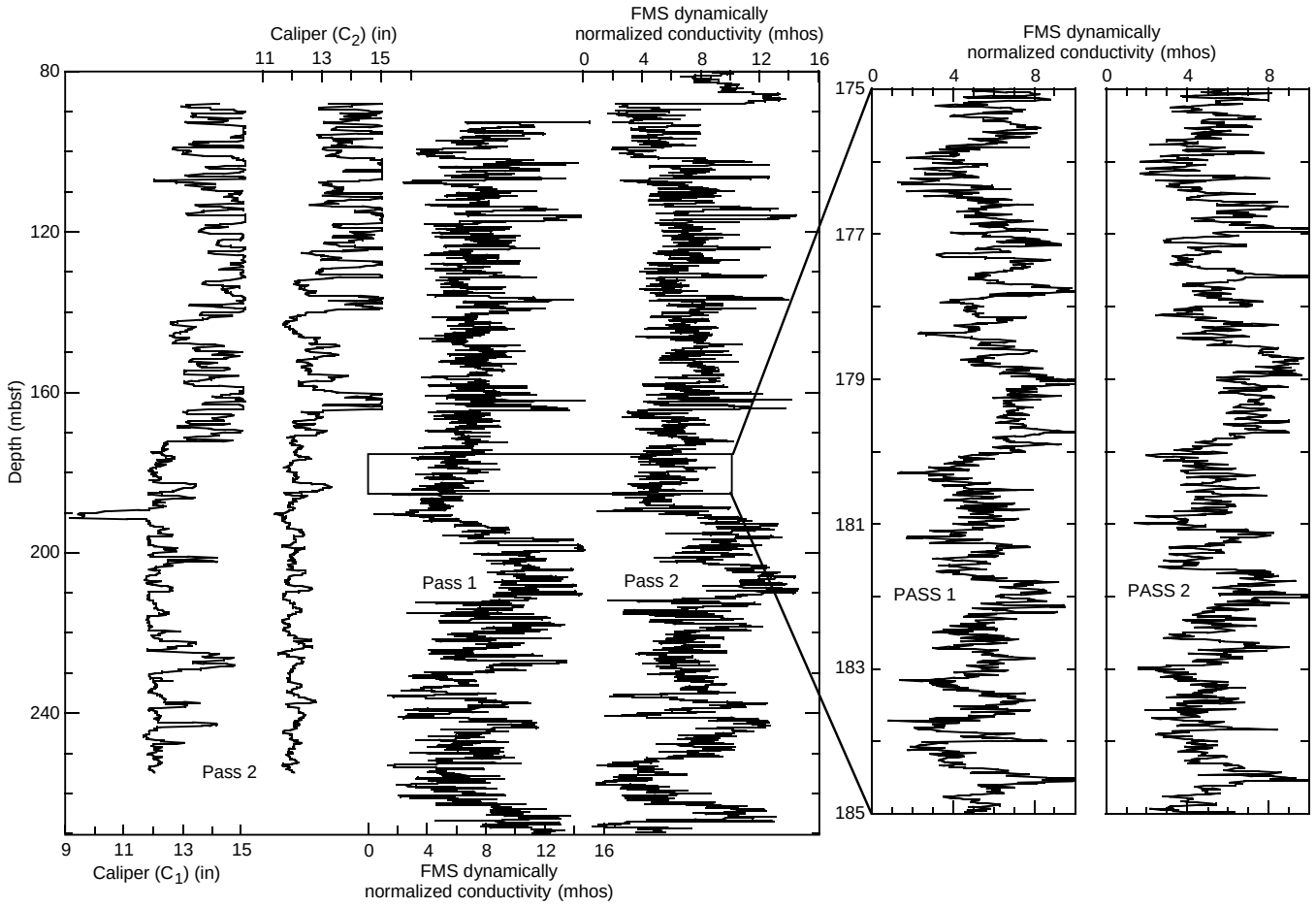


Figure 28. FMS data from pass 1 and pass 2 of the sonic-FMS tool string. On the left, the two orthogonal caliper records ($C_1$ and $C_2$) from pass 2 are shown. The washouts above 170 mbsf are where the FMS data are of poor quality. Below 170 mbsf, the hole is generally in fair to good condition. The caliper suggests that there is an interval of swelling at 190 mbsf, where a dolomitic clay was observed in the core. The middle two curves are the full FMS records from the two passes (20-point smoothing). On the right are the unsmoothed FMS data from the two passes in a 10-m interval.

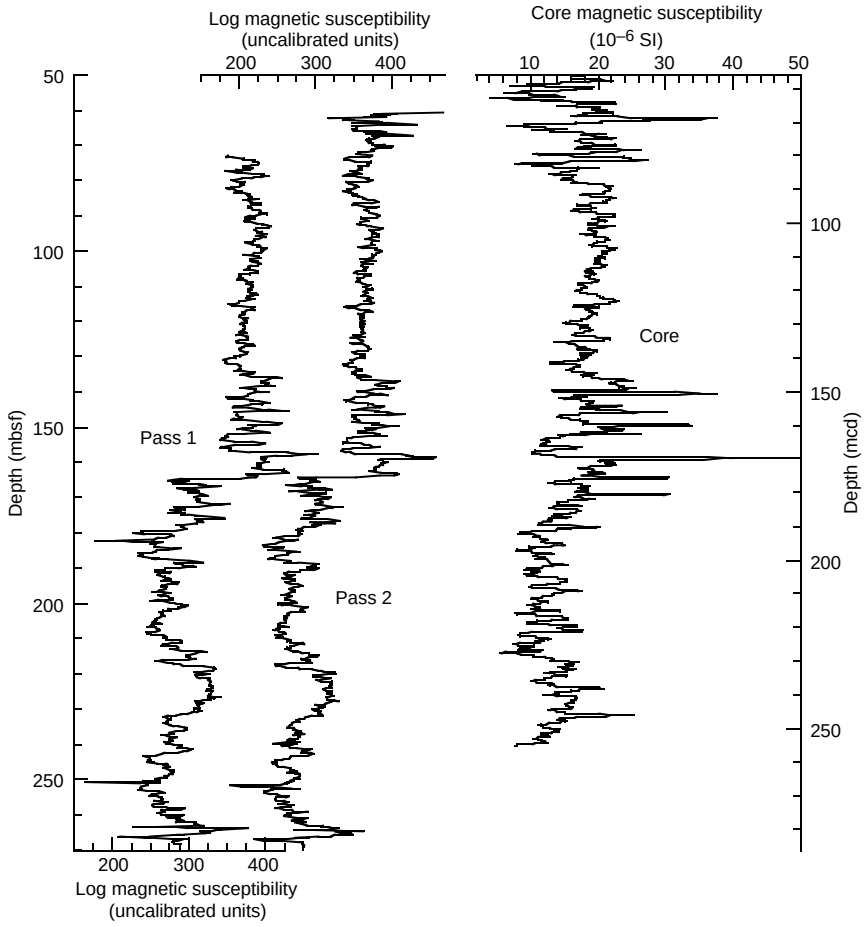


Figure 29. Comparison of log and core magnetic susceptibility data using the two passes of the GHMT tool string and the splice of MST whole-core magnetic susceptibility measurements (10-point smoothing).

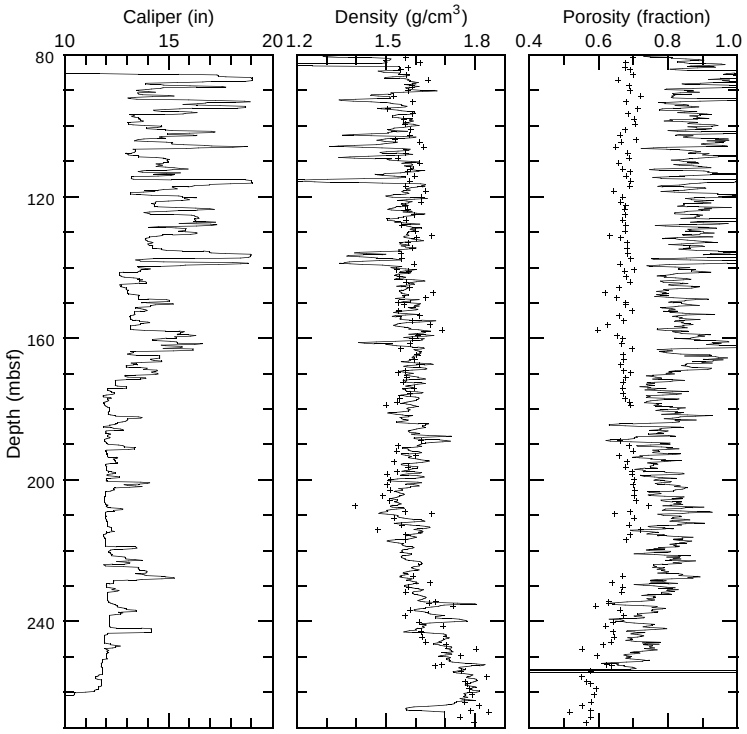


Figure 30. Comparison of log (lines) and core (crosses) density and porosity data.

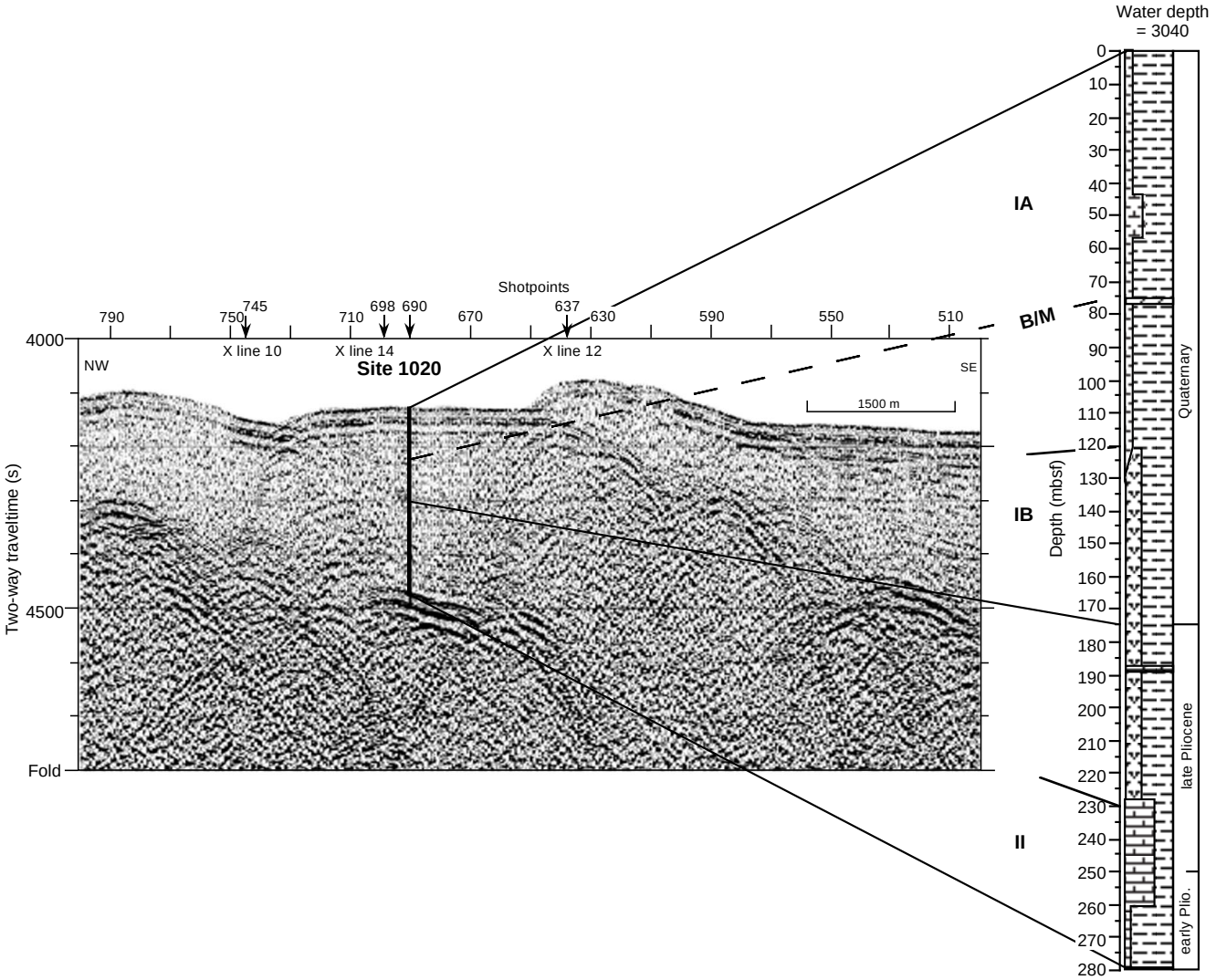


Figure 31. Comparison of the lithostratigraphic column at Site 1020 and a seismic reflection profile through it (Line W9406 CA4-4; Lyle, et al., 1995a, 1995b). Ties are calculated from shipboard seismic velocity measurements (see “Physical Properties” section, this chapter). B/M = Brunhes/Matuyama boundary. On y-axis, (s) = milliseconds.

# SHORE-BASED LOG PROCESSING
# HOLE 1020B

**Bottom felt:** 3049.7 mbrf (used for depth shift to seafloor)
**Total penetration:** 278.8 mbsf
**Total core recovered:** 265 m (95%)

## Logging Runs

**Logging string 1:** DIT/HLDT/APS/HNGS (2 passes)
**Logging string 2:** FMS/SDT/GPIT/NGT (2 passes)
**Logging string 3:** GHMT/NGT (2 passes)
Wireline heave compensator was used to counter ship heave.

## Bottom-Hole Assembly

The following bottom-hole assembly depths are as they appear on the logs after differential depth shift (see "Depth shift" section) and depth shift to the seafloor. As such, there might be a discrepancy with the original depths given by the drillers on board ship. Possible reasons for depth discrepancies are ship heave, use of wireline heave compensator, and drill string and/or wireline stretch.

DIT/HLDT/APS/HNGS: Recorded open hole (pass 1).
DIT/HLDT/APS/HNGS: Bottom-hole assembly at ~60 mbsf (pass 2).
FMS/GPIT/NGT: Recorded open hole (pass 1).
FMS/GPIT/NGT: Bottom-hole assembly at ~60 mbsf (pass 2).
GHMT/NGT: Recorded open hole (pass 1).
GHMT/NGT: Bottom-hole assembly at ~60 mbsf (pass 2).

## Processing

**Depth shift:** Original logs have been interactively depth shifted with reference to HNGS from DIT/HLDT/APS/HNGS pass 2 and to the seafloor (–049.7 m). Pass 1 of the GHMT and FMS tool strings have been depth shifted with reference to Pass 2 of the same tool string, by using caliper and magnetic data for correlation.

**Gamma-ray and environmental corrections:** Corrections for borehole size and type of drilling fluid were performed on the NGT data from the FMS/GPIT/SDT/NGT and GHMT/NGT tool strings. HNGS data from the DIT/HLDT/APS/HNGS tool string were corrected in real-time during the recording.

**Acoustic data processing:** The array sonic tool was operated in standard depth-derived, borehole compensated, long spacing (8-10-10-12 ft) and short spacing (3-5-5-7 ft) mode. Because of an offset the transit times, no standard processing has been performed. An uncompensated velocity value has been computed from the edited LTT4 (10-ft spacing) channel from Pass 2.

## Quality Control

Data recorded through bottom-hole assembly, such as the HNGS, NGT, and APS data above 60 mbsf, should be used qualitatively only because of the attenuation on the incoming signal.

Hole diameter was recorded by the hydraulic caliper on the HLDT tool (CALI) and on the FMS string (C1 and C2).

**Note:** Details of standard shore-based processing procedures are found in the "Explanatory Notes" chapter, this volume. For further information about the logs, please contact:

Cristina Broglia
Phone: 914-365-8343
Fax: 914-365-3182
E-mail: chris@ldeo.columbia.edu

Zhiping Tu
Phone: 914-365-8336
Fax: 914-365-3182
E-mail: ztu@ldeo.columbia.edu

Hole 1020B: Natural Gamma Ray-Density-Porosity Logging Data-Pass 2

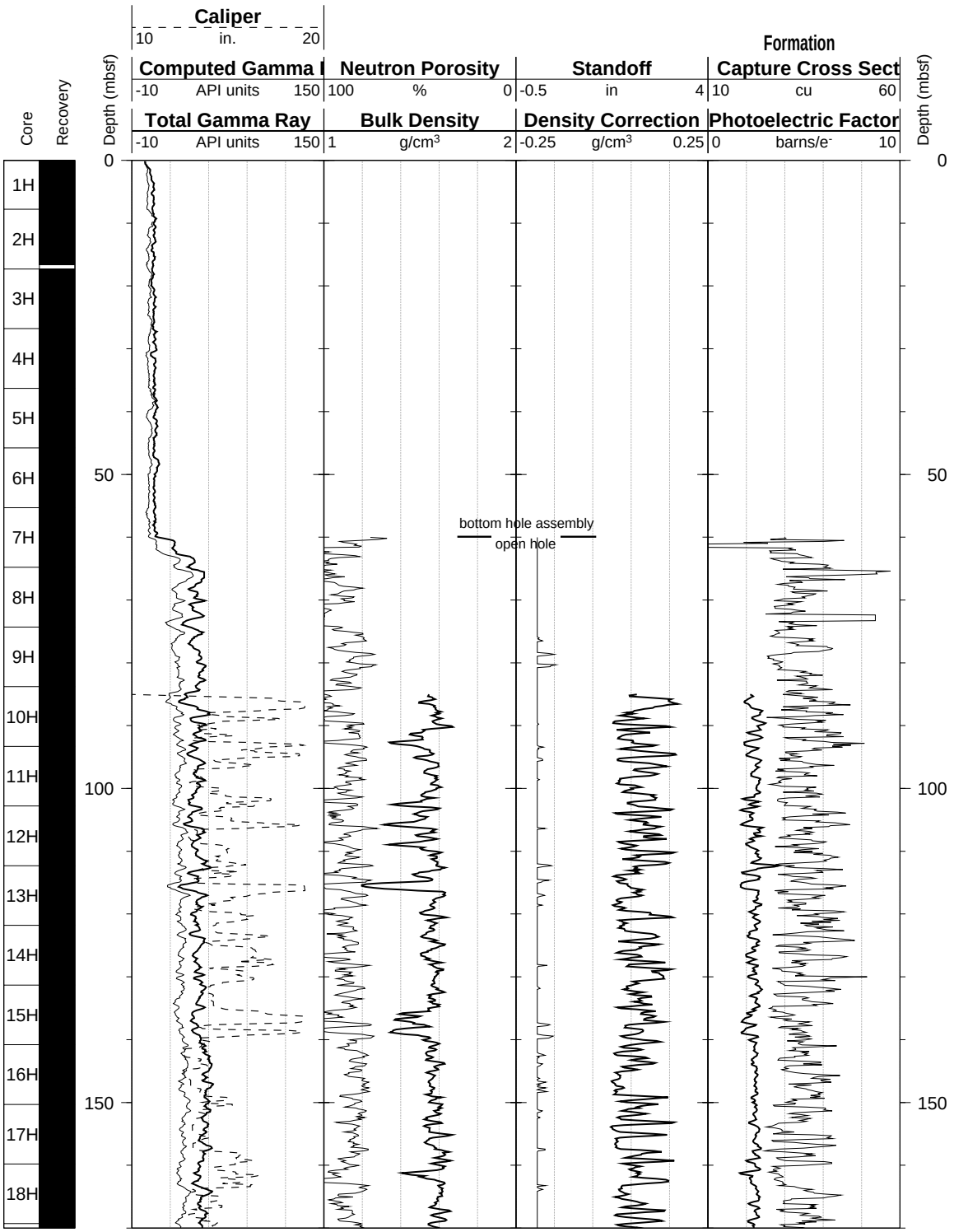

Hole 1020B: Natural Gamma Ray-Density-Porosity Logging Data-Pass 2 (cont.)

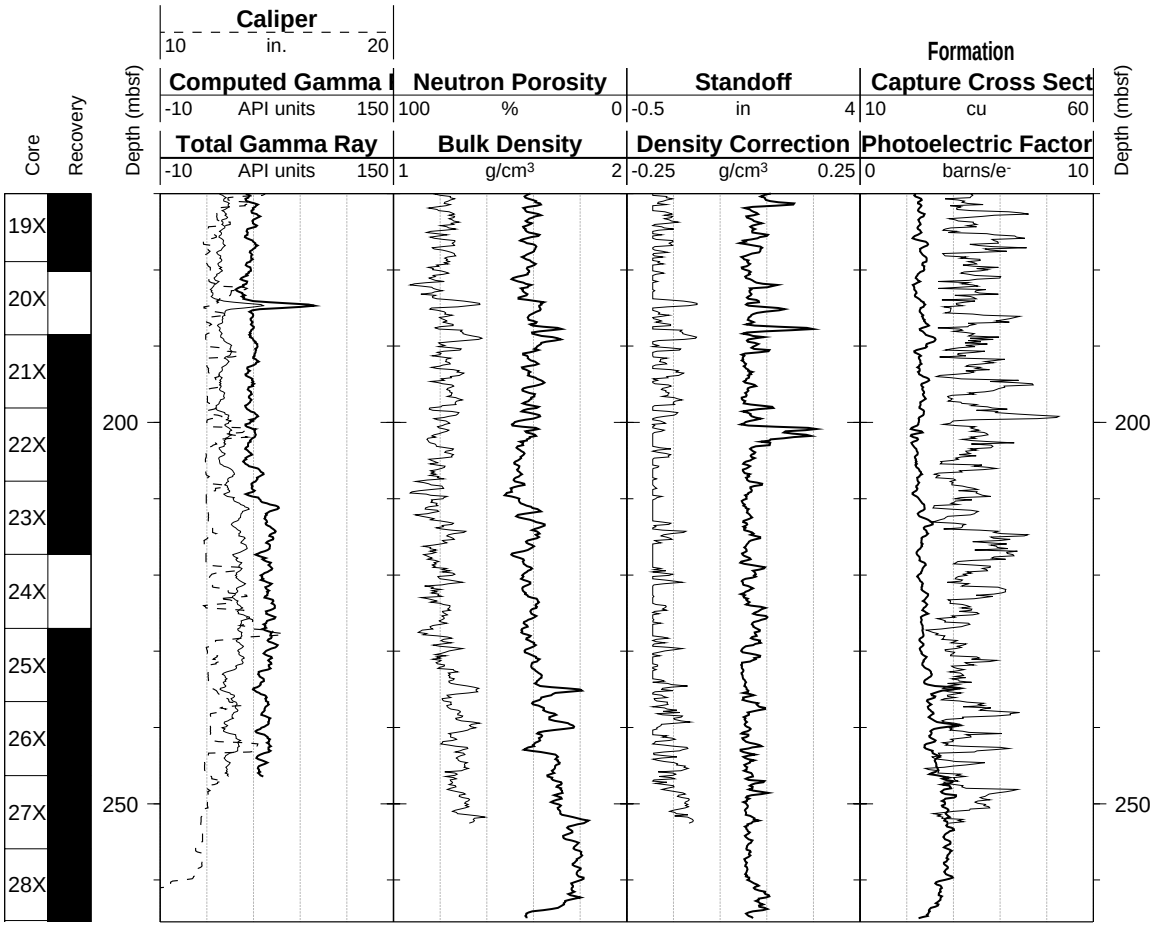

Hole 1020B: Natural Gamma Ray-Resistivity-Sonic Logging Data-Pass 2

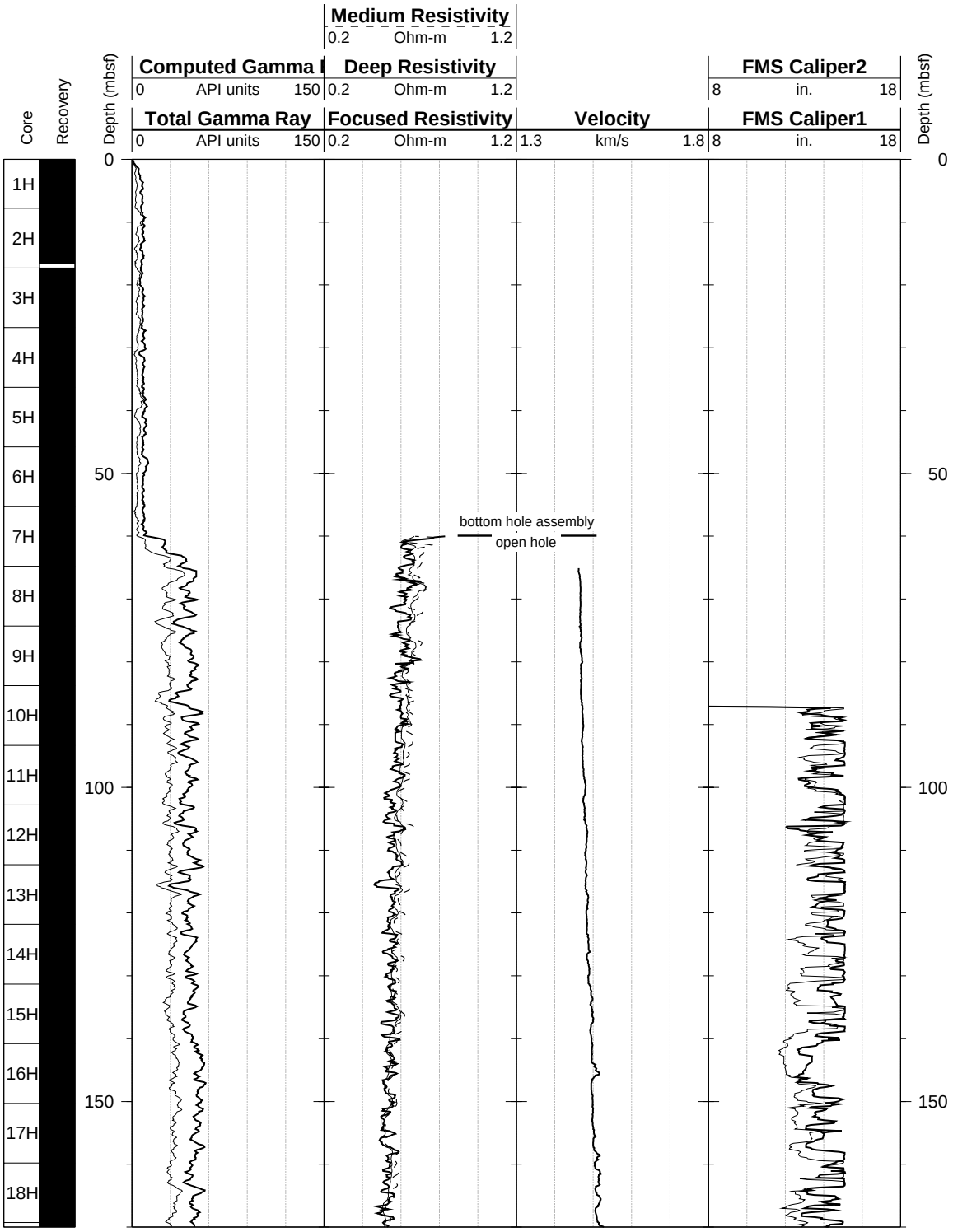

Hole 1020B: Natural Gamma Ray-Resistivity-Sonic Logging Data-Pass 2 (cont.)

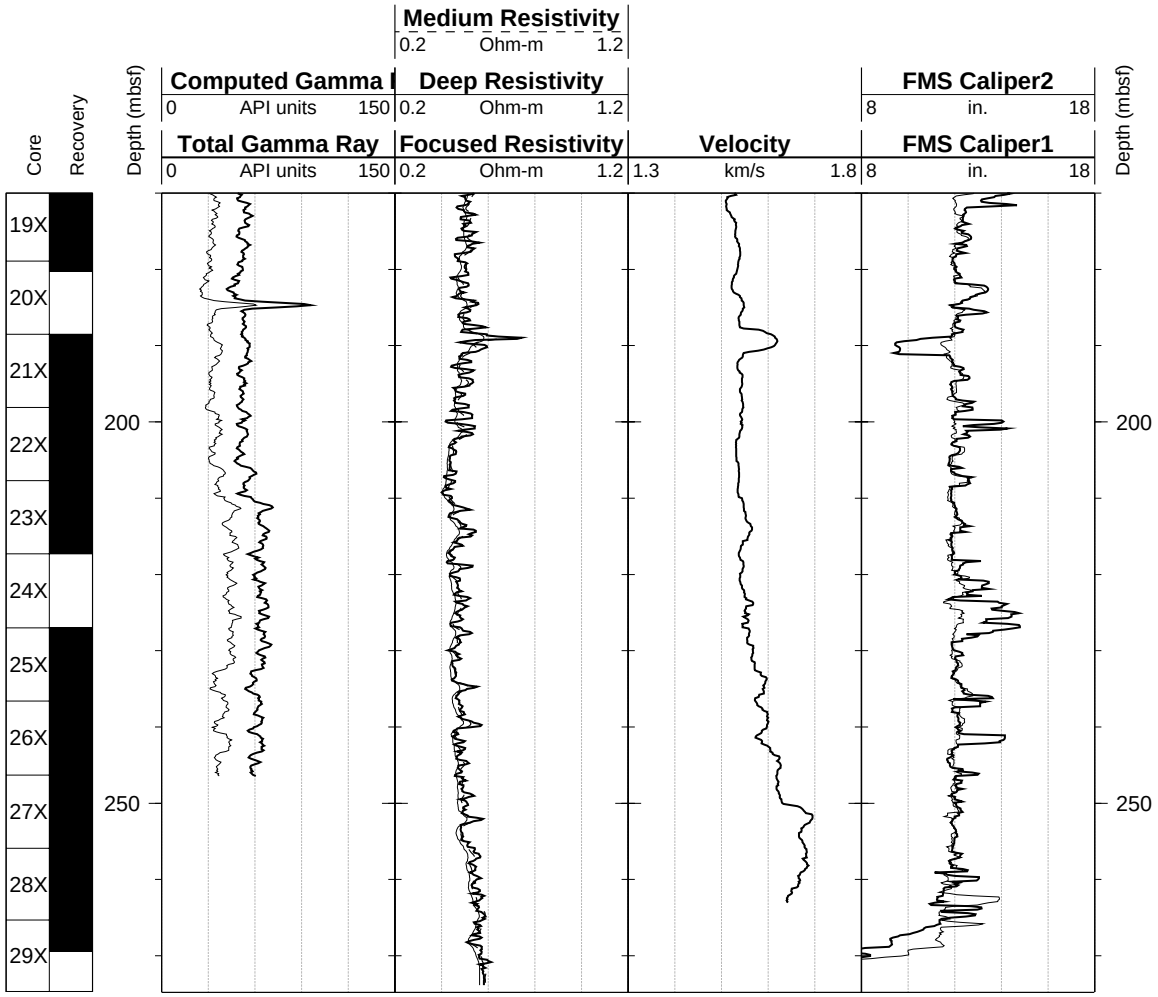

Hole 1020B: Natural Gamma Ray Logging Data-Pass 2

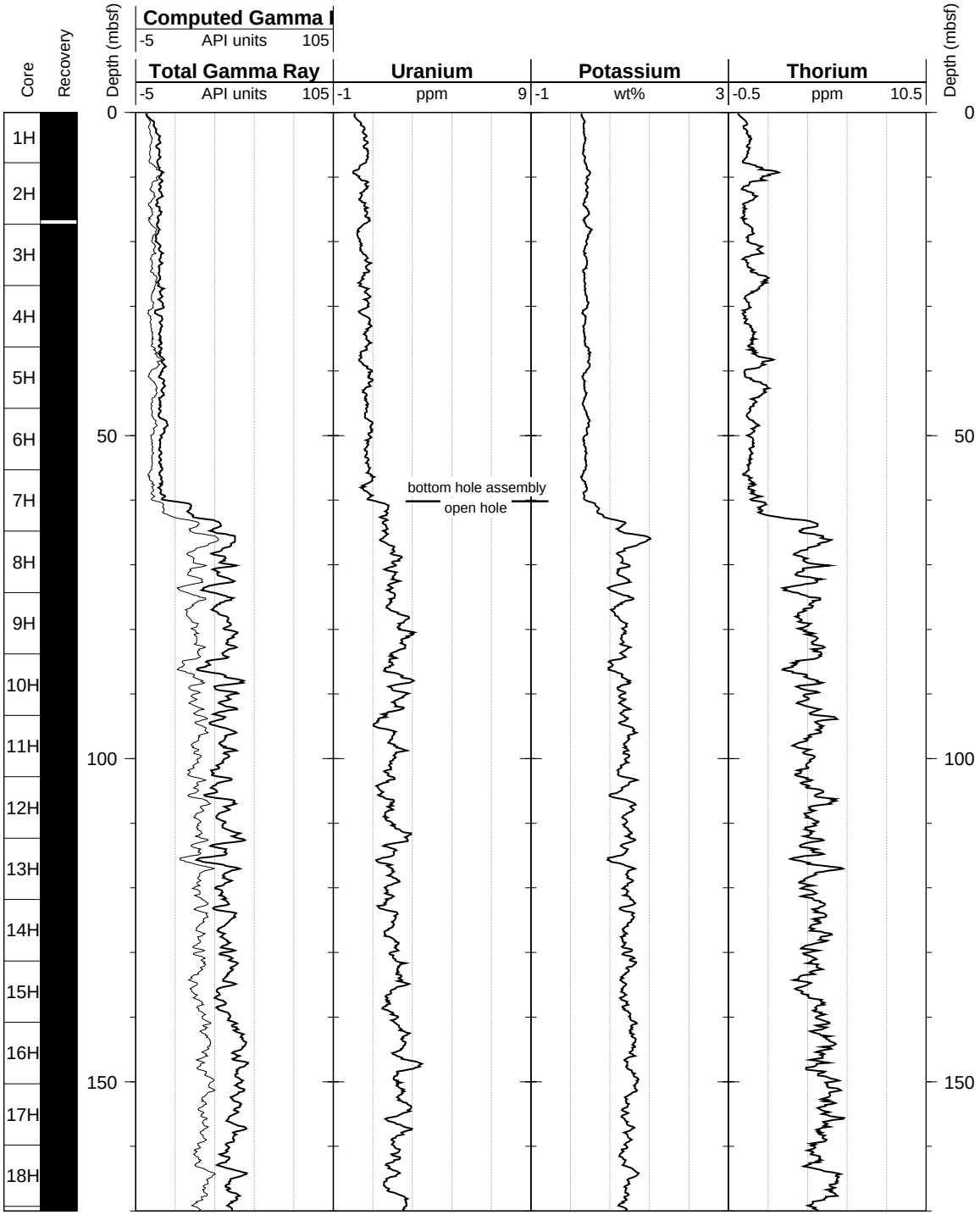

Hole 1020B: Natural Gamma Ray Logging Data-Pass 2 (cont.)